tekstilec (ISSN: 0351-3386 tiskano, 2350-3696 elektronsko) je znanstvena revija, ki podaja temeljne in aplikativne znanstvene informacije v fizikalni, kemijski in tehnološki znanosti, vezani na tekstilno in oblačilno tehnologijo, oblikovanje in trženje tekstilij in oblačil. V prilogah so v slovenskem jeziku objavljeni strokovni članki in prispevki o novostih v tekstilni tehnologiji iz Slovenije in sveta, prispevki s področja oblikovanja tekstilij in oblačil, informacije o raziskovalnih projektih ipd.

tekstilec *(ISSN: 0351-3386 printed, 2350-3696 online) the scientific journal gives fundamental and applied scientific information in the physical, chemical and engineering sciences related to the textile and clothing industry, design and marketing. In the appendices written in Slovene language, are published technical and short articles about the textile-technology novelties from Slovenia and the world, articles on textile and clothing design, information about research projects etc.*

Dosegljivo na svetovnem spletu/*Available Online at*
www.tekstilec.si

tekstilec

Revija Tekstilec izhaja štirikrat letno */*
Journal Tekstilec appears quarterly

Revija je pri Ministrstvu za kulturo vpisana v razvid medijev pod številko 583. Letna naroč-nina za člane Društev inženirjev in tehnikov tekstilcev je vključena v članarino.
Letna naročnina za posameznike 38 €
za študente 22 €
za mala podjetja 90 € za velika podjetja 180 €
za tujino 110 €

Cena posamezne številke 10 €

Na podlagi Zakona o davku na dodano vrednost sodi revija Tekstilec med proizvode, od katerih se obračunava DDV po stopnji 5 %.

Transakcijski račun 01100–6030708186
Bank Account No. SI56 01100–6030708186
Nova Ljubljanska banka d. d.,
Trg Republike 2, SI–1000 Ljubljana,
Slovenija, SWIFT Code: LJBA SI 2X.

Elise Diestelhorst [1], Jan Lukas Storck [1], Bennet Brockhagen [1], Timo Grothe [1], Inken Blanca Post [2], Thorsten Bache [2], Rumen Korchev [2], Anke Rattenholl [1], Frank Gudermann [1], Andrea Ehrmann [1]
[1] Bielefeld University of Applied Sciences, Faculty of Engineering and Mathematics, Bielefeld, Germany
[2] Bache GmbH, Rheinberg, Germany

Necessary Parameters of Vertically Mounted Textile Substrates for Successful Cultivation of Cress for Low-Budget Vertical Farming
Lastnosti vertikalno nameščenih tekstilij, potrebne za uspešno gojenje kreše pri nizkocenovnem vertikalnem kmetovanju

Corresponding author/*Korespondenčna avtorica:*
Prof. Dr. Dr. Andrea Ehrmann
E-mail: andrea.ehrmann@fh-bielefeld
ORCID ID: 0000-0003-0695-3905

Abstract
A growing population needs an expansion of agriculture to ensure a reliable supply of nutritious food. As a variable concept, vertical farming, becoming increasingly popular, can allow plant growth for local food production in the vertical sense on, e.g. facades in addition to the classical layered structure in buildings. As substrates, textile fabrics can be used as a sustainable approach in terms of reusability. In our experiment, we investigated which properties a textile should possess in order to be suitable for an application in vertical farming by the example of cress seeds. To determine the best-fitted fabric, four different textiles were mounted vertically, and were provided with controlled irrigation and illumination. Our results showed that a hairy textile surface as provided by weft-knitted plush is advantageous. There, the rooting of cress plants used in this experiment is easier and less complicated than along tightly meshed, flat surfaces, as for woven linen fabrics.
Keywords: vertical farming, textile substrates, cress, cost-effectiveness, germination

Izvleček
Naraščajoče prebivalstvo potrebuje širitev kmetijstva, da bi si zagotovilo zanesljivo oskrbo s hranljivimi živili. Vertikalno kmetovanje, ki postaja čedalje bolj priljubljeno, lahko kot spremenljiv koncept omogoči rast rastlin za lokalno pridelavo hrane v navpični legi, na primer ob klasičnih večplastnih strukturah na fasadah stavb. Za podlago lahko uporabimo tekstilije, ki pomenijo trajnostni pristop v smislu njihove ponovne uporabe. Na primeru semen kreše v našem poskusu raziskujemo, katere lastnosti bi morala imeti tekstilija, da bi bila primerna za uporabo v vertikalnem kmetovanju. Za določitev najboljše tekstilije so bile štiri različne tekstilije nameščene vertikalno, z nadzorovanim namakanjem in osvetlitvijo. Naši rezultati kažejo, da ima prednost kosmatena tekstilna površina, ki jo zagotavlja votkovni pliš, pri katerem je ukoreninjenje rastlin kreše, uporabljenih v tem poskusu, lažje in manj zapleteno kot na tesno povezanih, ravnih površinah, kot so na primer lanene tkanine.
Ključne besede: vertikalno kmetovanje, tekstilni substrat, kreša, nizkocenovno, kalitev

1 Introduction

The system of vertical farming (VF) has generated increasing attention in recent years. This development is due to the many advantages of the system, when compared to conventional agriculture, as well as due to the flexibility of the structure, the components and materials used. In view of a growing population [1], the rising demand for nutritious food [2, 3] is expected to increase by about 70% until 2050 [4, 5], while the available arable land is decreasing in the face of growing cities and climate change [6]. One of the challenges to meet this demand lies in the phenomenon of urbanisation, which results in pushing green spaces further out of the city centre, thereby lengthening the transport routes of food products and significantly reducing their quality in terms of nutrients and freshness [7–9]. Furthermore, the carbon footprint caused by the transportation contributes to heavy air pollution and thus global warming [10, 11].

Apart from the insufficient quantity of land, conventional agriculture entails a variety of problems including the ongoing destruction of forests [7], which can lead to the loss of native plant and animal species [12], to a loss of biodiversity and degradation of ecosystems due to the use of fertilisers and pesticides [3], and to the intense utilisation of water [10, 13], to name just a few.

Another challenge of conventional agriculture lies in the invariable external factors such as weather conditions. In view of the changing climate due to global warming, the food supply can often not be ensured, as phenomena like droughts, heatwaves or floods can lead to crop failures [7, 10, 13] with agriculture itself contributing to those risks by using methods like intensive groundwater pumping [13].

These issues can partly be solved by transferring plant cultivation from the fields into buildings and utilising systems like VF as an alternative concept to conventional agriculture. This makes the supply of food more reliable for several reasons. The independence from weather and climate change prevents weather-related crop failures and production can be carried out regardless of the season [7], leading to a higher food security. In addition, no new areas need to be developed and production can be conducted centrally in existing buildings [7, 8, 14]. At the same time, by cultivating into the vertical plane, the productivity per unit area increases compared to conventional agriculture [4, 7, 15–17].

Local production can further reduce transport emissions, while the nutrient content can increase by shortening the storage time of plants. The overall environmental pollution is reduced since a local VF system offers a more sustainable solution in terms of used materials and the cultivation of plants regarding the usage of water and energy resources [7, 8, 18].

Initially, VF is often associated with constructions in the form of ceiling-high shelves in high-rise buildings with the use of hydroponics as an approach for a sustainable production of herbs and plants in general, and the ability of manipulating factors that mimic the natural growing environment, e.g. artificial light sources and heating [8, 16]. Although control over temperature and lighting brings many benefits in terms of plant growth, these are also the factors that can become problematic when it comes to sustainable crop production, depending on building characteristics and location. If outdoor temperature differs greatly from the required indoor temperature, or if the amount of daylight is extremely low or cannot be distributed sufficiently evenly, VF can have high-energy requirements. For example, in large cities with many surrounding high-rise buildings, this cannot be optimally met by renewable energy sources, e.g. solar panels, due to the shading from surrounding buildings [19]. Alternative concepts, e.g. living walls, utilise substrates like textile fabrics or nonwovens and attach them to walls vertically for city greening or for air improvement indoors [18, 21]. Apart from plants, another possibility is the cultivation of algae on textile substrates [22]. The term "agro textile" refers to a variety of textiles applied in areas like agriculture, landscaping and forestry [23] that are used, e.g. as mulch mats [24], hail protection or windshields, in agricultural contexts, all mainly with the purpose of crop protection [25]. Due to their numerous application possibilities, the textiles themselves differ considerably in their properties and can be woven, nonwoven or knitted [18, 23, 26]. Textiles, however, are usually not applied in VF [22], although they can be more sustainable than the often-used mineral wool. Thus, we are presenting here the findings on inherent textile fabric characteristics which enable successful plant growth. This form of farming can easily be adapted for home growth, e.g. herbs on a small scale in the kitchen, and thus generally enable a more widespread acceptance in the population for this relatively new

form of soilless plant cultivation. In this context and with a low-budget system, the study aimed to investigate basic parameters of textile substrates for successful germination and cultivation of plants on the example of cress.
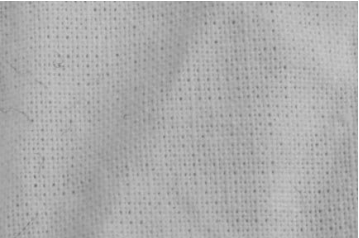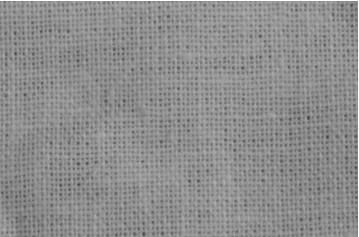
2 Experimental

The used textiles included woven linen, woven cotton (both plain weave), weft-knitted plush (from 5 threads 100% poly(ethylene terephthalate) (PET) 400 dtex, from Technofibres s.a., Wasserbillig, Luxembourg) and another weft-knitted fabric (1 thread merino wool 100%, Nm 30/2 (2 threads Nm 30), from Zegna Baruffa, Biella, Italy). The textiles were categorised according to their mass per unit area, thickness and capillary water height. An overview of fabric parameters can be found in Table 1.

These textiles were selected to allow a comparison of materials that differ significantly in their properties to find an indication which textiles are most suitable for a VF application. Another aspect was the reusability of textiles, which should be cleanable after the plants have been removed and reused to cultivate plants again, since their mechanical properties have not substantially changed after the cleaning.

Table 1: Parameters of fabrics used in investigation

Sample number	Composition	Mass per unit area (g/m²)	Thickness (mm)	Capillary rise (cm)	Photograph
1	Weft-knitted merino wool	970	3.84	12.3	
2	PET weft-knitted plush	1020	6.91	2.6	
3	Cotton woven	85	0.22	5.8	
4	Linen woven	142	0.30	8.4	

The mass per unit area was determined according to DIN EN 12127 with an analytical balance SE-202 (VWR International GmbH, Darmstadt, Germany). Thickness was measured according to DIN EN ISO 5084 with a digital gauge J-40-T (Wolf-Messtechnik GmbH, Freiberg, Germany) and capillary rise according to DIN 53924 after 30 min, using 5 specimens per fabric. A digital microscope VHX-600D (Keyence, Neu-Isenburg, Germany) was utilised for the microscopic images of textiles with the roots of plants to see which fabric offers plants optimal growth conditions, e.g. secure attachment of roots in the meshes, pile and through the stitches.

Textiles (60 cm × 20 cm) were attached to a coated metal grid (45 cm in height, 180 cm in width) as shown in Figure 1, which is the same basic structure as in the previous experiment [27]; however, with larger pieces of fabric and a different irrigation rhythm.

The irrigation of textiles with supply water (water hardness level 16 °d, i.e. 16 degrees of hardness) took place every 15 minutes using a pump INDOOR P300-I (3.6 W) (Heissner, Lauterbach, Germany), which reuses dripping water and pumps it from a water reservoir under the textiles to the distribution tube above them. Zip ties allowed the water to exit the tube and to irrigate the grid in a well-directed flow, reducing splashes and thus the waste of water. The flow rate was measured per irrigation hole (cf. Figure 2). In the previous experiment, it was found that although water was distributed slightly unevenly throughout the openings, this had no measurable impact on the plant growth [27]. With this type of irrigation, one of the evaluation criteria

for samples was the water storage capacity according to DIN 53923:1978-01.
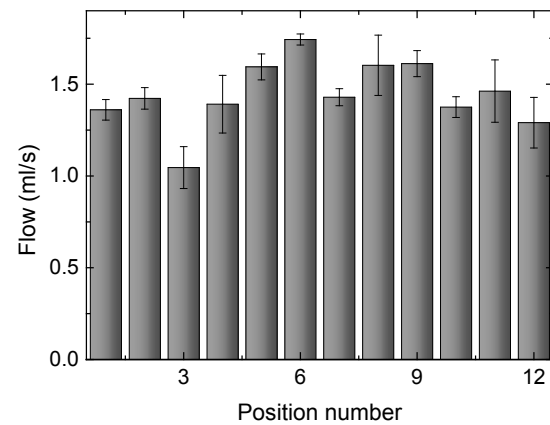
Figure 2: Flow rate through openings; samples were placed in positions 1–3, 4–6 etc. (cf. Figure 1)

Illumination was provided by an Osram lamp with the colour temperature of 3011 K, radiant flux of 6.25 W and luminous flux of 2.02 lm for 16 h per day (6 a.m.–10 p.m.). This lamp was chosen due to its wavelength peaks in the areas of chlorophyll A and B absorption, and its broad spectrum, which has been found to be suitable for plant cultivation in the context of VF [28]. Two of these lamps were placed one above the other in front of the test stand at the distance of 50 cm to illuminate it frontally. The resulting irradiance (in W/m²) was measured with a KIMO SL-200.

The preparation of samples was the same as in the previous test, using a biodegradable Konjac Gum Powder (Special Ingredients, Chesterfield, UK)
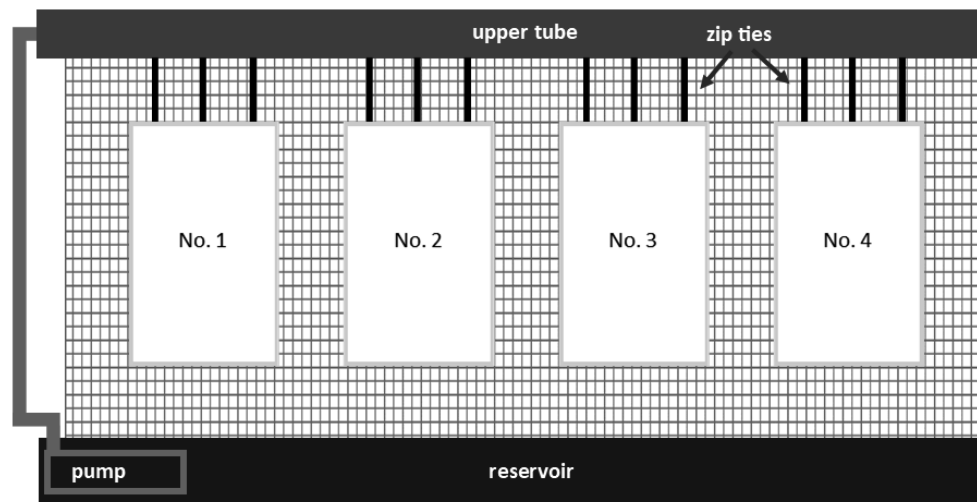
Figure 1: Schematic construction, showing fabrics numbered according to Table 1

hydrogel (2 g Konjac Gum Powder dissolved in 240 ml deionised water) to provide the seeds with a better hold and to prevent them from immediately falling [27]. One side of each textile was completely coated with the hydrogel and then the seeds were attached to the textiles. Subsequently, they were immediately attached vertically to the test stand.

Cress (Lepidium sativum L., Kiepenkerl, Everswinkel, Germany) was again used as a model organism. The reason was the easy handling due to the fast growth and the usability as food and potential for urban greening. On each piece of fabric, the seeds were arranged in 13 homogeneously spaced rows, each containing 5 seeds, i.e. overall 65 seeds per fabric.

In order to be able to make a statement about the quality of plant growth, the fresh mass was determined by cutting the plants above the textile at the end of the test and weighing them directly afterwards. Furthermore, the dry mass was determined to give a better indication of the biomass growth. The dry mass is the pure biomass without water, which is obtained by letting the plants dry in an oven for 48 h at 60 °C.

During the course of the experiment, which lasted over the period of 30 days, the main focus was on the water storage capacity of fabrics and the rooting of plants in the materials, which was investigated subjectively with microscopic images.

3 Results and discussion

The measured irradiance (W/m2) is presented in Figure 3.

The lamp was aligned in such a way that the illumination of fabrics was symmetrically distributed. As already stated in the previous paper [27], the slight varying intensity in the central area does not affect the comparability of plant development on different pieces of fabric as this low level of (varying) irradiance only triggers phototropism and the focus can be placed on the suitability of different textiles for the usage in VF [27, 29].

The suitability of textiles for the application in VF was first evaluated on the basis of lost seeds (cf. Figure 4). The reason for some seeds falling off from the textiles was the rinsing away of the Konjac Gum hydrogel, which inevitably happens after a certain period of time due to its water solubility in combination with late germination of the seeds. A large number of lost seeds on Sample 3 is the indication that, despite the Konjac Gum Powder and formed roots, it was not possible for the roots to adhere to the surface of this fabric. This can clearly be attributed to Sample 3 being the thinnest fabric with the smallest pores between the neighbouring warp and weft threads, which does not enable the plant roots to penetrate through these pores to get fixed. Sample 2 is considered the most suitable regarding the rooting or the adherence of roots to the substrate as the low number of lost seeds (cf. Figure 4) suggests.

It should be mentioned that this is in contrast to Khandaker and Kotzen [20] where a "living wall" with vertically mounted pots was applied, using soil and different substrates, hence showing another way to implement the vertical approach without the danger of losing seeds since the substrates inside these vertically mounted pots were only slightly tilted with respect to the ground and not fully vertical.

Focusing on the amount of germinated and growing plants (cf. Figure 5), Samples 1 and 2 are advantageous, i.e. relatively thick weft-knitted fabrics. Sample 4 had the lowest percentage of grown plants, followed by Sample 3, which can be explained by the poor possibility of rooting in these thin fabrics.

1	2	3	4	5	6	7	8	9	10	11	12	13	14	15
5	7	9	9	10	10	10	10	10	10	10	9	8	6	5
5	7	9	9	10	10	11	10	10	10	11	9	9	7	6
5	7	8	9	9	10	10	10	10	11	10	9	9	6	6
5	6	8	8	8	8	8	10	9	10	9	8	8	6	6
5	5	7	7	7	8	8	8	8	9	8	6	7	5	5

Figure 3: Measured irradiance in W/m²; samples were placed in positions 1–3, 4–6, 7–9 and 10–12.
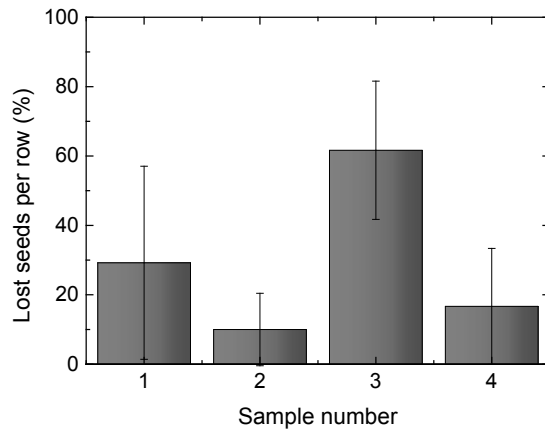
Figure 4: Lost seeds on different samples; error bars show standard deviations, calculated from percentage of lost seeds in each of 13 rows.
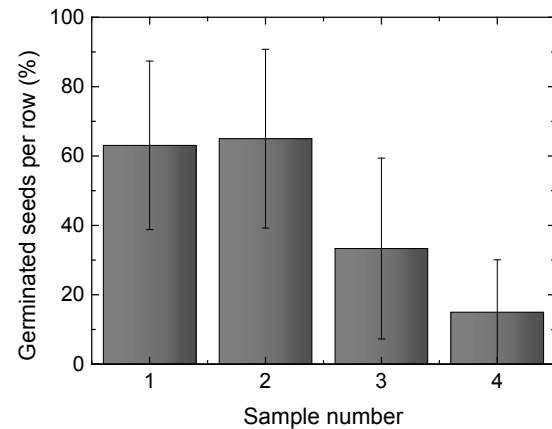
Figure 5: Germinated seeds; error bars show standard deviations, calculated from percentage of lost seeds in each of 13 rows.

It should be mentioned that some of the seeds were stuck on the fabric without germination; therefore, adding the percentages in Figures 3 and 4 does not result in 100%.

When observing the rooting of plants under a microscope, it is noticeable that the roots in Samples 3 and 4 could not find a hold through the interaction with meshes (cf. Figure 6c), but instead developed along the surface with the aid of small root hairs (cf. Figure 6d). Looking at the microscopic pictures of knitted Samples 1 and 2 (cf. Figures 6a, b), a good rooting through the hairy surface and plush threads, respectively, can be seen. In addition, a less intensive formation of root hairs is visible, which
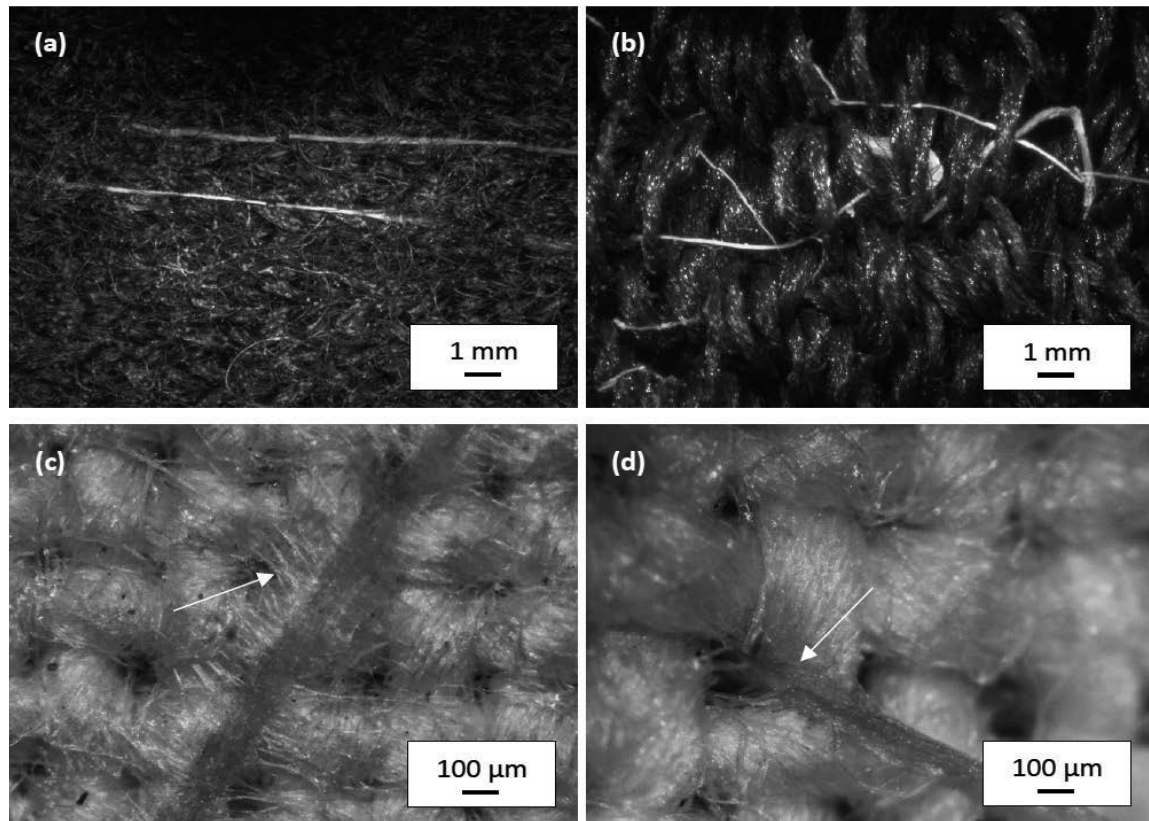
Figure 6: Roots on (a) Sample 1, (b) Sample 2, (c) Sample 3 and (d) Sample 4; arrows indicate root hairs

also supports the thesis that the fixation in the textile is a prerequisite for better plant growth due to the reduced requirement of an intensive root development. Due to a small amount of textile fabrics, it can be assumed that textile substrates should have for successful plant growth high porosity with a hairy surface for the seeds not to fall down before the formation of their germ roots, and to take root in the meshes and the pile without difficulty in further growth. These parameters are interestingly identical to those found for the growth of micro- and macro-algae [30, 31].

The fact that the surfaces of Samples 3 and 4 require a more intensive formation of root hairs to prevent the plant from falling down may result from the plants on Samples 3 and 4 being shorter than those of Samples 1 and 2 (cf. Figure 7).

The latter is also supported by the previous experiment [27] which indicated that the water solubility of the Konjac Gum Powder hydrogel can be problematic if it dissolves before the root could anchor in the textile. This makes a high porosity fabric with large pores or a raised surface the roots can grow easily in more advantageous for the application in VF. Nevertheless, it must be mentioned that the differences among all four samples are not significant, as it is directly visible from the large error bars. Thus, there is only a tendency of plants growing on Samples 1 and 2 to have larger stem lengths.

Another factor that is beneficial in promoting growth is the material's ability to distribute and store water. Samples 1 and 2 have the best water storage properties (cf. Figure 8) and can therefore provide plants with a constant supply of water over a longer period of time. The capillary height, as a measure for water distribution inside the fabric, is less important here due to the irrigation with relatively small spaces between the irrigation holes, so that all fabrics were fully wetted.

The harvested aboveground fresh mass per plant of each textile is shown in Figure 9a. Sample 2 produced the highest yield, which is also reflected in the amount of dry mass (cf. Figure 9b).

Again, a strong difference can be seen between Samples 2 and 4, obtaining by more than 50% less dry mass at Sample 4 compared to Sample 2. However, it must be mentioned again that most differences are not significant, i.e. standard deviations overlap.

Furthermore, while a large number of seeds (65 seeds per sample) was used, especially for Sample 4 where less than 20% germinated (cf. Figure 5), the statistical significance based on standard deviations is lower than it could be expected at first glance.

Finally, it must be mentioned that the results presented here are valid for a certain period during the year (in this case end of July until the end of August in Western Europe) and may be different in other seasons. This effect is well known from indoor plant growth experiments, even inside climate rooms, which is why such experiments are usually repeated subsequently [32–34]. In consequence, the results obtained in this study can only serve to choose textile fabrics for future experiments where objective, time-independent findings can be reported, i.e. for the differentiation between the two thin-woven
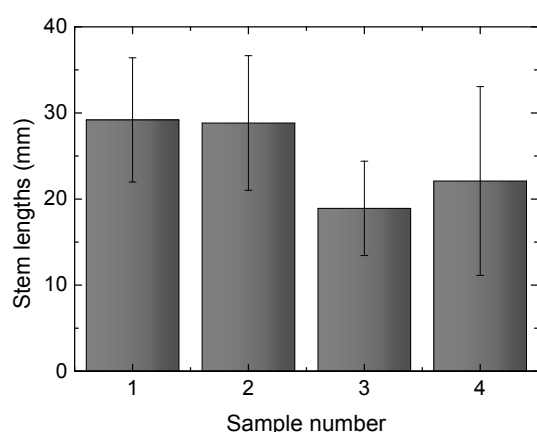
Figure 7: Plant lengths; error bars show standard deviations, calculated from all germinated seeds with grown stems (depending on germination rate, 10–42 plants per sample)
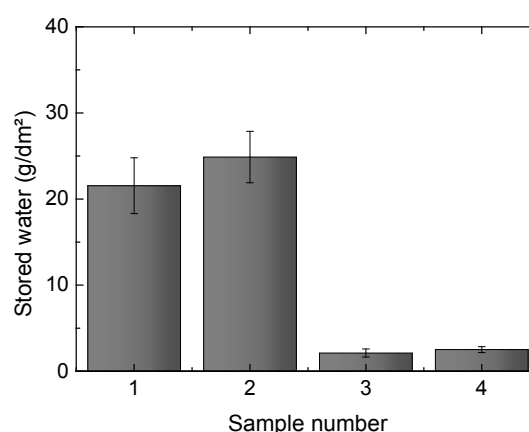
Figure 8: Water storage capacity
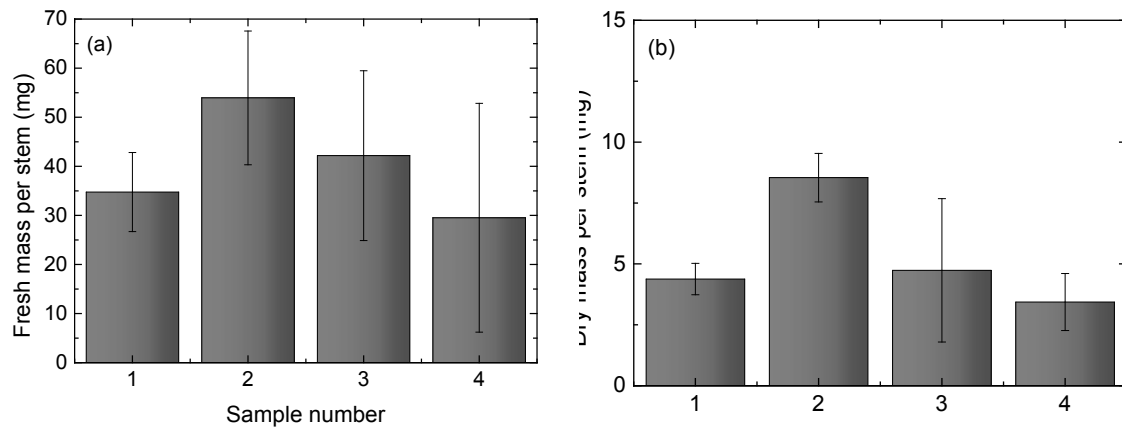
Figure 9: (a) Total aboveground fresh mass per plant, (b) total dry mass per stem; error bars show standard deviations, calculated from all germinated seeds with grown stems.

fabrics (Samples 3 and 4), which are clearly not suitable for root fixation, and different thicker knitted fabrics (Samples 1 and 2) which allowed the penetration by plant roots and will thus be investigated in further studies.

4 Conclusion and outlook

In this experiment, four different fabrics were compared regarding their applicability in vertical farming, i.e. vertically positioned substrates, with cress as a test plant over the course of 30 days.

In general, it was found that textile substrates should have for successful plant growth high porosity with a hairy surface to enable the penetration of roots into the fabric. Furthermore, a correlation between the water absorption capacity and biomass growth can be assumed. Overall, Sample 2 (weft-knitted plush) showed the best combination of good rooting properties, high germination rate, good water storage capacity, and high fresh and dry matter.

For future trials, considering water usage and sustainability, we will investigate these and other relatively thick, open-pore materials with different water-storage properties, and change the duration and frequency of irrigation to see if the amount of used water can be reduced by less frequent irrigation. Additionally, other more agronomically important plants should be in the scope of future research.

References

1. Selected Results of the 2019 UN World Population Projections. *Population and Development Review,* 2019, **45**(3), 689–694, doi: 10.1111/padr.12288.
2. ICKOWITZ, A., POWELL, B., ROWLAND, D., JONES, A., SUNDERLAND, T. Agricultural intensification, dietary diversity, and markets in the global food security narrative. *Global Food Security,* 2019, **20**, 9–16, doi: 10.1016/j.gfs.2018.11.002.
3. HUNTER, Mitchell C., SMITH, Richard G., SCHIPANSKI, Meagan E., ATWOOD, Lesley W., MORTENSEN, David A. Agriculture in 2050: recalibrating targets for sustainable intensification. *BioScience*, 2017, **67**(4), 386–391, doi: 10.1093/biosci/bix010.
4. TOULIATOS, Dionysios, DODD, Ian C., MCAINSH, Martin. Vertical farming increases

lettuce yield per unit area compared to conventional horizontal hydroponics. *Food Energy Security*, 2016, **5**(3), 184–191, doi:10.1002/fes3.83.

5. TILMAN, David, BALZER, Christian, HILL, Jason, BEFORT, Belinda L. Global food demand and the sustainable intensification of agriculture. *Proceedings of the National Academy of Sciences*, 2011, **108**(50), 20260–20264, doi: 10.1073/pnas.1116437108.
6. ZHANG, Xioa, CAI, Ximing. Climate change impacts on global agricultural land availability. *Environmental Research Letter,* 2011, **6**, 014014, doi: 10.1088/1748-9326/6/1/014014.
7. KALANTARI, Fatemeh, NOCHIAN, Ashkan, DARKHANI, Faiza, ASIF, Nayeem. The significance of vertical farming concept in ensuring food security for high-density urban areas. *Jurnal Kejuruteraan*, 2020, **32**(1), 105–111, doi: 10.17576/jkukm-2020-32(1)-13.
8. AVGOUSTAKI, Dafni Despoina, XYDIS, George. Indoor vertical farming in the urban nexus context: business growth and resource savings. *Sustainability*, 2020, **12**(5), 1965, doi: 10.3390/su12051965.
9. FAO [accessible online]. Nutrition-sensitive agriculture and food systems in practice. 2017. [accessed 8.10.2021]. Available on World Wide Web: <http://www.fao.org/publications/card/en/c/9ca3cf89-6109-4a38-855f-6e218eae543b/>
10. MANOS, Dimitrios-Panagiotis, XYDIS, George. Hydroponics: are we moving towards that direction only because of the environment? A discussion on forecasting and a systems review. *Environmental Science and Pollution Research*, 2019, **26**, 12662–12672, doi: 10.1007/s11356-019-04933-5.
11. PANDEY, Divya, AGRAWAL, Madhoolika, PANDEY, Jai Shanker. Carbon footprint: current methods of estimation. *Environmental Monitoring and Assessment*, 2011, **178**(1-4), 135–160, doi: 10.1007/s10661-010-1678-y.
12. JALETA, Olani Ganfure, JEBESSA DEBELLA, Habte. The impact of large scale agriculture on forest and wildlife in Diga Woreda, Western Ethiopia. *Asian Journal of Agriculture*, 2017, **1**(02), 100–113, doi: 10.13057/asianjagric/g010207.
13. GRUÈRE, Guillaume, LE BOËDEC, Hélène. Navigating pathways to reform water policies in agriculture. *OECD Food, Agriculture and Fisheries Papers*, 2019, **128**, 63 p., doi: 10.1787/906cea2b-en.
14. DESPOMMIER, Dickson D. The vertical farm: Controlled environment agriculture carried out in tall buildings would create greater food safety and security for large urban populations. *Journal für Verbraucherschutz und Lebensmittelsicherheit*, 2011, **6**(2), 233–236, doi: 10.1007/s00003-010-0654-3.
15. PENNISI, Giuseppina, ORSINI, Francesco, BLASIOLI, Sonia, CELLINI, Antonio, CREPALDI, Andrea, BRASCHI, Ilaria, SPINELLI, Francesco, NICOLA, Silvana, FERNANDEZ, Juan A., STANGHELLINI, Cecilia, GIANQUINTO, Giorgio, MARCELIS, L. F. M. Resource use efficiency of indoor lettuce (*Lactuca sativa L.*) cultivation as affected by red:blue ratio provided by LED lighting. *Scientific Reports*, 2019, **9**(1), doi: 10.1038/s41598-019-50783-z.
16. MOLIN, Elvira, MARTIN, Michael Alan. Assessing the energy and environmental performance of vertical hydroponic farming. Report number: C299.IVL. Swedish Environmental Research Institute, 2018. Available online: <https://www.researchgate.net/publication/324088096_Assessing_the_energy_and_environmental_performance_of_vertical_hydroponic_farming>.
17. TOULIATOS, Dionysios, BREYNON-DAVIES, Rhydian, MCAINSH, Martin. Vertical farming. *eLS*, 2020, 1–8, doi: 10.1002/9780470015902.a0028908.
18. SHARATHKUMAR, Malleshaiah, HEUVELINK, Ep, MARCELIS, Leo F.M. Vertical farming: moving from genetic to environmental modification. *Trends in Plant Science*, 2020, **25**(8), 724–727, doi: 10.1016/j.tplants.2020.05.012.
19. KALANTARI, Fatemeh, TAHIR, Osman Mohd, JONI, Raheleh Akbari, FATEMI, Ezaz. Opportunities and challenges in sustainability of vertical farming: a review. *Journal of Landscape Ecology*, 2018, **11**(1), 35–60, doi: 10.1515/jlecol-2017-0016.
20. KHANDAKER, Mohammed, KOTZEN, Benz. The potential for combining living wall and vertical farming systems with aquaponics with special emphasis on substrates. *Aquaculture Research*, 2018, **49**(2), 1454–1468, doi: 10.1111/are.13601.
21. FERNÁNDEZ-CAÑERO, Rafael, URRESTARAZU, Luis Pérez, PERINI, Katia. Vertical greening systems: classifications, plant species, substrates. In *Nature Based*

Strategies for Urban and Building Sustainability. Edited by Gabriel PÉREZ and Katia PERINI. Elsevier, 2018, pp. 45–54, doi: 10.1016/B978-0-12-812150-4.00004-5.

22. EHRMANN, Andrea. On the possible use of textile fabrics for vertical farming. *Tekstilec*, 2019, **62**(1), 34–41, doi: 10.14502/tekstilec2019.62.34-41.

23. CHOWDHURY, Md Jonayet, NASRIN, Shamima, AL FARUQUE, Md Abdullah. Significance of agro-textiles and future prospects in Bangladesh. *European Scientific Journal*, 2017, **13**(21), 1857–7881, doi: 10.19044/esj.2017.v13n21p139.

24. ABIDI, Houcine, RANA, Sohel, CHAOUCH, Walid, AZOUZ, Bechir, AISSA, Imed Ben, HASSEN, Mohamed Ben, FANGUEIRO, Raul. Accelerated Weathering of textile waste nonwovens used as sustainable agricultural mulching. *Journal of Industrial Textiles*, 2019, **50**(7), 1079–1110, doi: 10.1177/1528083719855326.

25. BHAVANI, K., MALLIKARJUN, Ningdalli, SUNILKUMAR, N.M. Agro textiles - their applications in agriculture and scope for utilizing natural fibers in agro tech sector. *International Journal of Applied Home Science*, 2017, **4**(7&8), 653–662.

26. STORCK, Jan Lukas, BÖTTJER, Robin, VAHLE, Dominik, BROCKHAGEN, Bennet, GROTHE, Timo, DIETZ, Karl-Josef, RATTENHOLL, Anke, GUDERMANN, Frank, EHRMANN, Andrea. Seed germination and seedling growth on knitted fabrics as new substrates for hydroponic systems. *Horticulturae*, 2019, **5**(4), 1–9, doi: 10.3390/horticulturae5040073.

27. BÖTTJER, Robin, STORCK, Jan Lukas, VAHLE, Dominik, BROCKHAGEN, Bennet, GROTHE, Timo, HERBST, Sabine, DIETZ, Karl-Josef, RATTENHOLL, Anke, GUDERMANN, Frank, EHRMANN, Andrea. Influence of textile and environmental parameters on plant growth on vertically mounted knitted fabrics. *Tekstilec*, 2019, **62**(3), 200–207, doi: 10.14502/Tekstilec2019.62.200-207.

28. HICKEM, Taylor, O'MARA, Colin. THE FOOD WALL - open source engineering design software for vertical farming greenhouse. *HELVA PTE,* 2019. Available online: https://www.research-gate.net/publication/335543711_THE_FOOD_WALL_Open_source_Engineering_Design_Software_for_Vertical_Farming_Greenhouse.

29. CHRISTIE, John Mackie. Phototropin blue-light receptors. *Annual Review of Plant Biology*, 2007, **58**(1), 21–45, doi: 10.1146/annurev.arplant.58.032806.103951.

30. BROCKHAGEN, Bennet, STORCK, Jan Lukas, GROTHE, Timo, BÖTTJER, Robin, EHRMANN, Andrea. Improved growth and harvesting of microalgae *Chlorella vulgaris* on textile fabrics as 2.5D substrates. *AIMS Bioengineering*, 2021, **8**(1), 16–24, doi: 10.3934/bioeng.2021003.

31. SEBÖK, Stefan, BROCKHAGEN, Bennet, STORCK, Jan Lukas, POST, Inken Blanca, BACHE, Thorsten, KORCHEV, Rumen, BÖTTJER, Robin, GROTHE, Timo, EHRMANN, Andrea. Growth of marine macroalgae *Ectocarpus sp.* on various textile substrates. *Environmental Technology*, 2020, online first, doi: 10.1080/09593330.2020.1829086.

32. HORLING, Frank, LAMKEMEYER, Petra, KÖNIG, Janine, FINKEMEIER, Iris, KANDLBINDER, Andrea, BAIER, Margarete, DIETZ, Karl-Josef. Divergent light-, ascorbate-, and oxidative stress-dependent regulation of expression of the peroxiredoxin gene family in Arabidopsis. *Plant Physiology*, 2003, **131**(1), 317–325, doi: 10.1104/pp.010017.

33. POORTER, Hendrik, FIORANI, Fabio, STITT, Mark, SCHURR, Uli, FINCK, Alex, GIBON, Yves, USADEL, Björn, MUNNS, Rana, ATKIN, Owen K., TARDIEU, Francois, PONS, Thijs L. The art of growing plants for experimental purposes: a practical guide for the plant biologist. *Functional Plant Biology*, 2012, **39**(11), 821–838, doi: 10.1071/FP12028.

34. POORTER, Hendrik, FIORANI, Fabio, PIERUSCHKA, Roland, WOJCIECHOWSKI, Tobias, VAN DER PUTTEN, Wim H., KLEYER, Michael, SCHURR, Uli, POSTMA, Johannes. Pampered inside, pestered outside? Differences and similarities between plants growing in controlled conditions and in the field. *New Phytologist,* 2016, **212**(4), 838–855, doi: 10.1111/nph.14243.

Aleksandra Micic [1], Ivanka Ristic [2], Suzana Djordjevic [2], Nebojsa Ristic [2], Dragan Djordjevic [1]
[1] University of Nis, Faculty of Technology, Bulevar oslobodjenja 124, 16 000 Leskovac, Serbia
[2] Academy of Vocational Studies Southern Serbia, Department of Technological Art Studies, Vilema Pušmana 17, Leskovac, Serbia

Adsorbent from Textile Waste for Removal of Textile Reactive Dye from Water – Equilibrium Adsorption and Kinetics

Adsorbent iz tekstilnih odpadkov za odstranjevanje tekstilnega reaktivnega barvila iz vode –adsorpcijsko ravnotežje in kinetika

Corresponding author/*Korespondenčni avtor:*
Prof dr. Dragan Djordjevic
Phone: ++381 1 62 47 203
E-mail: drag_64@yahoo.com
ORCID ID: 0000-0002-8223-9474

Abstract

The removal of textile reactive dye from an aqueous solution on a new adsorbent prepared from waste cotton knitted fabric was investigated in this study. Waste cotton textile, used for the production of adsorbents, is a by-product of the cutting of stacked parts of cotton knitwear planned for the production of women's T-shirts. The degree of efficiency of a paper pattern determines the amount of collected waste. The qualitative and quantitative characterization of the new adsorbent showed carbon and oxygen to be dominant in the chemical composition. A longer contact time means a greater amount of dye on the adsorbent, i.e. the dye concentration in the solution decreases with the duration of the adsorption process. The percentage of removed dye decreases with an increase in the initial dye concentration in the solution. However, the actual amount of adsorbed dye increases as the initial dye concentration increases. The results for equilibrium adsorption show that the Langmuir isotherm can be used for the interpretation of reactive dye adsorption on a new adsorbent. The pseudo-first order model can be fully used to describe the kinetics of dye adsorption on an adsorbent, with respect to valid results for statistical indicators. Based on the results, it can be concluded that the new adsorbent obtained from waste textiles has the potential to remove textile reactive dye from aqueous solutions.
Keywords: cotton knitted fabric, cutting, adsorbent, reactive dye, the Langmuir model, kinetics

Izvleček

V članku je bila raziskana odstranitev tekstilnega reaktivnega barvila iz vodne raztopine s pomočjo novega adsorbenta, pripravljenega iz odpadnega bombažnega pletiva. Uporabljena odpadna tekstilija je bila stranski proizvod krojenja bombažnega pletiva, položenega v plasti za izdelavo ženskih kratkih majic, pri čemer izkoristek papirnatega kroja določa količino zbranega odpadka. Kvalitativna in kvantitativna karakterizacija novega adsorbenta kaže, da sta v kemični sestavi prevladujoča elementa ogljik in kisik. Daljši kontaktni čas pomeni večjo količino barvila na adsorbentu, torej se s časom trajanja procesa adsorpcije koncentracija barvila v raztopini zmanjšuje. Odstotek odstranjenega barvila se zmanjšuje s povečevanjem začetne koncentracije barvila v raztopini, vendar se dejanska količina adsorbiranega barvila

z naraščanjem začetne koncentracije barvila poveča. Rezultati adsorpcijskega ravnotežja kažejo, da se Langmuirjeva izoterma lahko uporabi za interpretacijo adsorpcije reaktivnega barvila na novem adsorbentu. Model psevdoprvega reda se lahko v celoti uporabi za opis kinetike adsorpcije barvila na adsorbentu glede na veljavne rezultate statističnih kazalnikov. Na podlagi rezultatov lahko sklepamo, da ima novi adsorbent, pridobljen iz odpadnega tekstila, potencial odstranjevanja tekstilnih reaktivnih barvil iz vodnih raztopin.

Ključne besede: bombažno pletivo, krojenje, adsorbent, reaktivno barvilo, Langmuirjev model, kinetika

1 Introduction

The textile industry consumes an extensive amount of synthetic dyes. The aim is to use dyes that are more exhausted from the bath during dyeing, as well as those that are more degradable and environmentally friendly, or that can be more easily removed from water after textile dyeing [1, 2].

Reactive dyes belong to the class of very successful modern synthetic dyes thanks to their wide range of shades, flexibility in application and excellent fastness properties, particularly when wool, silk and cotton, as well as regenerated cellulose fibres, are dyed. These dyes contain certain groups capable of forming covalent bonds with nucleophilic sites on the fibre, which is an assumption of the extraordinary properties of colour fastness in terms of washing. Reactive dyes for wool are considered alternatives to chrome dyes. Certain classes of reactive dyes have a positive effect on the amount of damage to wool during dyeing at the boiling point [3].

After textile dyeing of natural or artificial origin, waste water from the textile industry is inevitably dyed, as it contains a higher or lower amount of organic dye residues. One of the methods for removal of organic matters from dyed water is the use of porous solid sorbents. The properties of these substances that make them useful are high porosity and their surface, as well as the physical and chemical nature of the inner surface. Such and similar adsorbents, e.g. activated carbon, are most frequently used in separation and purification processes. Research aimed at finding alternative adsorbents that could replace expensive activated carbon have intensified recently.

Industrial waste materials are potentially inexpensive adsorbents for removing organic matter from water. To date, researchers have used various waste materials of cellulose origin, e.g. agricultural or agro-industrial waste of cellulose origin, such as barley straw, rice husks, cotton stalks, the pits of various fruits and vegetables, etc. There was no example of the use of waste from a garment plant for the production of active adsorbent that would be used for the adsorption of waste reactive dye from aqueous solutions [2, 4–6]. If other types of dye and a similar adsorbent are taken into account, there are studies that describe, for example, the adsorption processes of methylene blue (basic thiazine dye) on an adsorbent of cotton stalk, cotton waste fibres and cotton dust [7, 8]. It has been observed that these types of adsorbents can be successfully used to remove methylene blue from aqueous solutions using the sorption technique. Sorption increases by increasing the initial dye concentration, temperature, sorbent dose and solution pH. The time required for maximum dye removal was 90 minutes. Maximum dye removal of up to 97.50% was achieved in all tested experimental conditions [7, 8].

The research presented in this paper uses precisely that waste material which thus far has typically been incinerated or disposed of in a landfill. This research proposes a new way of disposing of this waste, turning it into a useful product for the purification of coloured water. The aim is to use the resulting waste textile material, transform it into an adsorbent and use it for the removal of colour from water. Applying the equilibrium isotherm and the adsorption kinetics of textile dye has led to significant knowledge about the adsorption mechanism and feasibility of the decolorization process of aqueous solution.

2 Experimental

2.1 Materials

An adsorbent is made of the waste textiles from cotton knitted fabric after the cutting process in the manufacture of women's T-shirts. It is a by-product obtained from the cutting of the stacked parts of cotton knitted fabric during the clothing manufacture process. The raw material for the production of adsorbent was collected from a professional workshop. The amount of raw material waste was about

6 kg per one cutting of a multilayer stacked textile knitted fabric.

Since the waste cotton material was collected from the cutting of the cut parts of the future garment, the construction preparation of the women's T-shirt was monitored using a Gerber Technology computer software system. The optimal width of the basic material (140, 145 and 152 cm) was selected on the basis of the use of the paper pattern made using a CAD system during the production of the selected model of the women's T-shirt.

Knitted fabric made of 100% cotton fibres was used to make the selected model of a women's T-shirt with raglan sleeves. Table 1 shows the basic characteristics of the material (knitted fabric) that was used to make women's T-shirt as the by-product of cutting.

Table 1: Basic characteristics of knitted fabric for women's T-shirt production

Properties	Description/values
Raw material composition	Cotton, 100%
Colour	White
Weaving	Double knit plated
Horizontal density (1/cm)	14.6
Vertical density (1/cm)	20.5
Fineness of yarn (tex)	18
Surface mass (g/m²)	165

The new adsorbent was obtained through the chemical and physical modification of cotton waste. After its collection, the waste was washed (distilled water, bath ratio 1 : 100, 60 minutes at 90 °C), dried and cut into pieces as small as possible. Such a prepared waste was treated with a solution of H_3PO_4

(Oleohemija, Serbia, 85%, ratio 1:4) for 48 hours at room temperature. After decantation, the samples were heated at 600 °C for 2 hours. Cooling and shredding followed, then rinsing with distilled water and neutralization with an aqueous solution of sodium carbonate (Tehnohemija, Serbia). Finally, the drying (100 °C) and grinding of the material was performed, and samples were prepared for adsorption.

2.2 Adsorption process

An adsorption model test was performed in reaction vessels in which the adsorbent was suspended in a reactive dye solution (adsorbate). The reaction vessels were placed on a shaker (130 rpm) at a temperature of 20 °C and maintained for some time. The amount of adsorbent was fixed at 2 g, whereas the solution in a constant amount of 0.1 dm^3 contained a reactive dye concentration of 30, 50, 75, 100, 125 and 150 mg/dm^3. Processing time was 5, 10, 20, 30, 40, 50 and 60 minutes. The pH for all dye solution was 3.

The reactive dye used, CI Reactive Red 84 (RR84), belongs to the group of monoazo dyes with two sulfo groups and one amino. The structure comprises sulfonyldibenzen, naphthalene and bromoacrylamide part. The dye is water-soluble, and is used for the dyeing and printing of wool and silk fabrics.

2.3 Analyses and measurements

Solution absorption was measured on a UV-VIS spectrophotometer (Cary 100 Conc UV-VIS, Varian) at λ = 490 nm (the maximum wavelength of the spectrum of the used dye solution). The moisture content in the sorbent was determined according to the SRPS EN ISO 18134 standard. The ash content in the sorbent was determined according
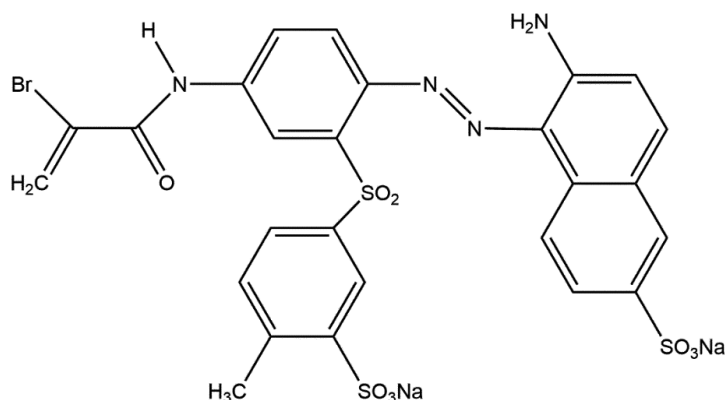
Figure 1: Structure of the used reactive RR84 dye

to the SRPS ISO 5984 standard. The density of the sorbent by pycnometer was determined according to the SRPS EN ISO 2811-1 standard. SEM and EDS measurements were performed on a TESCAN MIRA3 microscope. The samples were applied to an adhesive graphite strip and fixed to the supports, and then ion-coated with a thin layer of gold using a PO-LARON SC502 Sputter Coater.

The degree of dye removal [5] or degree of exhaustion was calculated on the basis of the dye concentration before and after this treatment:

$$E = \frac{C_0 - C_{t,e}}{C_o} \cdot 100 \tag{1}$$

where: C_0 and $C_{t,e}$ (mg/dm³) represent the initial and final (equilibrium) concentration of the dye solution, respectively.

The amount of adsorbed dye (adsorbate) per unit mass of adsorbent [9] at time t, q_t (mg/g), or equilibrium time, q_e, (mg/g), was determined using the equation:

$$q_{t,e} = \frac{(C_0 - C_{t,e}) \cdot V}{M} \tag{2}$$

wherein: M (g) represents the mass of adsorbent and V (dm³) represents the volume of solution from which the adsorption was performed.

The *Langmuir* isotherm [4] is presented using following equation:

$$\frac{1}{q_e} = \left[\frac{1}{b \cdot Q_0}\right] \cdot \frac{1}{C_e} + \frac{1}{Q_0} \tag{3}$$

where: Q_0 (mg/g) represents the maximum amount of adsorbate that can bind to the adsorbent and b (dm³/mg) represents the ratio of the adsorption rate constant and the adsorbate desorption rate constant.

Adsorption kinetics data are described using the *Lagergren* model [9] of pseudo-first order:

$$\log(q_e - q_t) = \log(q_e) - \frac{k_1}{2.303} \cdot t \tag{4}$$

where k_1 (1/min) represents the rate constant of adsorption *pseudo-first* order.

The adsorption kinetics can also be described using the *pseudo-second* order model [9]:

$$\frac{t}{q_t} = \frac{1}{k_2 \cdot q_e^2} + \frac{1}{q_e} \cdot t \tag{5}$$

where k_2 (g/mgmin) represents the adsorption rate constant of the *pseudo-second* order.

3 Results and discussion

3.1 Origin of textile waste

Figure 2 is a graph showing the efficiency of paper patterns in the manufacture of women's T-shirts, resulting in waste used to create a new adsorbent for the adsorption of reactive dyes. All paper patterns show the expected efficiency obtained when fitting the cutting parts. On the basis of these results, the paper pattern with a width of 152 cm had the highest material efficiency (85.82%) in relation to the other widths, due to more suitable combinations of cutting parts.
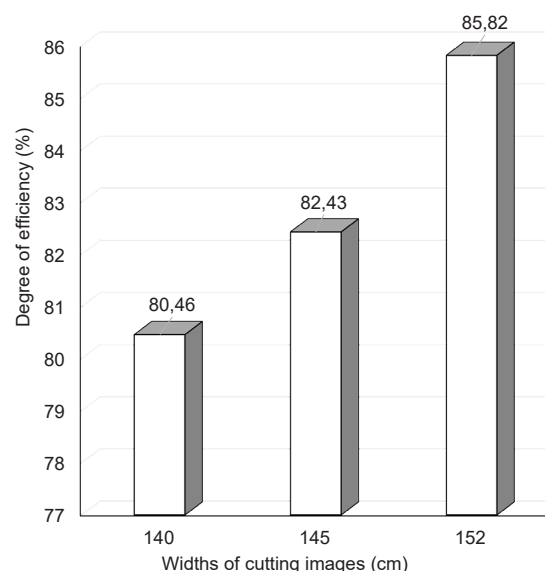
Figure 2: Graphic representation of the degree of efficiency of paper patterns with respect to their widths

3.2 Adsorbent characterization

The characterization of the absorbent was performed for the purposes of the representation of physical properties, as well as the introduction of morphological characteristics, or the actual chemical structure, as a very important factor for successful adsorption.

The determination of yield, density, ash content, moisture, etc. are techniques that provide information regarding the structure of the tested samples, but also regarding their reactivity and the possibility of application in appropriate conditions.

The loss after washing of raw cotton waste, before transformation into an adsorbent, was approximately 8% in relation to the sample of waste before washing. The yield of adsorbent from waste cotton textiles was approximately 42%.

The moisture content of the new adsorbent was 7.8%. The presence of moisture affected the activity in adsorption processes. Namely, the moisture that was largely adsorbed in the structure of the adsorbent obtained from waste textiles blocks the pores of the material, making them inaccessible to dye ions from the solution. The consequence of this effect was a decrease in the adsorption capacity towards the dye ions that were adsorbed from the solution into the porous structure of the adsorbent.

The ash content in the adsorbent may indicate a conversion pathway from the used precursor-waste cellulose textile. Typically, a powder adsorbent with high values of ash content show weaker adsorption power with respect to different adsorbates. The proportion of ash in the structure of the new adsorbent was 6%. The amount of ash was moderate, in this case, so there would be no obstacles to good sorption characteristics of the adsorbent in the processing of dyed water.

The determination of adsorbent particle density, including pore volume within the particles, was performed using a pycnometer. The new adsorbent had a density of 1.2 g/cm^3. Density values of the adsorbent were in a range typical for materials from cellulosic raw materials. Density is an important property of powder materials and illustrates porosity and the way the particles are packed in space. Porous materials with lower density have more air trapped in the structure.

The used adsorbent is a granular material with heterogeneous porous particles of divergent shape and form. Cracks, cavities and channels are present in the depth of the particles that are the basis of the porosity of the material. The micrograph in Figure 3 shows the appearance of adsorbent particles at a magnification of 2000x.

The EDS system enables a quick assessment of the elementary composition of the sample. The following chemical elements were detected: C (41.87%), O (54.34%) and Na (3.79%). According to the EDS analysis, there was carbon, as expected, while the increased presence of oxygen related to the oxides of metals (Na), while an adsorbent might have reacted with oxygen from the air during the annealing process.
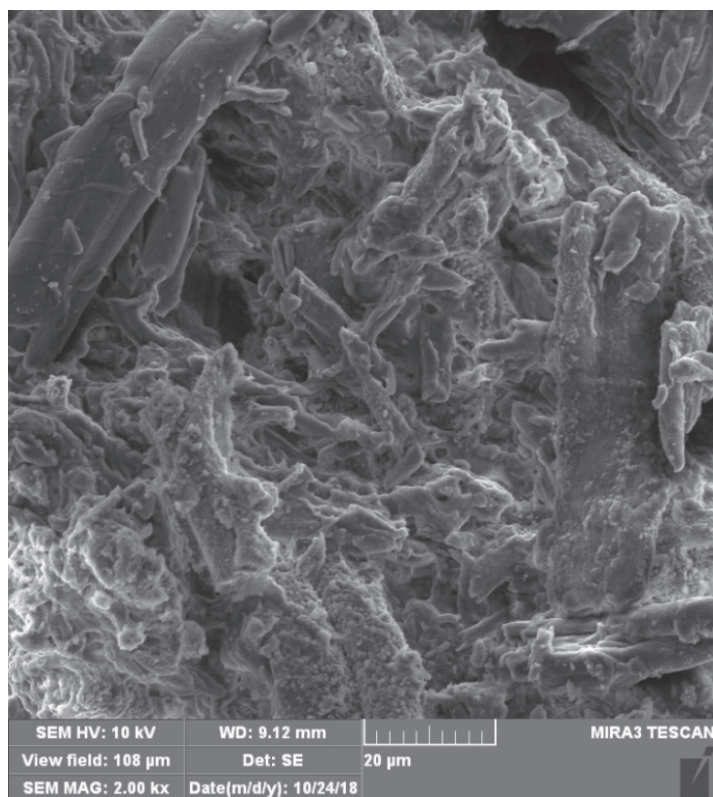
Figure 3: SEM micrograph of the applied adsorbent form textile waste

A similar morphology and chemical composition were seen in research [10] that deals with the preparation of cheaper and environmentally friendly adsorbents from biomass, with the use of phosphoric acid as the activator. Via SEM and EDXA spectra, the existence of the porous structure was asserted, as well as the presence of carbon and oxygen, which were dominant amongst chemical elements. The presence of potassium, sodium and phosphorus was negligible.

The selected RR84 dye has good solubility with respect to the existence of two sulfo groups, and shows a good affinity to the adsorbent in contact, given that there is no greater affinity towards the aqueous phase. The present sulfo groups represent a negative characteristic of this dye, whereas an amino group increases reactivity in the aromatic ring due to the electron donor [11].

It is known that adsorption from a solution towards a solid surface begins to occur when dipoles or charged types of adsorbent and adsorbate interact with each other. Also, the exchange of anions or cations occurs when the neutral molecules get close enough to each other. Similarly, an interaction occurs between the dissolved organic components

(dyes), the molecule of the solvent (water) and the surface of the adsorbent [12].

3.3 Influence of certain factors on adsorption

The influence of the time of adsorption on the exhaustion of the RR84 dye was tested in a concentration range of 30–150 mg/dm³ (Figure 4). As time increases, the initial dye concentration decreases in all cases. The initial dye concentration in the solution provides an important driving force for overcoming the mass transfer resistance between the aqueous and solid phases.

According to the curves in the graph presented in Figure 4, the higher initial dye concentrations of RR84 declined slightly more over time, while lower initial concentrations showed a more moderate change over time. All curves in the graph have a similar appearance of change over time, which shows similar or identical mechanisms of adsorption of dye molecules on the outer surfaces and inside the adsorbent particles.

Figure 5 presents a graph that explains the change in the level of exhaustion of RR84 dye relative to the duration of adsorption. The highest percentage of dye exhaustion occurs at the lowest initial dye
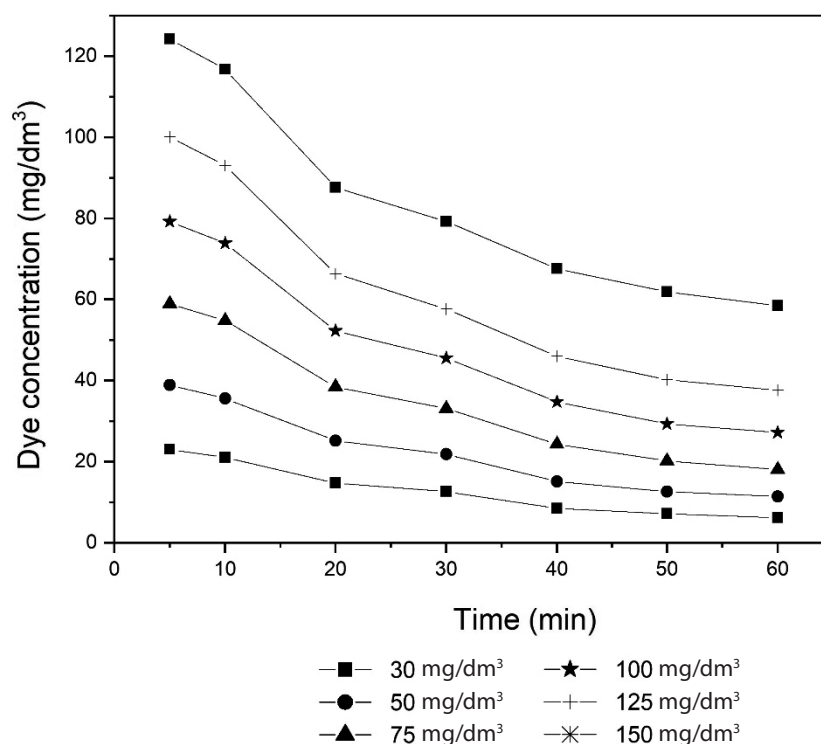
Figure 4: Change of the initial dye concentration of RR84 during adsorption
to a new adsorbent for different initial concentrations
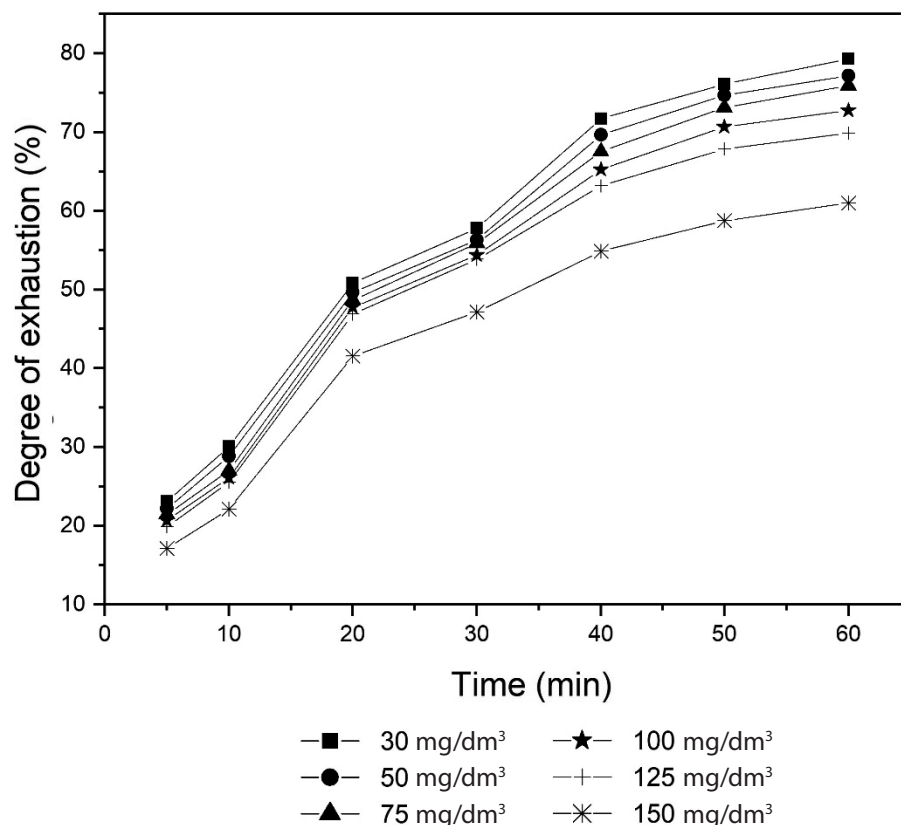
*Figure 5: Degree of exhaustion of RR84 dye during adsorption
to a new adsorbent for different initial concentrations*

concentrations, while the lowest percentage is present at the highest initial concentrations. All curves demonstrate an upward trend. On the other hand, the largest amount of the adsorbed dye from the aqueous solution in absolute terms, is found with the highest initial concentrations.

Thus, for example, in equilibrium (after 60 minutes):
- at the highest initial concentration (150 mg/dm³), the degree of exhaustion was 61% or 91.5 mg in absolute terms; and
- at the lowest initial concentration (30 mg/dm³), the degree of exhaustion was 79.33% or 23.8 mg in absolute terms.
- There was thus almost four times more of the adsorbed dye to the new sorbent (91.5 mg >> 23.8 mg) at the highest initial concentration, although a lower percentage of the degree of exhaustion occurred here (61% < 79.33%).

Similar results are shown by a study of the adsorption potential of rice husk and alkali-treated rice husk to remove yellow reactive dye from an aqueous solution. The highest adsorption was achieved after 40 minutes and did not change after that time. The first adsorbent was found to remove 65% of the dye within 40 minutes compared to the second which removed 92% [5].

The graph in Figure 6 shows the change in the adsorbed amount of dye per unit mass of adsorbent during adsorption (adsorption capacity) for different initial dye concentrations of RR84. The graph confirms that the amount of adsorbed dye increases relative to the duration of adsorption, and that the highest adsorption was observed at the highest initial concentrations. Since the curves have a similar appearance in the graph, it is assumed that the mechanism of adsorption at all initial concentrations is identical.

Similar behaviour in terms of the degree of exhaustion of the reactive dye (Bezaktiv Red S-Maks) was seen in a study [6] that estimated the different activated carbon prepared from by-products from agricultural waste. It was observed that adsorption was more rapid during the initial phase of the adsorption process, followed by a slower stage until equilibrium was reached. This phenomenon was due a large number of free positions exposed to
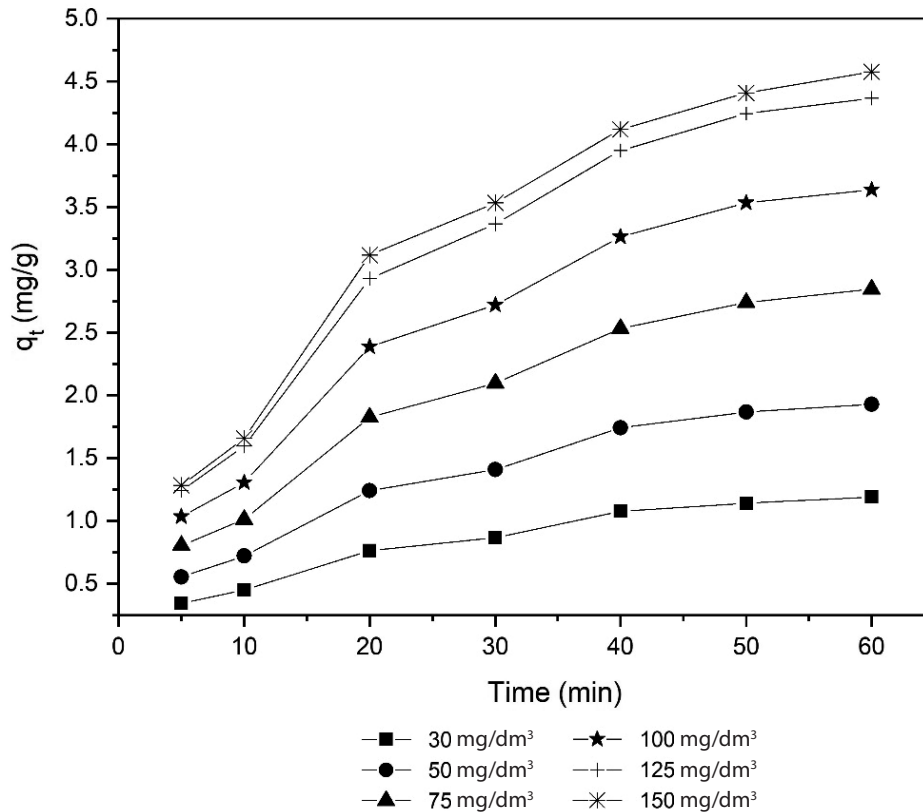
Figure 6: Change of adsorption capacity of RR84 dye during adsorption on a new adsorbent for different initial concentrations

adsorption in the initial phase, which made the taking of the remaining places on the surface harder because of the refusal between the adsorbate and adsorbent.

3.4 Adsorption izotherms

The graph in Figure 7 represents the linear interpretation of the *Langmuir* adsorption isotherm, showing the dependency of the parameter ($1/q_s$) in relation to the equilibrium dye concentration ($1/C_s$). The values of the *Langmuir* constants were determined from this graph, i.e. the slope and cut of the functional line.

The significant functionality of this parameter was observed from this graph, i.e. the fitting curve perfectly covers the experimental points. It can thus be concluded that the *Langmuir* adsorption isotherm can be used for the analysis of this specific case of RR84 dye adsorption onto the adsorbent.

The *Langmuir* constants Q_0 and b represent to the maximum amount of adsorbate that can bind to the adsorbent and the free adsorption energy, respectively. The values of these constants were 8.35 mg/g

and 0.027 dm³/mg, respectively. In this particular case, the *Langmuir* model had a very high value of R^2, which was 0.997.

The features of the *Langmuir* isotherm can be expressed in dimensionless constant, equilibrium parameter R_L. In the specific case of $R_L = 0.2$, it was confirmed that the applied *Langmuir* isotherm was suitable since the equilibrium parameter was between 0 and 1.

Similarly, in other research, [10] the application of cheaper and more environmentally friendly adsorbents from biomass for the needs of purification of reactive dye (Reactive red 23) from aqueous solution confirmed the dominance of the *Langmuir* model after comparison with the four most frequently used equilibrium adsorption models.

3.5 Adsorption kinetics

According to the linear forms of kinetic model in Figure 8, it can be concluded that the rate of adsorption, in the presented experimental conditions, can be functionally described in full by the *pseudo-first* order.
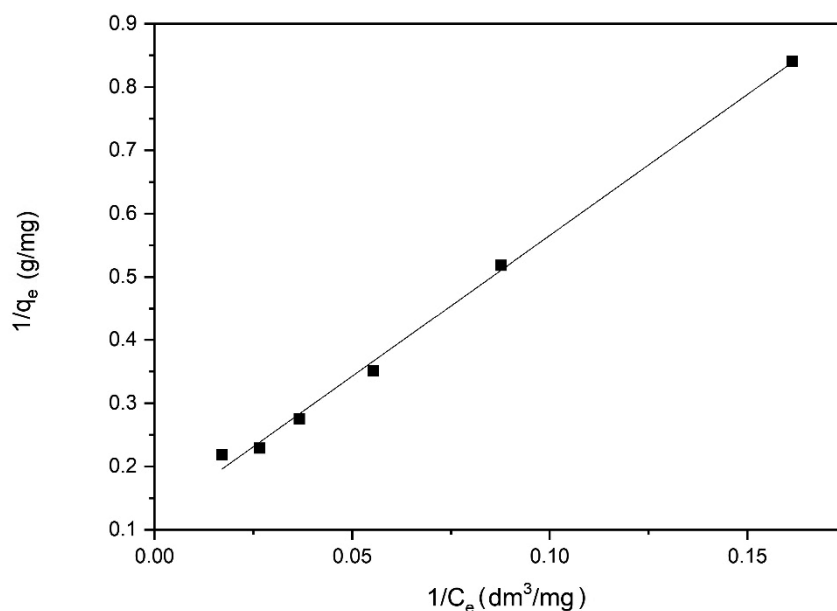
Figure 7: Modelling of RR84 dye adsorption on new adsorbent using the Langmuir model
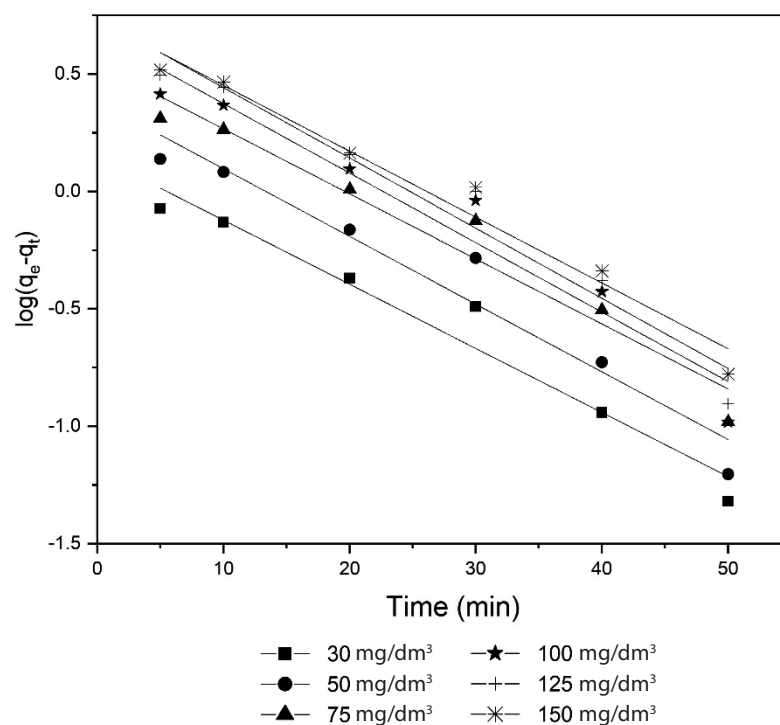
Figure 8: Kinetic curves of RR84 dye adsorption on a new adsorbent according to the pseudo-first order model

Thus, according to the appearance of curves on this graph, as well as the positions of the experimental points around the ideal fitting curves, it was determined that the kinetic adsorption of RR84 dye on the adsorbent from cotton textiles, obtained from waste after cutting of cotton knitted fabric, is perfectly described by the *pseudo-first* order model.

Table 2 presents the value of the kinetic parameter of the RR84 dye adsorption process on the adsorbent from the waste cotton (equilibrium constant rate of the *pseudo-first* order) for all of the initial

dye concentrations, values for the parameter q_e (calculated, $q_{e,izr}$ and experimental, $q_{e,exp}$) and statistical indicators of validity. The *pseudo-first* order model has, in all cases, a coefficient of determination greater than 0.940 (0.945-0.971), resulting in a high functionality, where the model can be accurately used to describe the process of dye adsorption on the adsorbent. Also, according to the statistical parameter *residual sum of squares (RSS)*, whose values are approximately zero, the validity of the results of the modelling of kinetics using the *pseudo-first* order model can be confirmed.

The differences between parameters $q_{e,izr}$ and $q_{e,exp}$ are approximate for this model, but again not completely identical.

According to the data presented in Table 2, the rate constant of *pseudo-first* order is not dependent on the initial dye concentration in the solution, which in turn confirms the validity of the results of that model.

The adsorption kinetics according to the *pseudo-second* order model (Figure 9) are presented using the graph of the dependence of t/q_t on time. By fitting the data to a graph, functional straight lines for all the initial dye concentrations were obtained. This model includes all phases of adsorption, such as external diffusion, adsorption and internal diffusion in particles, since it is *pseudo* model. It was established by comparing the curves from the graph, as well as the appearance and the dispersion of the

Table 2: Kinetic parameters of the RR84 dye adsorption process on new adsorbent (pseudo-first order, 20°C)

Dye concentration (mg/dm³)	$q_{t,exp}$ (mg/g)	$q_{t,izr}$ (mg/g)	k_1 (g/mg×min)	R^2	RSS
30	1.19	1.41	0.063	0.957	0.05
50	1.93	2.42	0.066	0.945	0.07
75	2.85	3.49	0.064	0.952	0.06
100	3.64	4.67	0.068	0.942	0.08
125	4.37	5.50	0.069	0.956	0.06
150	4.57	5.39	0.064	0.971	0.04
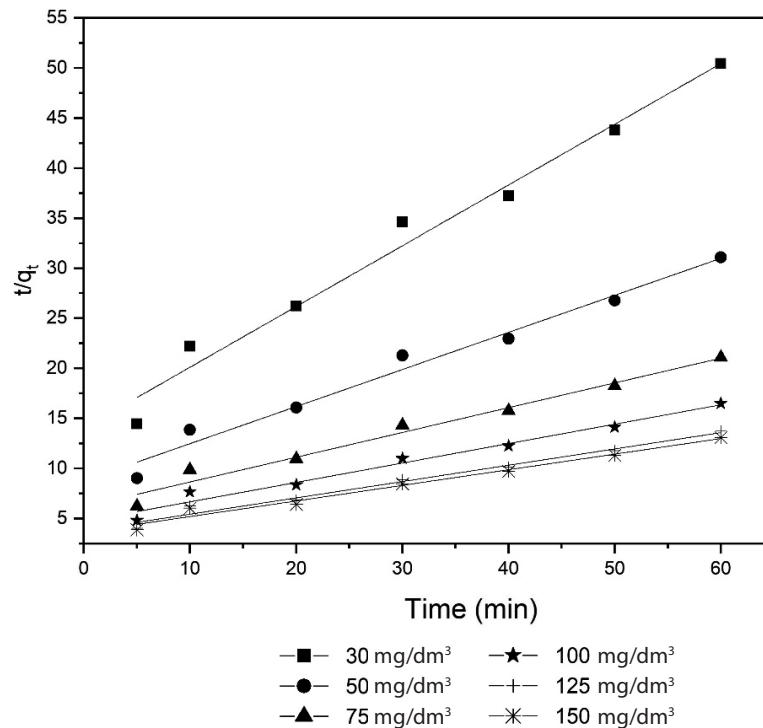
Figure 9: Kinetic curves of RR84 dye adsorption on a new adsorbent according to the pseudo-second order model

points around the ideal curve fitting, that the kinetics of RR84 dye adsorption to the adsorbent are sufficiently described by the *pseudo-second* order model.

Table 3 shows the value of the kinetic parameters of the adsorption process of the reactive dye on the adsorbent (the equilibrium rate constant for the *pseudo-second* order) for all the initial dye concentrations, values for parameter qe (calculated, $q_{e,calc}$ and experimental, $q_{e,exp}$) and statistical indicators of validity. In all cases, the kinetic *pseudo-second* order model had a coefficient of determination of $R^2>0.97$, thereby achieving a high degree of functionality (better than that of the pseudo-first order model), when the model can be used to describe the dye adsorption process on the adsorbent with sufficient certainty.

On the other hand, the differences between parameters $q_{e,izr}$ and $q_{e,exp}$ are more significant for this model than in the *pseudo-first* order model. Also, a greater variation of the rate of constant k_2 with a change in the initial dye concentration, as well as a very high number of values for the *residual sum of square* far greater than zero, push the *pseudo-second* order model into the background and give preference to the *pseudo-first* order model.

It can be concluded that the adsorption of RR84 dye on an adsorbent is of a physical nature, although it can be supported at any time by chemisorption, given the results of kinetic analysis, as well as the fact that the rate of equilibrium is rapid, which characterizes physisorption and activated chemisorption [13]. A similar observation was made in the study of the adsorption kinetics of reactive yellow and blue dyes on an adsorbent made by modifying agricultural residues from sugar cane processing. Dye adsorption is well described by the kinetic pseudo-first order model for reactive yellow and pseudo-second order for reactive blue dye [14].

4 Conclusion

With phosphoric acid as an activating agent, the thermochemical conversion of waste cotton textile into a powder adsorbent was performed. The obtained adsorbent was tested for physical and chemical properties. The element composition of the produced adsorbent was dominated by carbon and oxygen, while the surface morphology shows porosity.

The removal of reactive azo-dye with the help of the adsorbent was tested under different conditions. It was found that the adsorption depended on contact time and initial dye concentration.

The *Langmuir* equilibrium model perfectly describes the process of adsorption of reactive dye on the adsorbent from waste cotton textiles from the cutting of knitted fabric during the production of women's T-shirts.

The kinetic *pseudo-first and pseudo-second* order models excellently described the change in the adsorption rate of the reactive dye on the adsorbent, but preference was still given to the *pseudo-first* order model.

Based on these results, it can be concluded that the adsorbent obtained from the waste cotton textile may be an effective adsorbent for the removal of the reactive azo-dyes from an aqueous solution, with a reasonable tendency of application in industrial conditions, as well.

References

1. PUASA, S.W., ISMAIL, Khairul N., KHAIRI, N.A.I.A. Cleavable surfactant-impregnated activated carbon for enhanced adsorptive removal of reactive dye from an aqueous solution. *Materials*

Table 3: Kinetic parameters of RR84 dye adsorption process on new adsorbent (pseudo-second order, 20°C)

Dye concentration (mg/dm³)	$q_{t,exp}$ (mg/g)	$q_{t,izr}$ (mg/g)	k_2 (g/mg×min)	R^2	RSS
30	1.19	1.65	0.026	0.980	18.47
50	1.93	2.70	0.015	0.980	7.18
75	2.85	4.04	0.010	0.977	3.65
100	3.64	5.16	0.008	0.978	2.16
125	4.37	6.14	0.007	0.982	1.24
150	4.57	6.41	0.006	0.981	1.16

Today: Proceedings, 2018, **5**(10), 22020–22028, doi: 10.1016/j.matpr.2018.07.063.

2. DASH, Subhajit, CHAUDHURI, Haribandhu, GUPTA, Radha, NAIR Udayabhanu G. Adsorption study of modified coal fly ash with sulfonic acid as a potential adsorbent for the removal of toxic reactive dyes from aqueous solution: kinetics and thermodynamics. *Journal of Environmental Chemical Engineering*, 2018, **6**(5), 5897–5905, doi: 10.1016/j.jece.2018.05.017.

3. LEWIS, David M. Developments in the chemistry of reactive dyes and their application processes. *Coloration Technology,* 2014, **130**, 382–412, doi: 10.1111/cote.12114.

4. IBRAHIM, Shariff, SHUY, Wan Z., WANG, Ha-Ming, WANG, Shaobin. Preparation of bio-adsorbents for effective adsorption of a reactive dye in aqueous solution. *Asia-Pacific Journal of Chemical Engineering*, 2010, **5**(4), 563–569, doi: 10.1002/apj.446.

5. RACHNA, Km., AGARWAL, Anupam, SINGH, N.B. Rice husk and Sodium hydroxide activated Rice husk for removal of Reactive yellow dye from water. *Materials Today: Proceedings*, 2019, **12**(3), 573–580, doi: 10.1016/j.matpr.2019.03.100.

6. DAOUD, Mounir, BENTURKI, Oumessaad, KECIRA, Zoubida, GIRODS, Pierre, DONNOT, Andre. Removal of reactive dye (BEZAKTIV Red S-MAX) from aqueous solution by adsorption onto activated carbons prepared from date palm rachis and jujube stones. *Journal of Molecular Liquids*, 2017, **243**, 799–809, doi: 10.1016/j.molliq.2017.08.093.

7. ERTAS, Murat, ACEMIOGLU, Bilal M., ALMA, Hakki, USTA Mustafa. Removal of methylene blue from aqueous solution using cotton stalk, cotton waste and cotton dust. *Journal of Hazardous Materials*, 2010, **183**(1–3), 421–427, doi: 10.1016/j.jhazmat.2010.07.041.

8. TENEV, Maria D., FARIAS, Alejandro, TORRE, Camila, FONTANA, Gimena, CARACCIOLO, Nestor, BOEYKENS Susana P. Cotton industry waste as adsorbent for methylene blue. *Journal*

of Sustainable Development of Energy Water and Environment Systems, 2019, **7**(4), 667–677, 10.13044/j.sdewes.d7.0269.

9. ASGHER, Mahwish, BHATTI, Haq N. Removal of reactive blue 19 and reactive blue 49 textile dyes by citrus waste biomass from aqueous solution: equilibrium and kinetic study. *The Canadian Journal of Chemical Engineering*, 2012, **90**(2), 412–419, doi: 10.1002/cjce.20531.

10. FARISSI, Hammadi E., LAKHMIRI, Rajae, ALBOURINE, Abdallah, SAFI, Mohamed, CHERKAOUI, Omar. Adsorption study of charcoal of cistus ladaniferus shell modified by H3PO4 and NaOH used as a low-cost adsorbent for the removal of toxic reactive red 23 dye: kinetics and thermodynamics. *Materials Today: Proceedings*, 2021, **43**(2), 2021, 1740–1748, doi: 10.1016/j.matpr.2020.10.438.

11. NAEBE, Maryam, COOKSON, Peter G., RIPPON, John A., WANG, Xungai G. Effects of leveling agent on the uptake of reactive dyes by untreated and plasma-treated wool. *Textile Research Journal*, 2010, **80**(7), 611–622, doi: 10.1177/0040517509340603.

12. GIANNAKOUDAKIS, Dimitrios A., KYZAS, George Z., AVRANAS, Antonis, LAZARIDIS, Nikolaos K. Multi-parametric adsorption effects of the reactive dye removal with commercial activated carbons. *Journal of Molecular Liquids*, 2016, **213**, 381–389, doi: 10.1016/j.molliq.2015.07.010.

13. HONG, Gui-Bing, WANG, Yi-Kai. Synthesis of low-cost adsorbent from rice bran for the removal of reactive dye based on the response surface methodology. *Applied Surface Science,* 2017, **423**, 800–809, doi: 10.1016/j.apsusc.2017.06.264.

14. SAID, Abd El-Aziz, A., ALY, Aref A. M., EL-WAHAB, Mohamed M., SOLIMAN, Soliman A., EL-HAFEZ, Aly A., Helmey, V., GODA, Mohamed N. Application of modified bagasse as a biosorbent for reactive dyes removal from industrial wastewater. *Journal of Water Resource and Protection*, 2013, **5**(7A), 10–17, doi: 10.4236/jwarp.2013.57A003.

Ilda Kazani [1, 2]*, Majlinda Hylli* [1]*, Pellumb Berberi* [3]
[1] Polytechnic University of Tirana, Department of Textile and Fashion, Mother Teresa Square No.1, Albania
[2] Albanian Young Academy, Shëtitorja Murat Toptani 1000 Tirana, Albania
[3] Polytechnic University of Tirana, Department of Engineering Physics, Bulevardi Dëshmorët e Kombit Nr. 4, Tirana, Albania

Electrical Resistivity of Conductive Leather and Influence of Air Temperature and Humidity
Električna upornost prevodnega usnja ter vpliv temperature in vlažnosti zraka

Corresponding author/*Korespondenčna avtorica:*
Assoc Prof dr. Ilda Kazani
E-mail: ikazani@fim.edu.al
ORCID ID: 0000-0002-5727-5553

Abstract
Leather is a material that has been used in different applications for centuries. Today, living in the era of high-technology, we are surrounded by smart products. For this reason, traditional products must be changed or improved in order to support and make us more comfortable while using them. For instance, the touch screen display in electronics products is a smart phone's or a tablet computer's primary input device. Still, traditional leather will not function properly in a cold climate or other specific conditions. To make it conductive in such conditions, the double in-situ polymerization of the pyrrole coating method was used. The aim of this study was to observe the electrical properties of conductive leather. At the same time, it stands up to a wide range of different air temperatures, and relative and absolute humidity. These properties are essential because designers and textile engineers should be familiar with them when they decide to use materials in different smart products. Electricity conductivity tests were carried out in year-round temperatures from 7.5 °C to 28.1 °C, with a relative humidity from 18% to 77% and a vapor air concentration from 2.77 g/kg to 12.46 g/kg. The so-called "multiple-step method" was used to test leather's electrical resistivity for the first time. The method considers a material's compressional properties and provides an indicator inherent for a material's electrical properties, regardless of the mass and shape of samples. The results showed a strong dependence between water vapor air concentration and electrical resistivity, described using the formula $\rho = 1.310^3 \, H^{-1.04} \, \Omega m$, with a correlation coefficient of 0.87. There was no relation between relative humidity and electrical resistivity, and resistivity and air temperature. Also, the results confirmed again that changes in the shape of the sample used during tests did not influence the measurement's results, but supported the appropriateness of the measuring method.
Keywords: air humidity, conductive leather, electrical resistivity, multiple-step method.

Izvleček
Usnje se kot material že stoletja uporablja v različnih aplikacijah. Danes, ko živimo v dobi visoke tehnologije, smo obkroženi s pametnimi izdelki. V ta namen je treba tradicionalne izdelke spremeniti ali izboljšati, da bi jih nadgradili in naredili primernejše za rabo. Na primer, v elektronskih izdelkih je zaslon na dotik primarna vhodna naprava pametnega telefona ali tabličnega računalnika. Ker tradicionalno usnje v hladnem okolju ali drugih posebnih razmerah ne deluje,

je bilo površinsko obdelano z metodo dvojne in situ polimerizacije pirola. Cilj te študije je opazovati električne lastnosti prevodnega usnja v širokem razponu različnih temperatur, relativne in absolutne vlažnosti zraka. Te lastnosti so bistvene, ker oblikovalci in tekstilni inženirji morajo poznati te lastnosti, ko se odločijo za uporabo materiala v različnih pametnih izdelkih. Testi elektroprevodnosti so potekali eno leto pri temperaturah od 28,1 °C do 7,5 °C, pri relativni zračni vlažnosti od 77 % do 18 % in koncentraciji vodne pare v zraku od 12,46 g/kg do 2,77 g/kg. Prvič je bila za testiranje električne upornosti usnja uporabljena t. i. „metoda z več koraki". Ta upošteva tlačne lastnosti materiala in zagotavlja indikator, ki je vezan na električne lastnosti materiala, ne glede na maso in obliko vzorcev. Rezultati so pokazali močno odvisnost med koncentracijo vodne pare v zraku in električno upornostjo, opisano z zvezo ρ = 1.310³ H⁻¹·⁰⁴ Ωm, s korelacijskim koeficientom 0,87. Med relativno zračno vlago in električno upornostjo ter upornostjo in temperaturo zraka ni bilo povezave. Prav tako so rezultati ponovno potrdili, da spremembe oblike vzorca, uporabljenega med preizkusi, niso vplivale na rezultate meritev, kar potrjuje vrednost merilne metode.
Ključne besede: zračna vlaga, prevodno usnje, električna upornost, večstopenjska metoda

1 Introduction

Leather is a natural product made by converting animal hides and skins using tannage [1]. This material has been used in different applications for centuries after numerous mechanical and chemical operations. Moreover, this material has excellent insulating properties [2, 3], making it essential for various applications such as clothing, upholstery, footwear, automotive products and accessories.

Today, however, we live in a high-tech world surrounded by smart products. For this reason, traditional products must be changed or improved to support and make us more comfortable while using them.

For instance, the touch screen display in electronics products is the primary input device of a smart phone or a tablet computer. Still, traditional leather will not function properly in a cold climate or other specific conditions.

A great deal of research has been done on the transformation of textiles into conductive materials, including leather in the last decade. In this way, electrically conductive materials can be applied to the leather's surface to be used as a touching operator for a capacitive touch screen panel.

Consequently, the treated leather samples show electrical conductivity and are expected to have a reasonable working performance on a capacitive touch screen [2–10].

Various methods are used to evaluate the electroconductive properties of textile and leather materials. Those methods provide indicators that are difficult to compare with each other. For this reason, we decided to use the so-called "multiple-step method" for measuring the electrical resistivity of our manufactured leather's electrical resistivity [5, 11, 12]. The method takes into consideration the compressional properties of a material. It provides an indicator inherent for a material's electrical properties, regardless of the mass and shape of samples.

When investigating the electrical resistivity of conductive leather, certain parameters such as environmental conditions must be considered. We typically take into account standard air temperature and humidity conditions for textile materials' physical and mechanical properties.

Nevertheless, it is important for applications of conductive leather to know what happens to the electrical properties in a wide range of air temperatures and relative and absolute humidity. In this paper, we attempt to give more information about this smart leather to designers and textile engineers, who should be familiar with these properties when they decide to use this smart material in different applications such as clothing, bags, footwear, automobile seats or furniture.

2 Experimental

2.1 Materials and methods

White sheep crust leather of Albanian origin was used in this research. The leather was initially cut into 8 cm x 8 cm pieces with a thickness of 0.97 mm ± 0.2 mm. The leather was only chrome tanned and dried. A double in-situ polymerization of pyrrole coating was used to make the material conductive. The chemicals used here were pyrrole, ferric chloride, anthraquinone-2-sulfonic acid sodium salt monohydrate of laboratory-grade and high purity [2]. The multiple-step method was used to measure the electroconductive properties of this conductive leather [11–12].

This method consists of measuring the electrical resistance of the sample compressed to different volume fractions within a measuring cell, as shown in Figure 1. A reciprocal power function then approximated the dependence of the textile material's electrical resistance on its volume fraction (V_f) within the measuring cell.
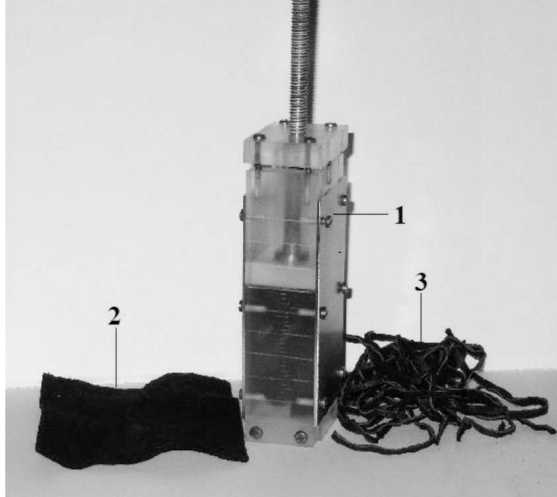
Figure 1: View of the measuring cell (1) and two sample shapes: sheet shape (2) and strip shape (3)

The specific resistance was calculated using the formula:

$$\rho = R * \left[\frac{m}{d \cdot a^2}\right] * Vf^b \rho = R_f \left(\frac{m}{da^2}\right) V_f^{-b} \qquad (1)$$

where ρ represents electrical resistivity in Ωm, m represents the mass of the sample, R_f represents the electrical resistance of the sample in volume fraction V_f calculated from the approximation function $Rf = f(V_f)$, Vf represents the ratio between the intrinsic volume of the sample $V_0 = m/d$ and volume occupied in the measuring cell, d represents the density of leather's material, a represents the distance between the measuring electrodes of the measuring cell, and b represents a power index calculated using the approximation of the set of resistances of the sample compressed in different volume fractions.

The double in-situ polymerization of the pyrrole coating method was used to make the leather conductive. The leather samples were first cut into in 8 cm x 8 cm squares and treated with a mixed pyrrole/AQSA solution for one hour at room temperature, rotating manually at 10 rpm. A ferric chloride solution, which plays an oxidant role, was then added to the mixture to initiate the polymerization, which was carried out for two hours at 5 °C, rotating manually at 10 rpm. The polypyrrole coated leather samples were washed with distilled water and dried at 35 °C. The concentration of monomer (pyrrole), AQSA as a dopant and $FeCl_3$ as an oxidant were varied and optimized to ensure the leather's maximum conductivity. The sample was then treated following the same procedure to obtain double in situ polypyrrole coated leather. In the end, the coated leather was washed four times with distilled water and dried at 35 °C.

The colour of the sheep leather samples treated using this method changed from white to black at the end of the experiments.

3 Results and discussion

The samples's electrical resistance compressed in different volume fractions (V_f) was measured using a Tektronix DMM4050 Multimeter. The voltage used was 10 V DC. For each sample, a set of electrical resistance results compressed by at least fifteen different volume fractions was used to calculate power index b of approximation power function of the form $R_f = f(V_f^{-b})$ needed to calculate the resistivity ρ. Correlation coefficients R^2 in each case were more than 0.95. Figure 2 illustrates a typical case of approximation.
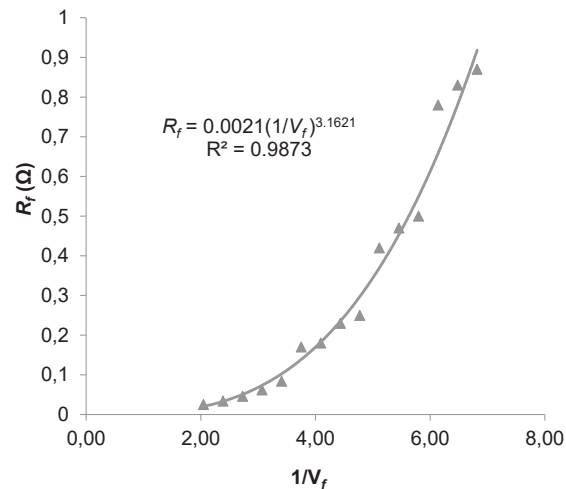
Figure 2: Typical curve of dependence between electrical resistance of the tested sample in Ω and inverse of volume fraction $1/V_f$

The mass of the sample used for these measurements was 4.54 g. The density of leather was 0.86 g/cm³, while intrinsic volume was V_0 = 5.28 cm³. Each sample was first tested in its initial square sheet shape (8 cm × 8 cm). It was then cut into thin strips and again tested for electrical resistance (Figure 1). We did this because our initial objective was to verify whether this method of measurement of resistivity, originally applied to textile fibres, could be successfully applied to leather, as well. The samples were randomly placed in the measuring cell.

In our previous research, [5] it was observed that the electrical resistivity of conductive leather, unlike the methods and standards used today for measuring surface resistance, was shown to be an inherent indicator of bulk conductivity of a leather assembly and was not influenced by sample shape or the way it is placed in the measuring cell.

After proving the objectivity of the method, we decided to continue the measurements for nearly one year to observe how the conductive leather will behave in natural environmental conditions. In this way, the tests were carried in natural weather conditions that included a wide range of humidity and air temperatures, using products made from this material. The objective of this research was to understand how the conductive leather applied in a smart product will react due to environmental conditions. Measurements of the sample's resistivity in two different shapes and different environmental conditions are shown in Table 1.

The results of resistivity were plotted versus relative the humidity and water vapor concentration of the air, as shown in Figures 3 and 4, respectively. Also, each figure contains two sets of data: curve 1 corresponds to the dependence of the sample's resistivity in the shape of strips on the relative humidity and vapor concentration in the air. Curve 2 shows the above dependencies, but all results are considered, both for samples in the form of strips and sheets.

As mentioned above, the preliminary objective of the actual study was to test the appropriateness of multiple-step method for measuring the resistivity of leather and its sensitivity to the shape of the sample. This explains why we tested two shapes of the same sample, initially in the form of a sheet and later in the form of strips. A problem arose when comparing the results of the resistivity taken from tests performed on different days when air humidity changed. The discrepancy of resistivity results in different temperatures and humidity raised doubts

about the appropriateness of the method. The sample in the shape of a sheet was tested during the summer when temperatures were higher, while tests of the sample in the shape of strips were performed mainly during winter when temperatures were low. The obvious difference between curve 1 and 2 in Figure 3 create the impression of the ambiguous influence of the sample's shape, air temperature and relative humidity. The correlation coefficient R^2 was 0.21 for curve 1 and 0.14 for curve 2. The values are too low to consider them reliable. In Figure 4, curves 1 and 2 match each other. The correlation coefficient is as high as 0.87, which makes them reliable.

We can conclude that the multiple-step method used to measure resistivity offers satisfactory results for testing leather electrical conductivity. Moreover, the leather's resistivity depends on the water vapor concentration in the air but not on relative humidity. Consequently, there is no visible dependence of the resistivity of conductive leather on temperature. A change in the resistivity of conductive leather with water vapor concentration in the air follows the equation:

$$\rho = 1.3 \ 10^3 H^{-1.04} \ \Omega m \qquad (2)$$

Curve 1: ρ = 3121.3 RH$^{-0.693}$; R² = 0.211

Curve 2: ρ = 1910.3 RH$^{-0.614}$; R² = 0.1408
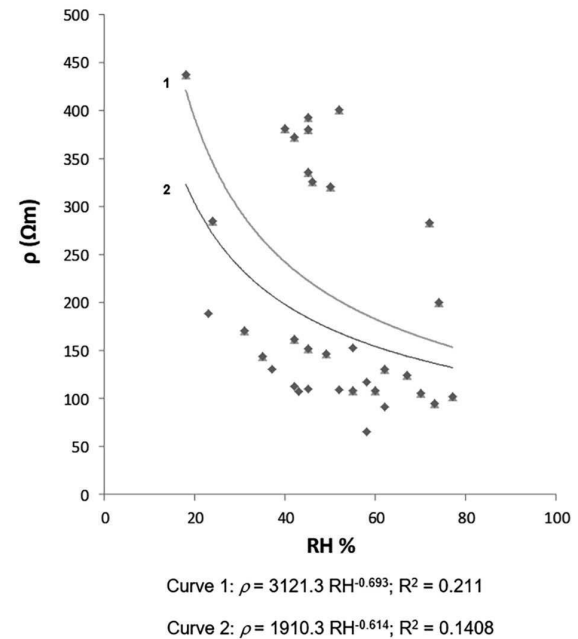
Figure 3: Change in the resistivity of conductive leather with air relative humidity

Curve 1 corresponds to sets of data taken from the sample in the shape of strips alone, while curve 2

Table 1: Resistivity of the sample in two different shapes and in different environmental conditions

Nr	Shape	Air temperature (°C)	Relative humidity (%)	Water vapor concentration (g/kg)	Resistivity $\times 10^2$ (Ωm)
1	strips	21.1	60	9.39	1.0846
2	strips	22.6	67	11.52	1.2421
3	strips	22.7	62	10.72	1.3104
4	strips	20.8	31	4.76	1.7104
5	strips	22.6	35	6.02	1.4418
6	strips	24.0	55	10.32	1.0846
7	strips	23.3	45	8.08	1.5174
8	strips	22.4	42	7.13	1.6218
9	strips	23.4	49	8.85	1.4693
10	strips	21.6	24	3.88	2.8489
11	strips	22.8	18	3.13	4.3787
12	strips	22.3	70	11.81	1.0599
13	strips	18.9	73	9.96	0.9529
14	strips	18.0	77	9.94	1.0194
15	strips	13.0	45	4.25	3.3581
16	strips	11.7	42	3.66	3.7270
16	strips	13.0	45	4.25	3.9341
18	strips	8.5	46	3.28	3.2578
19	strips	9.5	50	3.80	3.2091
20	strips	11.7	52	3.48	4.0133
21	strips	7.5	45	3.02	3.8110
22	strips	8.0	40	2.77	3.8150
23	strips	8.7	65	4.70	3.6590
24	strips	9.1	74	5.48	2.0040
25	strip	9.7	72	5.54	2.8300
26	sheet	24.2	55	10.45	1.5298
27	sheet	24.4	52	10.00	1.0922
28	sheet	25.0	45	8.98	1.1007
29	sheet	24.2	58	11.02	1.1714
30	sheet	25.1	62	12.46	0.9109
31	sheet	25.5	42	8.65	1.1321
32	sheet	24.9	58	11.51	0.6584
33	sheet	28.1	37	8.96	1.3086
34	sheet	27.4	43	9.97	1.0711
35	sheet	24.9	23	4.56	1.8825

corresponds to sets of data taken from samples in shape of both strips and sheets.

Curve 1: $\rho = 1300.7\ H^{-1.042}$; $R^2 = 0.8748$

Curve 2: $\rho = 1305.1\ H^{-1.059}$; $R^2 = 0.8701$
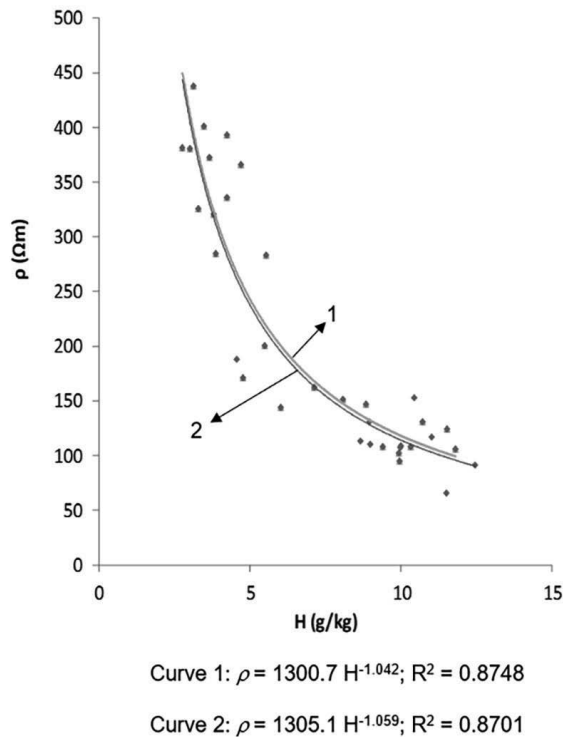
Figure 4: Change in the resistivity of conductive leather with vapor concentration in the air H.

Curve 1 corresponds to sets of data taken from the sample in the shape of strips alone, while curve 2 corresponds to sets of all data taken from samples in the shape of both strips and sheets.

4 Conclusion

We can conclude that the multiple-step method for measuring resistivity offers satisfactory results for testing the electrical conductivity of leather. The conductive leather's electroconductive properties were observed at different temperatures from 7.5 °C to 28.1 °C, relative humidity from 18% to 77% and water vapor concentration in the air from 2.77 g/kg to 12.46 g/kg, using the multiple-step method. The analyses of obtained data revealed that conductive leather's electrical resistivity was a property with a strong dependence on environmental conditions, particularly on the air humidity. Resistivity decreased with an increase in relative and absolute humidity. This study observed that the leather's resis-

tivity depends on the water vapor concentration in the air but not on relative humidity. Consequently, there was no visible dependence of the resistivity of conductive leather on temperature. This conclusion regarding the influence of environmental conditions on conductive leather can help researchers understand where and how to apply conductive leather in different smart textile applications.

References

1. HYLLI, M. Evaluation of extension set of different Albanian leathers. *Albanian Journal of Natural Technical Sciences*, 2014, **21**(1), 111–119, https://doczz.net/doc/3772801/some-results-of-green-s-relations.
2. HYLLI, M., SHABANI, A., KAZANI, I., BEQIRAJ, E., DRUSHKU, S., GUXHO, G. Application of double in-situ polymerization for changing the leather properties. In *Book of Proceedings of 8th International Textile Conference.* Edited by I. Kazani. Tirana : Polytechnic University of Tirana, Faculty of Mechanical Engineering, 2018, 42–47.
3. WEGENE, J.D., THANIKAIVELAN, P. Conducting leathers for smart product applications. *Industrial & Engineering Chemistry Research*, 2014, **53**(47), 18209–18215, doi: 10.1021/ie503956p.
4. HONG, K.H. Preparation of conductive leather gloves for operating capacitive touch screen displays. *Journal of the Korean Society for Clothing Industry*, 2012, **14**(6), 1018–1023, doi: 10.5805/KSCI.2012.14.6.1018.
5. SHABANI, A., HYLLI, M., KAZANI, I., BERBERI, P.G. Measurement of resistivity of conductive leather using multiple step method. In *Book of Proceedings of 8th International Textile Conference.* Edited by I. Kazani. Tirana : Polytechnic University of Tirana, Faculty of Mechanical Engineering, 2018, 120–125.
6. SHABANI, A., HYLLI, M., KAZANI, I., BERBERI, P., ZAVALANI, O., GUXHO, G. The anisotropic structure of electro conductive leather studied by Van der Pauw method. *Textile & Leather Review*, 2019, **2**(3), 136–144, doi: 10.31881/TLR.2019.16.
7. SHIN, J.E., HAN, S.S, CHOI, S.M. Fabrication of highly electrical synthetic leather with polyurethane/poly(3,4-ethylene dioxythiophene)/

poly(styrene sulfonate). *The Journal of The Textile Institute*, 2017, **109**(2), 241–247, doi: 10.1080/00405000.2017.1337296.

8. YANG, C., WANG, J., LI, L. A novel approach for developing high thermal conductive artificial leather by utilizing smart electronic materials. *Textile Research Journal*, 2016, **87**(7), 816–828, doi: 10.1177/0040517516641356.

9. BAO, Y., FENG, C., WANG, C., MA, J., TIAN, C. Hygienic, antibacterial, UV-shielding performance of polyacrylate/ZnO composite coatings on a leather matrix. *Colloids and Surfaces A: Physicochemical and Engineering Aspects*, 2017, **51**(C), 232–240, doi: 10.1016/j.colsurfa.2017.01.033.

10. SHABANI, A., HYLLI, M., KAZANI, I., BERBERI, P.G. Resistivity behavior of leather after electro-conductive treatment. *Textile & Leather Review*, 2019, **2**(1), 15–22, doi: 10.31881/TLR.2019.15.

11. BERBERI, P.G. Effect of processing on electrical resistivity of textile fibers. *Journal of Electrostatics*, 2001, **51-52**, 538–544, doi: 10.1016/S0304-3886(01)00112-7.

12. BERBERI, P.G. A new method for evaluating electrical resistivity of textile assemblies. *Textile Research Journal*, 1998, **68**(6), 407-412, doi:10.1177/004051759806800604.

Malek Alshukur[1,2]
[1] *Heriot-Watt University, School of Textiles and Design, Netherdale Road, Galashiels, TD1 3HF, UK*
[2] *Faculty of Mechanical and Electrical Engineering, Department of Mechanical Engineering of Textiles Industries and their Technologies, Damascus University, Airport Road, Post Box 86, Damascus, Syria*

Effect of Spinning Triangle and Production Speed of Hollow-Spindle System on the Bouclé Yarn Structure
Vpliv predilnega trikotnika in proizvodne hitrosti sistema z votlim vretenom na strukturo preje buklé

Corresponding author/*Korespondenčni avtor:*
Malek Alshukur
E-mail: malekshukur@yahoo.com
ORCID ID: 0000-0002-4042-7311

Abstract

This study aims to show the impact of both the width of the base of the spinning triangle and the production speeds of hollow-spindle spinning machines on the structure of ultimate multiple-thread-structure bouclé yarns and similar fancy yarns. A hollow-spindle spinning machine was used and bouclé yarns were made of a core thread, an effect thread and a (multifilament) binder. Initially, five bouclé yarns were made by setting the widths of the base of the spinning triangle at five levels, i.e. 4.5 mm, 7.5 mm, 10 mm, 13 mm and 16 mm. A further six bouclé yarns were made to show the changes that occur to the spinning triangle at various production speeds. The resulting fancy bouclé yarns were assessed by measuring the size, number and circularity ratio of bouclé profiles. It was found that at low production speeds, i.e. at start-up, that the spinning triangle was unstable, which adversely affected the structure of the final bouclé yarns. However, at production speeds higher than 17 m/min, the spinning triangle became stable, though such a stable spinning triangle had no impact on the structure of the resulting fancy bouclé yarns. The results of this study may help fancy yarn manufacturers to avoid making defective fancy yarns.
Keywords: fancy yarn, bouclé yarn, spinning triangle, hollow-spindle machine

Izvleček

Cilj te študije je bil ugotoviti, kako širina predilnega trikotnika in proizvodna hitrost predilnih strojev z votlim vretenom vplivata na strukturo večnitne preje buklé in drugih efektnih prej. Za izdelavo preje buklé je bil uporabljen predilni stroj z votlim vretenom. Preja buklé je bila izdelana iz niti v jedru, efektne niti in multifilamentne povezovalne preje. Najprej je bilo izdelanih pet prej buklé z nastavitvijo širine osnove predilnega trikotnika na pet nivojev, tj. 4,5 mm, 7,5 mm, 10 mm, 13 mm in 16 mm. Nadaljnjih šest prej buklé je bilo izdelanih zato, da bi ugotovili, kakšne spremembe nastanejo na predilnem trikotniku pri različnih proizvodnih hitrostih. Kakovost izdelanih efektnih prej buklé je bila ocenjena glede na velikost, število in razmerja kroglastih profilov buklé. Pokazalo se je, da je pri nizkih proizvodnih hitrostih, tj. ob zagonu stroja, predilni trikotnik nestabilen, kar je negativno vplivalo na strukturo izdelane preje. Pri proizvodnih hitrostih nad 17 m/min je postal predilni trikotnik stabilen, vendar to ni vplivalo na strukturo nastale efektne preje buklé. Rezultati te študije lahko pomagajo predilcem, da se izognejo napakam pri izdelavi efektnih prej.
Ključne besede: efektna preja, preja bukle (bouclé), predilni trikotnik, stroj z votlim vretenom

1 Introduction

1.1 Spinning triangle of multiple-thread-structure fancy yarns on hollow spindle-spinning machines

When using the hollow-spindle system to make fancy yarns by combining several (input) spun threads (or yarns), the final fancy yarn is said to have a multiple-thread structure. The spinning geometry of this final multiple-thread-structure fancy yarn forms part of the first spinning zone. This zone is located between the yarn supply rollers and the inlet mouth of the hollow-spindle [1, 2]. This zone is characterised by the formation of an approximately right-angle spinning triangle and effect-thread helices. An example is provided in Figure 1 for the Gemmill & Dunsmore MK#3 hollow-spindle spinning machine. This machine can make the effect component of fancy yarns using either drafted fibres (i.e. slivers or rovings) or previously spun threads as the input materials. When using a spun thread for the effect component, a spinning triangle forms when the effect thread emerges from the supply rollers to the point where it starts making a helix around the core thread. The sides of such a spinning triangle were the segments of the core thread (one side of the triangle), the effect thread (hypotenuse of triangle) and the distance between the nipping points of the upper and lower supply rollers on these two threads (i.e. the base of the triangle). Observations indicated that changing the width of the base of such a triangle may alter the size of such a spinning triangle. It is easily possible to change such a width using the grooves of the control cylinder, which is located before the upper supply roller (not shown in Figure 1). Several studies have been conducted on multiple-thread-structure fancy yarns made using the hollow-spindle system as shown below.

1.2 Literature survey

The structure of multiple-thread fancy yarns made by either wrapping or twisting was studied using several approaches. These include the mathematical modelling of the structure, the statistical or empirical modelling of the structural features of these yarns, technological studies of the parameters of the machines and their impact on the structure, engineering studies of the properties of the input yarns and their impact on the structure, engineering studies of the formation conditions of the structure and forces affecting the formation process, etc. In
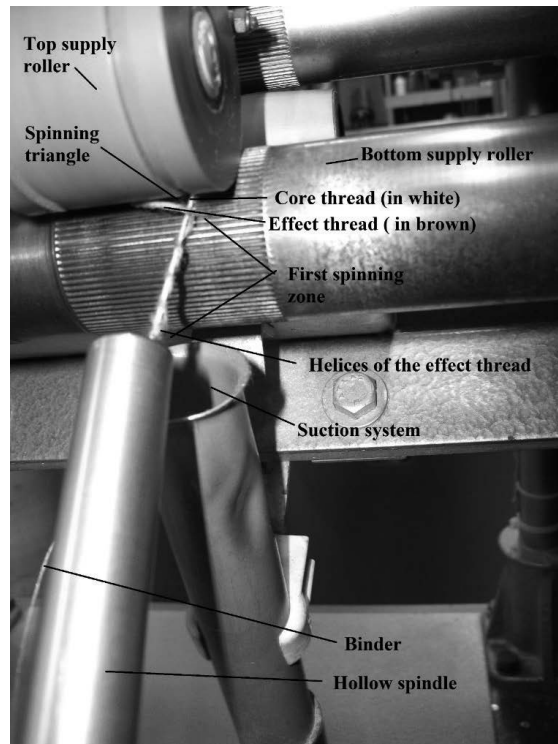
Figure 1: Spinning Triangle on the Gemmill & Dunsmore hollow-spindle spinning when making multiple-thread-structure fancy yarns

one analytical study based on mathematical equations, the structure and formation of several types of multiple-thread-structure fancy yarns were modelled analytically [3]. In such a purely theoretical study, no practical results were presented to test the accuracy of the theoretical equations. Further, the fancy yarns described in such a study were made by twisting, not wrapping, and using routes and technologies different from the hollow-spindle spinning system.

When using the hollow-spindle spinning or hollow-spindle twisting systems, the spinning geometry was shown to have an impact on the structure of multiple-thread final fancy yarns. A recent experimental investigation using the hollow-spindle system showed that the tension of the core thread can change the spinning geometry of fancy yarns [4], particularly within the first spinning zone. Consequently, it was used to regulate the style of the ultimate multiple-thread-structure fancy yarns by selecting suitable values for it. The practical benefit of such a study is that it showed it was possible to make good-quality multiple-thread-structure fancy bouclé yarns using a differential overfeed ratio of as low as +50% of only *one* effect thread in

comparison with the core thread [4]. Following this, two other studies were also conducted to provide a deeper understanding of the formation of the effect-thread helices within the first spinning zone of hollow-spindle spinning machines [1, 2]. In these two studies, it was shown that the shape and size of the effect-thread helices can change the structure of the ultimate multiple-thread-structure fancy yarns. These two studies also showed that the spinning geometry was also controlled by several factors, such as the overfeed ratio of the effect thread, the weight and stiffness of input effect thread and the dynamic forces affecting the segment of the effect thread within the first spinning zone [1, 2]. Dynamically, the diameter of the helices is controlled by external forces, such gravitational force, air drag, centrifugal force and centripetal force. It is also controlled by internal forces, such as tension and the bending force of the effect thread [1]. Mathematically, it was shown that the overfeed ratio and the number of helices can define the radius of the helices in the steady-state rotation or configuration of the effect-thread helices [2].

In another study, a universal, analytical model of the structure and geometry of several types of multiple-thread-structure fancy yarns was presented [5]. In other studies, another form of mathematical modelling of the geometry of bouclé yarns was used to build a mathematical model of the strength of such types of fancy yarn. In the same study, however, the structure was called loop yarn when the structural profiles were sinusoidal in shape, though these were similar to any typical bouclé yarn structural profiles [6, 7]. In another study, the *Structural ratio of multi-thread fancy yarn* was presented using a simple mathematical equation to account for the interaction of the number of wraps and the overfeed ratio, and to show how such an interaction may help in deciding the structure and type of fancy yarn [8]. Depending on the value of this ratio, the final fancy yarn can be bouclé yarns, gimp yarns, overfed fancy yarns or wavy yarns.

Other studies concerned the contribution of technological factors of the hollow-spindle system to the structure of multiple-thread fancy yarns. Examples of these studies are those that dealt with the impact of the supply speed of the effect thread, the rotational speed of the hollow-spindle and the delivery speed of the ultimate fancy yarns [9–14]. These studies were based on the design of experiment method using either the Box-Behnken design

or second-order composite models. The differences between these studies lie in the type of material used and types of fancy profile that resulted [9–14]. The researchers studied these overfed fancy yarns in terms of linear density, breaking tenacity, height of the effect projections, width of the effect projections, distance between the effect projections and the number of effect projects per unit length. In these studies, the effect threads that were studied were loop/knot and plain knot, plain knot-knot effect profiles, closed loop, opened loop, loop-knot, opened loop-plain knots, knot made from various loops and combinations thereof [9–14]. The impact of other factors was also reported, including the bending stiffness of effect threads [15, 16], the combined effect of the overfeed ratio and the number of wraps [8] and false twist [17].

Other forms of investigation were also based on the design of experiment method using factorial designs [18-21]. The multiple-thread-structure fancy yarns were gimp fancy yarns, derivatives thereof and generic overfed fancy yarns. The properties studied were the linear density of ultimate fancy yarns [18], their aesthetics and structural properties [19] and their tensile properties [20, 21]. This group of technological factors included the supply speed of effect thread, the delivery speed of ultimate fancy yarn, the rotational speed of the hollow spindle, the use of false-twist, the nature of the effect component (i.e. number of threads, linear density, type of spinning method and any special treatments), the nature of the core component and the nature of the (multifilament) binder. Significant results were obtained, as summarised in Table 1 [18–21].

Using the combined hollow-spindle system and ring-spindle system in one machine, two similar studies were conducted on multiple-thread-structure bouclé yarns and fancy knitted fabrics made from them [22, 23]. The factors of these two studies were the overfeed ratio of the effect thread, the number of wraps of the binder and the direction of wraps. The bouclé yarns were assessed by counting the number of bouclé profiles per unit length and by measuring their height. The fancy knitted fabrics made of these bouclé yarns were studied in terms of areal density, fabric thickness and abrasion resistance. The knitted fabrics were single jersey and (1×1) rib in the first study [22], and 2×1 and 2×2 rib fabrics in the second study [23]. The overfeed ratio had two levels, i.e. 100% and 200%, while the number of wraps had three levels, i.e. 400, 450 and

Table 1: Summary of results reported on multiple-thread-structure fancy gimp yarns using a fractional factorial design

Factor and levels	Advantages gimp yarn structure	Disadvantages to gimp yarn structure
Core component: two single threads versus a single thread	Thicker gimp yarns; higher value of the maximum load and load at the first peak; better extension at the first peak; higher number of the core ruptures; lower number of irregular non-gimp fancy projections with smaller sizes	Not applicable
Binder component: heavy textured multifilament versus lighter non-textured multifilament	Higher values for load at the first peak and extension at the first peak, lower number of non-gimp profiles with smaller sizes	Lower number of core ruptures
Effect component: heavy and stiff bamboo yarn versus lighter, softer cotton yarn	Thicker gimp yarns; higher value of load at the first peak; smaller number of non-gimp profiles with smaller sizes; and higher number of core ruptures	Lower value of the maximum load; less extension at the first peak
Supply speed: high versus low	Thicker gimp yarns	Not applicable
Rotational speed: high versus low	Reduced number of non-gimp profiles by increasing the number of wraps; slightly increase in the number of core ruptures	Not applicable
Delivery speed: high versus low	Not applicable	Thinner gimp yarns
False-twist: using versus not using it	Not applicable	Slight increases in the number of non-gimp profiles
Number of wraps: high versus low	Increase in the number of core breaks; reduced number of non-gimp profiles by increasing the rotations of the spindle	Decrease in the maximum load; slight increases in the size of abnormal distortions
Overfeed ratio: high versus low	Increase in the number of the core ruptures	Reduced number of core breaks; increases in the number of non-gimp profiles and their average size

500 wraps per metre. All these factors were found to have an influence on the results, but clear interaction plots for the effect of these factors were not provided and the experimental design was not a standard experimental design for either of the two studies [22, 23].

The spinning triangle was not studied in any of these published studies. However, since the spinning triangle on traditional ring spinning machines is important to the structure of typical spun yarns and controlling its dimensions has led to the invention of compact ring spinning, a similar investigation is required for the spinning triangle on the hollow-spindle system. Such an investigation may be completed in two cases. In the first case, which is beyond the scope of this study, the effect element of fancy yarns should be made by spinning draft-

ed fibres, i.e. sliver or roving. In the second case, the effect element of fancy yarns is made by combining previously made yarns. In this second case, since the spinning triangle forms part of the first spinning zone, studying it may help increase current knowledge of the spinning geometry of this category of fancy yarns. Based on all of that, this study was conducted to complete the experimental investigations that were reported for the most part in three studies [1, 2, 4]. The topic of this study was the distance between the core thread and the effect thread at the beginning of the first spinning zone, also known as the width of the base of the spinning triangle. Further, since the motion of the effect thread changes at different levels of production speeds, in particular at the start-up of the hollow-spindle machines or at low production speeds,

the spinning triangle may change. Therefore, the impact of running the hollow-spindle system at different levels of production speed on the structure of the ultimate fancy yarns was also studied.

2 Experimental

For this investigation, two experiments were conducted, and the ultimate fancy yarns were made by combining only three input yarns. This number of input threads was suitable for this kind of investigation, though fancy yarn can be made from more input threads. In the first experiment, five fancy bouclé yarns were made (i.e. group I of fancy bouclé yarns). The input effect component was a 67 tex wool thread and the input core component was a three-ply cotton thread (R72/3 tex), while the binder (or wrapper) was a nylon multifilament (R14.5/77 tex). The multiple-thread bouclé yarns were made on a Gemmill & Dunsmore (G&D) MK#3 hollow-spindle spinning machine. The supply speed of the machine was 54 m/min, the delivery speed was 30 m/min and the rotational speed of the hollow-spindle was 5700 revolutions per minute. Subsequently, the number of wraps was W = 5700 ÷ 30=190 wraps per metre, while the theoretical overfeed ratio was η = (54 ÷ 30) ×100 = 180%, i.e. the differential overfeed ratio is +80%. These values of machine speeds ensured that the spinning triangle was stable, while the effect thread helices were also stable. The tension of the core thread while running the machine was *approximately* zero in accordance with the results of a previous study [4]. The width of base of the spinning triangle was set to 4.5, 7.5, 10, 13 and 16 mm, one at a time, according to the machine design and limited by the width of the upper (rubber) supply roller. Due to the variability of the manufacturing process itself, the vibration of the machine parts and the variation in linear density of the core and effect threads, the aforementioned values for the base width changed continuously within a ± 0.5 mm range. The false-twist hook was used in this experiment, while its influence on the structure was revealed in a previous work [17]. False-twist may result in a transient impact on the structure at the start-up of the machine if drafted fibres are used, but this is not the case when using yarns as input materials due to differences in number, size and mass of the input threads in comparison with loose fibres.

Since the formation of a stable spinning triangle is related to the levels of production speeds, a further experiment (Experiment II) was conducted to assess the impact of production speed on the fancy bouclé yarn structure. This experiment may complement a previous investigation on the effect of the production speed of hollow-spindle machines on the structure of bouclé yarns that have the effect component made from drafted fibres [24]. In one case of Experiment II, the spinning triangle was made unstable by running the machine at a low production speed. This is similar to the case of a machine starting-up or changing speeds when the machine is already running at a suitable production speed. Six new bouclé yarns were made (i.e. called group II of fancy bouclé yarns) for Experiment II. The core component was an R120/2 tex lambswool/viscose blended spun yarn. The effect component was an R120/2 tex lambswool/cashmere blended spun yarn. The false-twist hook was used in the Experiment II. The full settings of the machine are given in Table 2.

Table 2: Machine settings and structural parameters of bouclé yarns for Experiment II

Fancy yarn	Delivery speed (m/min)	Supply speed (m/min)	Rotational speed (min⁻¹)	Overfeed ratio, η (%)	Number of wraps (m⁻¹)
Yarn II (1)	17	34	3400		
Yarn II (2)	24	48	4800		
Yarn II (3)	28	56	5600	200	200
Yarn II (4)	32	64	6400		
Yarn II (5)	34	68	6800		
Yarn II (6)	36	72	7200		

The ultimate multiple-thread structure fancy yarns were first preconditioned and then conditioned according to BSI ISO Standard 139:2005. They were then assessed according to the parameters and procedures given in previous studies for the objective assessment of such unique yarns [25, 26]. These parameters include the size of fancy profile, the number of fancy profiles and the circularity ratio of fancy profile. The size of fancy profile refers to the average area of an ultimate, fitted polygon drawn to match the circumference of the 2D projection of the fancy profile on a plane (if it is seen under a microscope). The number of fancy profiles refers to the number of the main fancy profiles of the effect component in a unit length (usually one meter) of the fancy yarn. The circularity ratio of fancy profile is a term that describes the circularity or the roundness of the representative projection of fancy profile on a plane. Fifteen specimens were sampled systematically to count the number of fancy bouclé (including semi-bouclé) profiles per dm. The sampling distance for this procedure was two metres. A manual winding reel (supplied by Doodbrand & Co. Ltd., England) was used to prepare the yarns for this purpose. A further fifteen specimens were also sampled systematically to measure the size (or area) and the circularity ratio of the fancy bouclé profiles. For these last two parameters, the sampling distance between each two bouclé profiles selected was 60 cm. The selected fifteen bouclé profiles were prepared before taking a digital image of each of them. The preparation was accomplished by placing the selected profiles, one at a time, underneath a suitable transparent plate made from glass. Doing so ensured that the fancy profiles lay in a plane if they were not already so. The plate and profile underneath it were all placed under a microscope with a magnifying power of 4×. The microscope was connected to an Olympus digital camera. Following this, a digital photo was taken of each fancy profile. A digital image analysis software package called 'analySIS FIVE®' was used to draw an ultimate, fitted polygon around the projection of fancy profile when viewed from above. This digital image analysis software was used to analyse the images and to measure both the size and the circularity ratio of the profile.

3 Results and discussion

The yarns made for the first experiment are shown in Figure 2. The fancy profiles that are marked with green colour were profiles that were selected to measure their size (mm) and circularity ratio (%). Subjectively, one may say that these bouclé yarns were *similar* in structure because they all had *similar* bouclé profiles and *regular* sigmoidal segments. These observations were confirmed objectively by the results of numerical testing procedures, as shown in Table 3. According to the p-values of ANOVA testing, no statistical differences were found amongst the yarns in terms of the size, the number and the circularity ratio of profiles. This means that the width of a stable spinning triangle had no effect on the structure of multiple-thread bouclé yarns. The similarities in the number, size and the circularity ratio of the fancy bouclé profiles mean that the effect-thread helices in the first spinning zone were similar in number and diameter [1, 2]. This also indicates that the influential factors controlling the diameter of effect-thread helices, as given previously [1, 2], exceeded any impact of the width of the spinning triangle base.

Table 3: Numerical results of Experiment I

Bouclé yarn	Width of spinning triangle (mm)	Size of bouclé profile (mm²)		Number of bouclé profile (dm⁻¹)		Circularity ratio of bouclé profile (%)	
		Average	SD [a]	Average	SD [a]	Average	SD [a]
Yarn I (1)	4. 5	13.39	3.80	7.3	0.90	57	17
Yarn I (2)	7.5	14.65	4.19	7.2	1.20	53	17
Yarn I (3)	10	12.85	6.72	7.8	1.60	55	20
Yarn I (4)	13	13.59	4.15	7.3	0.90	56	18
Yarn I (5)	16	14.40	6.59	6.5	1.40	56	18

[a] Standard deviation
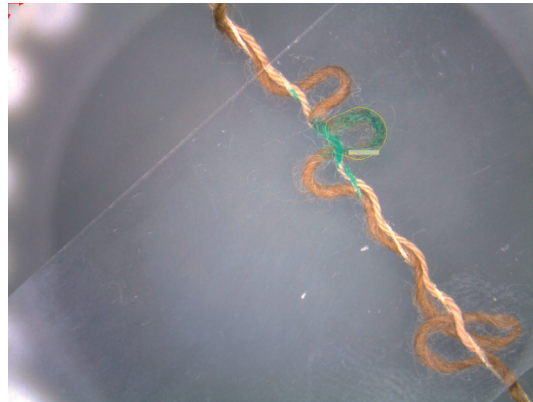
Yarn I (1)
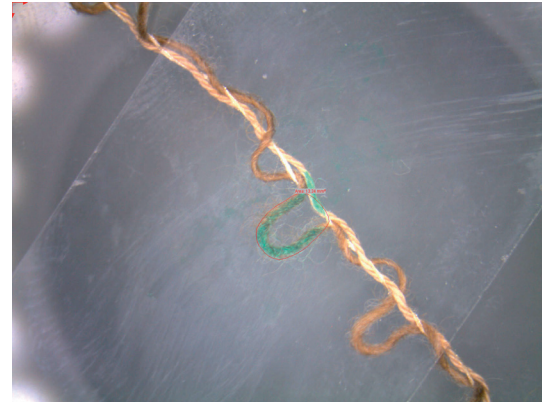
Yarn I (2)
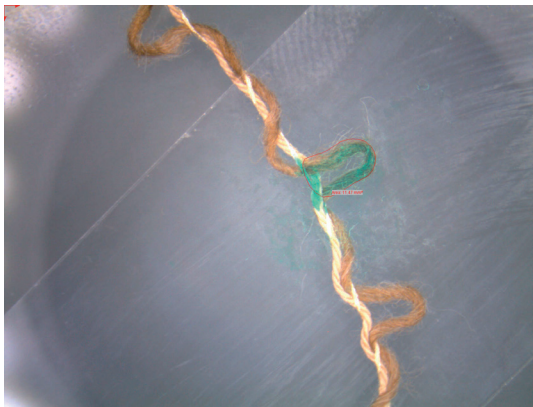
Yarn I (3)

Yarn I (4)

Yarn I (5)

Figure 2: Images of the bouclé yarns made for Experiment I

The yarns made for Experiment II are shown in Figure 3, while the results of the numerical testing of these yarns are given in Table 4. Subjectively, one may say that the first of these yarns had a lower number of bouclé profiles in comparison with the rest of the yarns. Additionally, the other yarns do not appear to differ profoundly in terms of the number of bouclé profiles. However, due to the 3D configuration of these profiles, it is necessary to rely on numerical values for the size of the profiles. Table 4, and Figures 4 and 5 all indicate that the use of low speeds on the machine resulted in the final bouclé yarn II (1) being different from those made at higher speeds. The main difference was that profoundly larger and less bouclé profiles were obtained. Figure 4 and Figure 5 also have two regions, with an

approximately stable region starting from a delivery speed of 24 m min-1. This region is characterised by approximately similar profiles within an acceptable level of variation that is typical for fancy yarns. This region is preceded by an initial region that has fancy bouclé yarns different in terms of size and number from the profiles of the second stable regions.

Dynamically, the effect thread segment within the spinning triangle is subjected to internal and external forces. The main internal forces are bending force and tension. The tension may initially have negative values, i.e. compression, at the start-up of the machine because the effect thread is forced forward by the supply rollers. However, once the

Yarn II (1)

Yarn II (2)

Yarn II (3)

Yarn II (4)

Yarn II (5)

Yarn II (6)

Figure 3: Images of bouclé yarns made for Experiment II

Table 4: Numerical results of Experiment II

Fancy yarn	Delivery speed (m/min)	Size of bouclé profile (mm²)		Number of bouclé profiles (1/dm)	
		Average	SD [a]	Average	SD [a]
Yarn II (1)	17	23.11	9.56	9.46	1.59
Yarn II (2)	24	18.45	5.73	11.87	2.50
Yarn II (3)	28	19.00	6.61	12.53	3.182
Yarn II (4)	32	20.89	6.19	12.67	2.28
Yarn II (5)	34	19.34	9.69	11.67	1.72
Yarn II (6)	36	19.90	6.66	12.53	3.638

[a] Standard deviation
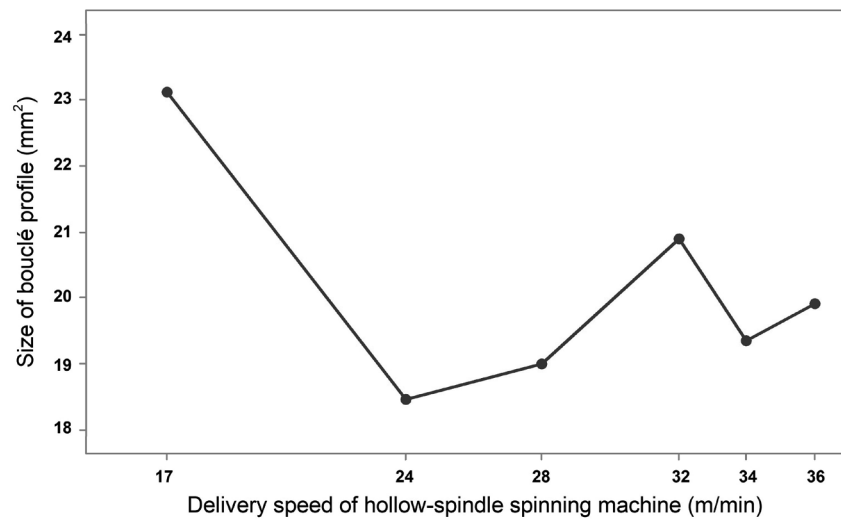
Figure 4: Relationship between the speeds of the hollow-spindle machine and the size of bouclé profiles
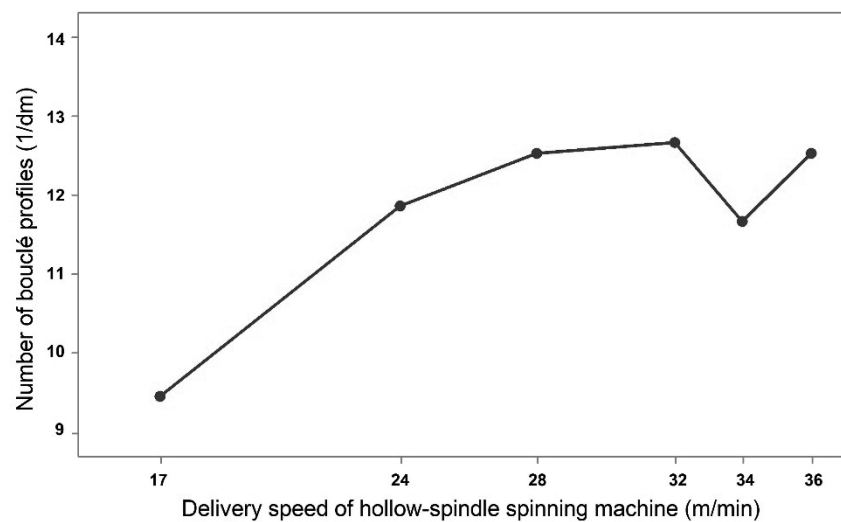
Figure 5: Relationship between the speeds of the hollow-spindle machine and the number of bouclé profiles

rotational speed and thus centrifugal and centripetal forces increase, a positive value of the tension will control the effect thread segment in all locations of the first spinning zone, including the spinning triangle. The main external forces in the spinning triangle are air drag and gravitational force. At the start-up of the machine, gravitational force (*G*) will be the dominating external force, and the effect-thread segments may fall downwards. As all speeds of the machine increase, air drag appears and comes into effect. Once the rotational speed reaches a specific limit, the effect thread segment starts to rotate around the core thread segment. The result of this is that a new force, called centripetal force, starts to appear and is directed outward from the centre of rotation, while centrifugal force acts in the opposite direction. Starting from this limit, the impact of air drag remains constant, and as such, it may not create substantial changes to the shape of the spinning triangle.

Gravitational force is greater than centripetal force (*F$_c$*) at the start-up of the machine. This is confirmed by the following calculations based on an *infinitesimally* small segment d*l* of the effect thread that has a linear mass *m*. This yarn segment is subjected to a gravitational force of d*G* = *mgdl*, where g represents the gravitational acceleration, g = 9806.65 mm/s². Due to rotation, this yarn segment is also subjected to centripetal force d*F$_c$* =*mrω²*d*l*, where ω represents angular velocity (measured in radians per second) and *r* represents the radius of the rotation of this yarn segment. Centripetal force must be greater than gravitational force for a fancy yarn to form, i.e. d*F$_c$* > d*G* or mrω²d*l* > *m*gd*l*; thus *r*ω² > g. Since ω = 2π*RS*, where *RS* represents rotational speed, therefore (2π*RS*)² > g, or:

$$RS > \sqrt{\frac{60 \, g}{2\pi \, r}} \tag{1}$$

where the number 60 is used to convert time from seconds into minutes for the revolutions.

At the start-up of the machine, the radius of rotation r may be equal to the base of the spinning triangle. When r = 4.5 mm, which is the setting used for the first setting of Experiment I, then RS must be > 144 revolution per minute for centripetal force to be greater than gravitational force. Once centripetal force increases, air drag comes into effect. Thus, higher values of centripetal force are required

to exceed such a drag. As centripetal force and centrifugal force increase in magnitude, they reach a point where they become the dominating forces and they balance out all other forces. Subsequently, both the spinning triangle and the helical configuration of the effect thread reach the steady-state case. Eventually, a *stable* spinning triangle followed by *stable* effect-thread helices are formed, and the spinning triangle smoothly merges with the top of the effect-thread helical configuration.

Since stable, *similar* helices are formed, regardless of the length of the hypotenuse of the spinning triangle, no changes will occur to their diameter or number within the first spinning zone. This means that the use of the overfeed ratio as a main element in Equation 5 in a previous study [2] remains valid. This Equation is reproduced here as follow:

$$r = \frac{L_c}{2\pi n}\sqrt{\eta^2 - 1} \tag{2}$$

where *r* represents the radius of helices, *n* represents their number within the first spinning zone, *η* represents the theoretical overfeed ratio of the effect thread and *L$_c$* represents the length of the core thread within the first spinning zone (which *approximately* equals the length of the first spinning zone).

It is thought that changes in the length of such a hypotenuse, when changing the width of the base, happen mainly at the start-up of the machine and also when changing the speeds of the machine. The case of machine start-up is also similar to the case of running the machine at low speeds. During the start-up time, once the machine reaches the set values of rotational, supply and delivery speeds, the hypotenuse will also be stable for the specific overfeed ratio used. The set values of speeds must be above a certain level to ensure the stability and regularity of both the spinning triangle and the effect thread helices. These results were explained dynamically above.

The result of Experiment II indicate that the spinning triangle was not stable at low production speed, but rather was irregular. This is because of gravity and air drag. These reasons concur with a previous investigation regarding effect-thread helices at low machine speeds, in particular the rotational speed [1, 2]. In some cases where the speeds of the machine are extremely low, the machine fails to make a spinning triangle or effect-thread helices. Consequently, it fails to make multi-

ple-thread-structure fancy bouclé yarns. Due to the similarities in structure with other fancy yarns as described mathematically in one universal geometrical model [5], similar results may be obtained for overfed fancy yarns such as gimp fancy yarns, wavy fancy yarns, generic overfed fancy yarns and all their derivatives.

4 Conclusion

It was concluded that the width of the base of the spinning triangle of hollow-spindle spinning machines had a profound influence on the structure of multi-thread fancy bouclé yarns when such machines run at low production speeds, i.e. ≤ 17 m/min. At these low production speeds, the spinning triangle was unstable. The resulting fancy bouclé yarns thus had an unacceptably low number of profoundly large bouclé profiles, which adversely affected their quality and commercial value. This problem was solved by increasing the production speed to a higher value, i.e. ≥ 24 m/min. At these higher production speeds, the stability of the spinning triangle was improved. This helped in regulating the structure, morphology and style of the resultant multi-thread fancy bouclé yarns. Similar results may be obtained for similar multiple-thread-structure fancy yarns, such as gimp fancy yarns, wavy fancy yarns, generic overfed fancy yarns and all their derivatives. The results of this research can help fancy yarn manufacturers to improve the quality of their yarns and also to avoid the aforementioned unfavourable situations, thus saving them money, effort and time.

References

1. ALSHUKUR, Malek, YURCHENKO, Daniil. Experimental study on the spinning geometry of multi-thread fancy yarn on hollow-spindle spinning machines: Part II. *International Journal of Clothing Science and Technology*, 2019, **31**(4), 454–461, doi: 10.1108/IJCST-05-2017-0065.
2. ALSHUKUR, Malek, YURCHENKO, Daniil. Experimental study on the spinning geometry of multi-thread fancy yarn on hollow-spindle spinning machines: Part I. *International Journal of Clothing Science and Technology*, 2018, **30**(4), 496–506, doi: 10.1108/IJCST-05-2017-0064.
3. MARTON, Erich, Theoretical principles of fancy yarn twisting. *Melliand Textilberichte [Eng. Ed.]*, 1987, **68**(8), E 242–243.
4. ALSHUKUR, Malek, SUN, Danmei. Effect of core thread tension on structure and quality of multi-thread bouclé yarn. *Indian Journal of Fibre & Textile Research*, 2016, **41**(4), 367–372, http://op.niscair.res.in/index.php/IJFTR/article/view/8176.
5. ALSHUKUR, Malek, GONG, Hugh, STYLIOS, George. Structural Modelling of multi-thread fancy yarn. *International Journal of Clothing Science and Technology*, 2018, **30**(2), 268–283, doi: 10.1108/IJCST-05-2017-0063.
6. GRABOWSKA, Katarynza Ewa. Mathematical modeling of tensile properties of fancy loop yarns. Theoretical: Part I. *Textile Research Journal*, 2010, **80**(18), 1905–1916, doi: 10.1177/0040517510369405.
7. GRABOWSKA, Katarynza Ewa. Experimental analysis of the tensile properties of fancy loop yarns. Part II. *Textile Research Journal*, 2010, **80**(18), 1917–1929, doi: 10.1177/0040517510369406.
8. ALSHUKUR, Malek, FOTHERINGHAM, Alex. Structural ratio of multi-thread fancy yarn: interaction effect of both the number of wraps and the overfeed ratio on fancy bouclé yarn structure. *Journal of Natural Fibers*, 2021, **18**(11), 1570-1579, doi: 10.1080/15440478.2019.1692320.
9. PETRULYTĖ, Salvinija, PETRULIS, Donatas. Influence of twisting on linen fancy yarn structure. *Journal of Natural Fibers*, 2014, **11**(1), 74–86, doi: 10.1080/15440478.2013.842512.
10. RAGAIŠIENĖ, Audrone. Interrelation between the geometrical and structural indices of fancy yarns and their overfeed and twist. *Fibres & Textiles in Eastern Europe*, 2009, **17**(4)/**76**(5), 26–30, http://fibtex.lodz.pl/article265.html.
11. RAGAIŠIENĖ, Audrone. Influence of overfeed and twist on fancy yarns structure. *Materials Science*, 2009, **15**(2), 178–182, https://www.matsc.ktu.lt/index.php/MatSc/article/view/26142.
12. PETRULYTĖ, Salvinija. Influence of technological parameters on the periodical effects of fancy yarns. *Fibres & Textiles in Eastern Europe*, 2008, **16**(3)/**68**(3), 25–29, http://fibtex.lodz.pl/article163.html.
13. PETRULYTĖ, Salvinija. Analysis of structural effects formation in fancy yarn. *Indian Journal of Fibre & Textile Research*, 2007, **32**(1), 21–26, http://hdl.handle.net/123456789/399.

14. RAGAIŠIENĖ, Audrone, PETRULYTĖ, Salvinija. Design of fancy yarns with worsted and elastomeric covered components. *Materials Science*, 2003, **9**(4), 414–418, https://matsc.ktu.lt/index.php/MatSc/article/view/26751.

15. ALSHUKUR, Malek, FOTHERINGHAM, Alex, GONG, Hugh. Influence of component stiffness on the structure of multi-thread, fancy bouclé yarn. *Journal of Industrial Textiles*, 2020, **49**(7), 889–905, doi: 10.1177/1528083718801365.

16. ALSHUKUR, Malek, FOTHERINGHAM, Alex, GONG, Hugh. Relationship between the interaction of bending stiffness of component yarns and the structure of fancy bouclé and semi-bouclé yarns. *Fibers and Polymers*, 2020, **21**(2), 437–446, doi: 10.1007/s12221-020-8156-0.

17. ALSHUKUR, Malek, FOTHERINGHAM, Alex. Role of false twist in the manufacturing process of multi-thread fancy yarn on hollow spindle spinning machines. *The Journal of The Textile Institute*, 2014, **105**(1), 42–51, doi: 10.1080/00405000.2013.810367.

18. ALSHUKUR, Malek, FOTHERINGHAM, Alex. Studying the linear density of multi-thread fancy yarn made from natural fibers using the design of experiments. *Journal of Natural Fibers*, 2018, **15**(5), 658–667, doi: 10.1080/15440478.2017.1354741.

19. ALSHUKUR, Malek, FOTHERINGHAM, Alex. Quality and structural properties of gimp fancy yarns using the design of experiments. *The Journal of The Textile Institute*, 2015, **106**(5), 490–502, doi: 10.1080/00405000.2014.927126.

20. ALSHUKUR, Malek, FOTHERINGHAM, Alex. Studying the tensile properties at the first break of multi-thread fancy gimp yarns using the design of experiments. *Journal of Natural Fibers*, 2020, **17**(5), 716–725, doi: 10.1080/15440478.2018.1527741.

21. ALSHUKUR, Malek, FOTHERINGHAM, Alex. Study of maximum tensile strength of fancy yarns using the design of experiments. *Mechanics & Industry*, 2019, **20**(4), 403–412, doi: 10.1051/meca/2019033.

22. NERGIS, Banu Uygun, CANDAN, Cevza. Performance of bouclé yarns in various knitted fabric structures. *Textile Research Journal*, 2006, **76**(1), 49–56, doi: 10.1177/0040517506059210.

23. NERGIS, Banu Uygun, CANDAN, Cevza. Performance of rib structures from boucle yarns. *Fibres & Textiles in Eastern Europe*, 2007, **15**(2)/**61**(2), 50–53, http://fibtex.lodz.pl/article1058.html.

24. BAOYU, Zhu, OXENHAM, William. Influence of production speed on the characteristics of hollow spindle fancy yarns. *Textile Research Journal*, 1994, **64**(7), 380–387, doi: 10.1177/004051759406400703.

25. ALSHUKUR, Malek. The quality of fancy yarn: Part I: methods and concepts. *International Journal of Textile and Fashion Technology*, 2013, **3**(1), 11–24, http://www.tjprc.org/publishpapers/2-29-1517224853-2.IJTFTMAR201302.pdf.

26. ALSHUKUR, Malek. The quality of fancy yarn: Part II: practical experiments and application. *International Journal of Textile and Fashion Technology*, 2013, **3**(1), 25–38, doi: 10.24247/ijtftmar201303.

Tetiana Ielina[1], Liudmyla Halavska[1], Nataliia Ausheva[2]
[1] Kyiv National University of Technologies and Design, Nemyrovych-Danchenko str. 2, Kyiv, Ukraine
[2] National Technical University of Ukraine "Igor Sikorsky Kyiv Polytechnic Institute", Ukraine

Macro-Modelling of Rib-Knitted Tubular Parts
Makromodeliranje rebrasto pletenih cevastih sestavnih delov

Corresponding author/*Korespondenčna avtorica:*
Tetiana Ielina
Phone: +38 0965403835
E-mail: yelina.tv@knutd.com.ua
ORCID ID: 0000-0002-9310-0582

Abstract
The aim of the research was to improve the process of knitted products design. The use of modern software helps us predict the physical and mechanical behaviour of materials, using their three-dimensional models. A macro-model of rib-knitted tubular parts was developed in the study. This model allows its implementation into algorithms, describing the peculiarities of the stretching process. Recent findings in the field of 3D modelling and simulation of knitwear behaviour aim at working with models of different scales of structural hierarchy. The use of macro-models provides the opportunity to simplify the geometry and significantly reduce the time required for simulation. Rib stitch structures are among the most popular weft-knitted ones. When using threads of usual stretchability (with breaking elongation that does not exceed 10–12%), the stretchability of some rib stitch structures in the course-wise direction can reach up to 350% and even more. When stretched in the course direction, rib-knitted stitches undergo a number of stages. The stretching process includes: decreasing the width-wise curling; mutual shifting of knit and purl stitches; reducing the curvature of the loop feet and loop heads; pulling the yarn from the loop legs to the loop feet; stretching of the yarn. The assumption was made that such parts of knitted garments as cuffs and borders on sweaters, cuffs on socks, where rib stitch patterns are used, can be described as thin-walled elastic shells. A part of a human body surface, covered with a rib-knitted garment part, can be approximated by a truncated cone. The mid-surface of the shell can be represented as a ruled surface created upon a set of Bezier curves, located along the circumference of the upper and lower bases of the truncated cone. The mathematical description, elaborated in the course of the research, was used for the computer program LastikTube, which was developed to create 3D macro-models of ribbed tubular garments.
Keywords: Rib stitch structures, macro-models, sock cuff, 3D modelling

Izvleček
Cilj raziskave je bil izboljšati proces oblikovanja pletenih izdelkov. Sodobna programska oprema nam z uporabo tridimenzionalnih modelov materialov pomaga predvideti njihovo fizikalno in mehansko obnašanje. V študiji je bil razvit makromodel rebrasto pletenih cevastih sestavnih delov. Model omogoča izpeljavo v algoritme, ki opisujejo posebnosti raztezanja. Najnovejša spoznanja na področju 3-D modeliranja in simulacije obnašanja pletenin so namenjena delu z modeli na različnih ravneh strukturne hierarhije. Uporaba makromodelov omogoča poenostavitev geometrije in znatno skrajšanje časa, potrebnega za simulacijo. Rebraste strukture so med najbolj priljubljenimi votkovnimi pletivi. Pri uporabi niti običajne raztegljivosti (s pretržnim raztezkom pod 10–12 %) lahko raztegljivost nekaterih rebrastih struktur

v smeri zančnih vrst seže do 350 % in celo več. Pri raztezanju v smeri zančnih vrst gredo rebrasta pletiva skozi več faz. Raztezanje zajema: zmanjšanje vihanja po širini; vzajemno premikanje levih in desnih zank; zmanjšanje ukrivljenosti igelnih in platinskih glav zank; odvzemanje preje od krakov zanke k platinski glavi zanke in raztezanje preje. Domnevali smo, da lahko dele pletenih oblačil, kot so rokavne in pasne obrobe na puloverjih in robovi nogavic, kjer so uporabljene rebraste pletene strukture, opišemo kot tankostenske elastične lupine. Del površine človeškega telesa, ki je prekrit z rebrasto pletenim delom oblačila, lahko poenostavljeno prikažemo kot prisekani stožec. Sredinsko površino lupine lahko predstavimo kot ravno površino, ustvarjeno s pomočjo niza Bezierovih krivulj, ki se nahajajo vzdolž oboda zgornje in spodnje osnovne linije prisekanega stožca. Matematični opis, izdelan med raziskavo, je bil uporabljen za računalniški program LastikTube, ki je bil razvit za izdelavo 3-D makromodelov rebrastih cevastih oblačil.

Ključne besede: rebrasta pletena struktura, makromodeli, rob nogavice, 3-D modeliranje

1 Introduction

The challenge of designing knitwear with predicted properties is widely discussed in the scientific community. Evidently, the demands for the quality and comfort of clothing are constantly rising. Some of the most important properties of apparel that affect the level of human comfort in the process of wearing clothes are air permeability, hygroscopicity and tactile comfort. This idea has been confirmed in various studies [1–4]. Other papers [5–7] focus on the pressure clothes exert on a human body and the conditions of maintaining their comfort when using them. Research [8–10] addresses the issue of designing various knitted structures by means of yarn level modelling. It provides high accuracy of yarn geometry, but significantly increases the time required for calculus [11, 12]. Depending on the algorithms and the purpose of physical process modelling, knitwear can be represented as an orthotropic shell of certain thickness, with specified parameters of elasticity, hygroscopicity, heat conductivity, stiffness etc. In a ready-made product, the level of indicators that affect the comfort of clothes in the process of wearing is predominantly determined by the properties of raw materials they are made of and their knitted structure. Furthermore, the latter is predetermined by the design of the product and the compliance of its size with body measurements. Circumference measurements depend on the position of a human body and the dynamics of its movements [13]. When used, the knitted garment is in a deformed state (especially if the clothing is tight fitted). Thus, the indicators of the above-mentioned properties differ significantly from the ones that refer to not deformed ones. The issues of knitted fabric deformation mechanism and fabric deformation modelling by means of computer tools were studied [14–19].

One of the most popular weft-knitted structures is a rib structure which provides high elasticity without creating any excessive compression. The surface of rib stitch structures possesses certain peculiarities and requires using special algorithms for the creation of macro-models of some parts of knitted products comprising rib structures.

2 Methodology

Within the apparel modelling system, the scale of modelling and corresponding fabric structure idealisation depends on the purpose of its design and input data availability as well as software and hardware tools. It is important to choose appropriate assumptions and idealisations, as well as numerical homogenisation methods. Within the systems of three-dimensional modelling and simulation, knitwear can be represented as an orthotropic textile shell with given thickness. In this case, the product, e.g. a sock, can be presented in the shape of a 3D model as shown in Figure 1.

Figure 1: 3D model of sock represented as shell with homogenised properties within system of three-dimensional modelling

The basic knitted structure element is a loop inter-meshed with the loops of the previous and subsequent courses. Furthermore, in the case of 2×2, 3×3, 4×4 and other rib stitch patterns, adjacent knit and purl stitches of the same course can change their mutual position; plain columns width-wise curling can exist as well. As for mechanical characteristics, it is necessary to mention that, depending on the rib stitch pattern and yarn properties, rib stitch structures can have variable levels of stretchability. To represent the physical and mechanical properties of rib stitch structures in macro-models more precisely and to design the mid-surface of tubular rib-knitted shells, the mathematical tool of Bezier curves and ruled surfaces can be used.

2.1 Rib stitch course-wise cross-section

The study of geometric transformations that occur in the process of course-wise stretching of rib-knitted structures [20–22] proved that the change in the configuration and position of separate elements within such a structure is irregular. In the course of stretching, some different processes occur: decreasing of width-wise curling, mutual shifting of adjacent knit and purl stitches, reduction of the curvature of the loop feet and loop heads, pulling the yarn from the loop legs to the loop feet, stretching of the yarn. To study the nature of a thread redistribution within the structure of knitwear, the authors of papers [20–22] used the following notions: the ribbing pattern unit width in mm (Wru), the

width of the projection of a convex part of a rib stitch pattern on the fabric plane (C) and the width of the projection of a visible segment of its concave part on the fabric plane (S), as shown in Figure 2. If we divide the process of stretching of knitwear in the course-wise direction into n discrete states T_m, where m is the number of a given state, we can say that $0 \leq m \leq f$, where 0 is the index of a free state particular to a knitted fabric before applying tensile forces and f is the index of the state of maximum tension that is reached by a sample before its destruction. Therefore, the above-mentioned geometric characteristics defined for T_m state can be noted as Wru_m, C_m and S_m (cf. Figure 2).

The cross-section of a 2×2 rib-knitted structure during the stretching process can be schematically represented as shown in Figure 3. The relative position of the loops before the process of stretching is shown in Figure 3a, while the change in the relative position of loops during the process of stretching (cf. Figures 3a and 3b) until they gain the state of T_f ($m = f$) is shown in Figure 3d.

Owing to their intrinsic elastic properties, rib stitch structures can often be used to design sock cuffs, necklines, waistlines, borders on sweaters etc.

2.2 Geometric approximation

In recent researches, different approaches are used for textile clothes simulation [23]. The most commonly used are mesoscale modelling [10–12] and macro-level garment simulation [24, 25]. However,
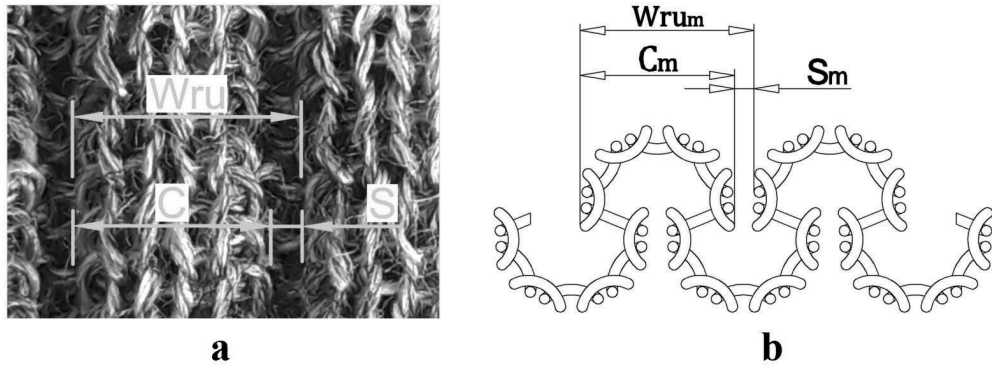

Figure 2: Parts of ribbed patterns within rib stitch structures
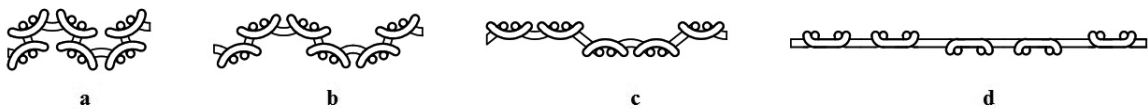
Figure 3: Transformation of knitted fabric elements of 2×2 rib structure in process of uniaxial course-wise stretching

according to the authors' knowledge, there is no published work dedicated to macro-modelling of rib-knitted garment parts. The body parts covered with a tubular rib-knitted garment or its segments can be approximated by a set of conical surfaces, e.g. to provide a mathematical analysis of a ribbed sock cuff, it is possible to approximate the leg surface with a frustum (cf. Figure 4b) with the radii of bases R_{s1} and R_{s2}, the perimeters of which correspond to the leg girths in sections 1 and 2, respectively (cf. Figure 4a).
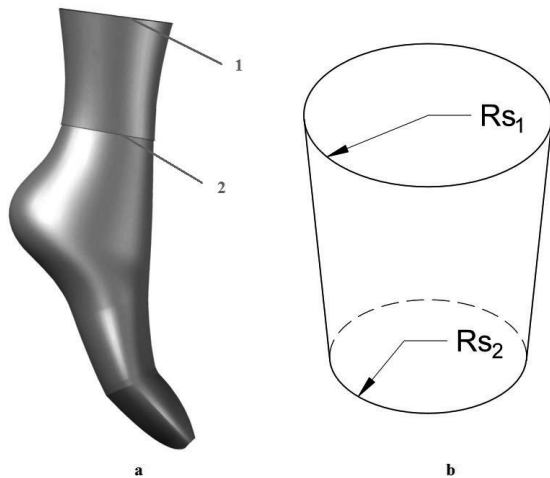
Figure 4: Simplification of shin surface shape with frustum with equivalent base circumferences

3 Results and discussion

In general, if a tubular shell made of an even rib stitch pattern knit is put onto a conical surface, the knitted structure may undergo various levels of stretching in the course-wise direction. In case the tubular rib-knitted garment was produced without changing the number of working needles and stitch density, the number of loops in one course and the loop length do not change.

3.1 Stretching geometry
When the number of rib stitch patterns in one circular course is denoted as N_{ru} and the perimeter of a ribbed tube in a free state as Q_0 (mm), then the pattern width in a free state Wru_0 (mm) can be determined with equation 1:

$$W_{ru_0} = \frac{Q_0}{N_{ru}} \tag{1}$$

If putting a tube with Q_0 perimeter onto a conical surface as shown in Figure 5, three cross-sections with R_1, R_2 and R_3 radii, and Q_1, Q_2 and Q_3 perimeters, respectively, can be schematically represented by three discrete tensile states T_1, T_2 and T_3 as shown in Figure 6. The number of stitches remains unchanged. In the case of transition from T_1 to T_3, the relative elongation increases and the fabric thickness M_m decreases. The pattern width in T_1, T_2 and T_3 can be determined by using equations 2–4.

$$W_{ru_1} = \frac{Q_1}{N_{ru}} \tag{2}$$

$$W_{ru_2} = \frac{Q_2}{N_{ru}} \tag{3}$$

$$W_{ru_3} = \frac{Q_3}{N} \tag{4}$$
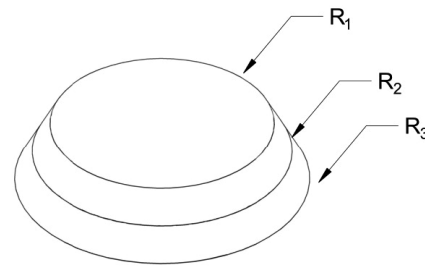
Figure 5: Conical surface with radii of cross-sections R_1, R_2, R_3
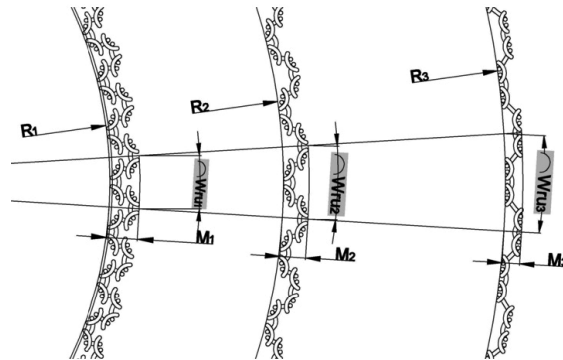
Figure 6: Transformation of knitted fabric elements in case of conical surface wrapped with tube

The correlation of Wru_m, C_m and S_m values for each state of tension depends on many factors and is currently determined experimentally [20–22]. Figure 7 presents macro-models of three stretching states of a sample of 2×2 rib structure made of PAN yarn of linear density 32×2 tex reproduced according to experimental data as described in [21].

Figure 7: Three states of tension of rib stitch structure sample represented in macro-models

If a ribbed tube is put onto a cylindrical or conical surface, the following algorithm can be used to describe the mid-surface.

3.2 Set of Bezier curves for one repeated unit mid-surface segment

If we assume that 2 × 2 rib stitch structure is wrapped around a cylinder with the perimeter Q_m, where $Q_m \geq Q_0$, then the relative elongation Δl_m (%), can be calculated according to equation 5:

$$\Delta l_m = 100 \times \frac{(Q_m - Q_0)}{Q_0} \tag{5}$$

Figure 8 represents a course-wise cross-section of a repeated pattern unit of a rib-knitted fabric wrapping a cylinder of radius R_m. The control points P_0, P_1, P_{15} and P_{16} belong to the circle line with the radius $R_{m-1} = R_m + D_c / 2$, where D_c is a yarn diameter. Then, the control points P_3, P_4, P_5, P_{11}, P_{12}, P_{13} are located on the circle line with the radius $R_{mc} = R_m + M_m / 2$, where M_m is the thickness of the fabric, which corresponds to a given state of stretching. Points P_7, P_8 and P_9 are located on the circle line with the radius $R_{m-2} = R_{m-1} + M_m - D_c / 2$.

$$\psi = \frac{Wru_m \cdot 180}{\pi \cdot R_{mc}} \tag{6}$$

$$\psi_1 = \frac{(C_m - Dc) \cdot 180}{\pi \cdot R_{mc}} \tag{7}$$

$$\psi_2 = \frac{(S_m + Dc) \cdot 180}{\pi \cdot R_{mc}} \tag{8}$$

3.3 Mid-surface geometry description

The ruled surface with guide curves described as quadratic Bezier curves can be used to describe the mid-surface of rib-knitted shells (marked as Ms in Figure 8) pulled over the cone base. The radius vector of the ruled surface $r\,(u, v)$ (cf. Figure 9) can be described as equation 9:

$$r(u, v) = r_1(u)(1 - v) + r_2(u)v \tag{9}$$

where $0 \leq v \leq 1$ is a point on the generating line, and $r_1(u)$, $r_2(u)$ are quadratic Bezier curves.
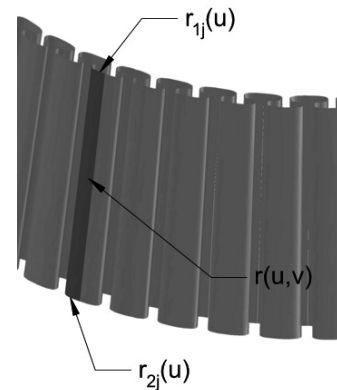
Figure 9: Building of ruled surface fragment upon Bezier curves

Figure 8: Location of control points of set of quadratic splines for description of 2 × 2 rib-knitted structures mid-surface

Curve lines $r_1(u)$ and $r_2(u)$ are represented as a combination of Bezier curves (equation 10):

$$r_i(u) = \{r_{i0}(u), r_{i1}(u), \ldots r_{in}(u)\}, \tag{10}$$

where $r_{ij}(u)$ is a quadratic Bezier curve.

In order to provide the geometric description of a rib stitch pattern (cf. Figure 6), eight quadratic Bezier curves are used. In such a case, a parametric equation of the elementary curve can be presented as follows (equation 11).

$$r_{ij}(u) = P_{i,k}(1-u)^2 + 2 \cdot P_{i,k+1}(1-u) \cdot u + P_{i,k+2}u^2 \tag{11}$$

where k = 0 … 14 corresponds to the aggregate number of control vertices that determine the directions of tangents for all elementa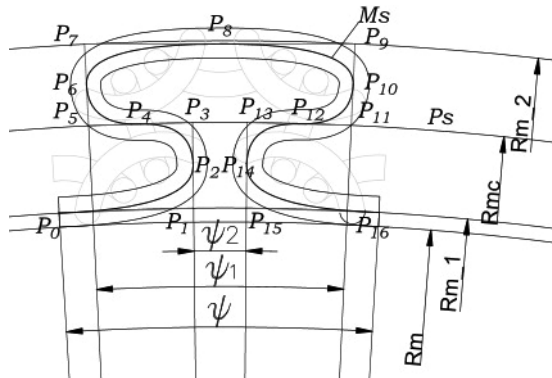ry curves. The combination of elementary curves represents the central line of a rib stitch pattern *Ms* (cf. Figure 8). To increase smoothness between adjoining quadratic Bezier curves, it is necessary that the last point of the first segment and the first point of the second segment coincide as shown in Figure 10. Therefore, the equation can be written as (equation 12):

$$r^{(1)}(1) = r^{(2)}(0) \tag{12}$$
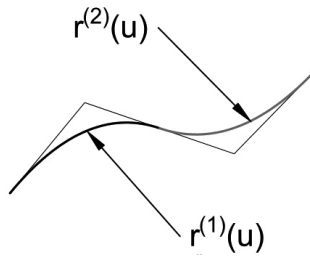
Figure 10: Ensuring smooth connection between adjoining Bezier curves

In addition, the joint segment must have a continuous inclination at the connection point (equation 13):

$$r^{(1)}(1) = \alpha_1 T; r^{(2)}(0) = \alpha_2 T, \tag{13}$$

where *T* is a unit vector of a common tangent, and α_1, α_2 are scalar constants that influence the completeness of a segment. It can be proved by the example (cf. Figure 8):

$$r^{(1)}(u) = P_0(1-u)^2 + 2P_1(1-u) \cdot u + P_2u^2 \tag{14}$$

$$r^{(2)}(u) = P_2(1-u)^2 + 2P_3(1-u) \cdot u + P_4u^2 \tag{15}$$

$$r^{(1)}(1) = P_2; r^{(2)}(0) = P_2; \tag{16}$$

The first condition is considered. For the continuity of a tangent tilt,

$$r'^{(1)}(1) = 2(P_2 - P_1); r'^{(2)}(0) = 2(P_3 - P_2); \tag{17}$$

the unit vector of a common tangent can be calculated as follows:

$$T = \frac{2(P_2 - P_1)}{\alpha_1} = \frac{2(P_3 - P_2)}{\alpha_2} \tag{18}$$

where α_1 and α_2 are tangent vector lengths.

Therefore, the equation for the segment of a cone surface can be represented with the following formula (equation 19):

$$r(u,v) = [P_{1,k}(1-u)^2 + 2P_{1,k+1}(1-u)u + P_{1,k+2}u^2] \cdot \\ \cdot (1-v) + \begin{bmatrix} P_{2,k}(1-u)^2 + 2P_{2,k+1}(1-u)u \\ + P_{2,k+2}u^2 \end{bmatrix} \cdot v \tag{19}$$

where $0 \le u, v \le 1$.

3.4 Software development

The above proposed mathematical calculations aimed at the geometric description of the mid-surface of rib-knitted shells were installed into the LastikTube program. The latter helps improving the process of designing rib-knitted structure tubular garment parts (cf. Figure 11).
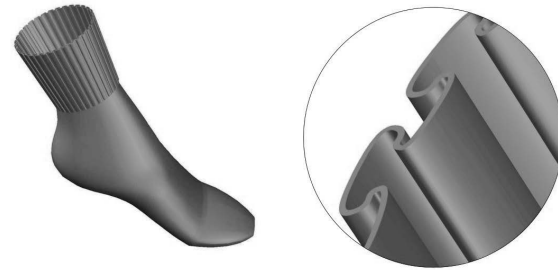
Figure 11: Macro-model of sock, designed as elastic shell, put upon surface approximated by shape of truncated cone

The program contains a database, created during experimental studies, which allows determining the relationship between the geometric characteristics of the surface, e.g. width of Wru pattern, and the widths of its structural parts, i.e. *C* convex and a visible part of a concave area *S* of the pattern unit, created on the base of the analysis of rib knits of various raw materials and pattern numbers.

4 Conclusion

Modelling the physical and mechanical knitwear behaviour in the program environment is one of the most promising ways to increase the usability and functionality of knitwear. During the study, the assumption was made that certain parts of knitwear made by even rib stitch patterns, e.g. 2 × 2, 3 × 3 etc., can be described as thin-walled elastic shells, the middle surface of which is a linear surface created upon a set of Bezier curves located along the contours of truncated cone bases. The software, developed in the course of the research, was used to broaden the capability of computer aided design of knitwear, including the macro-modelling of ribbed tubular garments. 3D models, generated by means of the program, can be used for the assessment of thermophysiological comfort.

References

1. NIIMI, Yoshitaka, HAVELKA, Antonin, KANAI, Hiroyuki. A proposal for designing knitted fabric for the "wear promotes exercise effect" with the purpose of improving comfort. *Fibres and Textiles*, 2018, **25**(4), 71–77, http://vat.ft.tul.cz/2018/4/VaT_2018_4_13.pdf.
2. HERCIKOVA, Eva, KOMARKOVA, Petra, GLOMBIKOVA, Viera, HAVELKA, Antonin, KUS, Zdenek. Evaluation of thermal properties of textile structures under fast flowing air conditions. *Fibres and Textiles*, 2018, **25**(4), 31–34, http://vat.ft.tul.cz/2018/4/VaT_2018_4_7.pdf.
3. ANGELOVA, Radostina, REINERS, Priscilla, GEORGIEVA, Elena, KONOVA, Hristina Plamenova, PRUSS, Bianca, KYOSEV, Yordan. Heat and mass transfer through outerwear clothing for protection from cold: influence of geometrical, structural and mass characteristics of the textile layers. *Textile Research Journal*, 2017, **87**(9), 1060–1070, doi: 10.1177/0040517516648507.
4. GÜNEY, Sestaç, AKGÜNOĞLU, Betül, KAPLAN, Sibel. Parameters affecting sport socks pressure and pressure prediction from tensile characteristics. *Fibres and Textiles*, 2017, **24**(1), 68–72, http://vat.ft.tul.cz/Archive/VaT_2017_1.pdf.
5. MENGNA, Guo, KUZMICHEV, Viktor. Pressure and comfort perception in the system "female body–dress". *AUTEX Research Journal*, **13**(3), 71–78, doi: 10.2478/v10304-012-0032-6.
6. NAKHAICHUK, Oleg, ZAKHAROVA, Elina, MIZRAKH, Arkadij, HOROBCHYSHYNA, Valentina. Pressure forecasting of textile materials in the "figure-dress" system. *Bulletin of Khmelnytskyi National University. Technical Sciences*, 2020, **283**(2), 135–140, doi: 10.31891/2307-5732-2020-283-2-135-140, http://journals.khnu.km.ua/vestnik/?p=1239.
7. BARDOS DE VASCONCELOS, Fernando, CASACA, Fabiano, GOMES DE VASCONCELOS, Fernanda, MARCICANO, Joao Paulo Pereira, SANCHES, Regina Aparecida. Design of elastic garments for sports in circular knitting. *International Journal of Textile and Fashion Technology (IJTFT)*, 2013, **3**(1), 39–48, http://www.tjprc.org/publishpapers/--1357879773-4.Design%20full.pdf.
8. KYOSEV, Yordan, Geometrical and mechanical modelling of textile structures at fiber and yarn level – software and data structures. *Vlakna a Textil*, 2017, **24**(1), 3–9, http://vat.ft.tul.cz/Archive/VaT_2017_1.pdf.
9. KURBAK, Arif, EKMEN, Ozgur. Basic studies for modeling complex weft knitted fabric structures. Part I: a geometrical model for widthwise curlings of plain knitted fabrics. *Textile Research Journal*, 2008, **78**(3), 198–208, doi: 10.1177/0040517507082352.
10. KALDOR, Jonathan, JAMES, Doug, MARSCHNER, Steve. Simulating knitted cloth at the yarn level. In *SIGGRAPH '08: Special Interest Group on Computer Graphics and Interactive Techniques Conference, Los Angeles, California, August 11 - 15, 2008*. New York : Association for Computing Machinery, 2008, doi: 10.1145/1399504.1360664.
11. LOGINOV, Alexey, GRISHANOV, Sergei. and HARWOOD, R. (2002a), Modelling the load-extension behaviour of plain-knitted fabric. Part I: a unit-cell approach towards knitted-fabric mechanics. *The Journal of The Textile Institute*, **93**(3, Parts 1 and 3), 218–238, doi: 10.1080/00405000208630566.
12. *Modelling and predicting textile behaviour*. Edited by X. Chen, X. (Woodhead Publishing Series in Textiles: No 94.) Woodhead Publishing, CRC Press, 2010, 536 p.
13. PETRAK, Slavenka., MAHNIC NAGLIC, Maja. Dynamic anthropometry – defining

protocols for automatic body measurement. *Tekstilec*, 2017, **60**(4), 254–262, doi: 10.14502/Tekstilec2017.60.254-262.

14. ABGHARY, Mohammad Javad, NEDOUSHAN, Reza Jafari, HASANI, Hossein. Simulation of the spherical deformation of biaxial weft-knitted fabrics using meso and macro models. *Fibres and Polymers*, 2016, **17**(10), 1702–1708, doi: 10.1007/s12221-016-6511-y.

15. ABGHARY, Mohammad Javad, HASANI, Hossein, NEDOUSHAN, Reza Jafari. Geometrical modeling for bi-axial weft-knitted fabrics based on rib structure. *Indian Journal of Fibre & Textile Research*, 2017, **42**(4), 431–438, http://nopr.niscair.res.in/handle/123456789/43245.

16. LIU, Dani, CHRISTE, Daniel, SHAKIBAJAHROMI, Bahareh, KNITTEL, Chelsea, CASTANEDA, Nestor, BREEN, David, DION, Genevieve, KONTSOS, Antonios. On the role of material architecture in the mechanical behavior of knitted textiles. *International Journal of Solids and Structures*, 2017, **109**, 101–111, doi: 10.1016/j.ijsolstr.2017.01.011.

17. WEEGER, Oliver, SAKHAEI, Amir Hosein, TAN, Ying Yi et al. Nonlinear multi-scale modelling, simulation and validation of 3D knitted textiles. *Applied Composite Materials*, 2018, **25**(4),797–810, doi: 10.1007/s10443-018-9702-4.

18. QI, Yexiong, JIANG, Yaming, XIANG, He, QASEEM, Saood, LI, Xuezhen & WANG, Menghua. Macro-geometric method based modeling of the uniaxial tensile properties of tri-axial knitted fabrics. *The Journal of The Textile Institute*, 2020, **111**(10), 1502–1510, doi: 10.1080/00405000.2019.1706224.

19. POINCLOUX, Samuel, MOKHTAR, Adda-Bedia, LECHENAULT, Frederic. Geometry and elasticity of a knitted fabric. *Physical Review X*, 2018, **8**(2), 021075, doi: 10.1103/PhysRevX.8.021075.

20. ZUBRYTSKAYA, Halyna, YELINA, Tetiana, HALAVS'KA, Liudmyla. Study of the process of uniaxial deformation of 2+2 rib fabrics under the action of tensioning force. *Bulletin of Khmelnytskyi National University,* 2020, **285**(3), 222–226 [in Ukrainian], doi: 10.31891/2307-5732-2020-285-3-35, http://journals.khnu.km.ua/vestnik/?p=1343.

21. YELINA, Tetiana, HALAVSKA, Liudmyla, MANOILENKO, Oleksandr, Development of a parametric surface model of rib 2x2 knits. Bulletin of the Kyiv National University of Technologies and Design, 2020, **144**(2), 80–89 [in Ukrainian], doi: 10.30857/1813-6796.2020.2.8.

22. YELINA, Tetiana, PUKHOVA, Angelina, ROMANIUK, Veronika, HALAVSKA, Liudmyla. Study of the process of stretching in the course-wise direction of different knitting rib structure. *Bulletin of the Kyiv National University of Technologies and Design*, 2020, **148**(4), 98–106 [in Ukrainian], doi: 10.30857/1813-6796.2020.4.9.

23. LONG, James, BURNS, Katherine, and YANG, Jingzhou (James). Cloth Modeling and simulation: a literature survey. In *Proceedings. Third International Conference, ICDHM 2011, Orlando, Florida, USA, July 9-14, 2011.* Edited by Vincent G. Duffy. Berlin, Heidelberg : Springer, 2011, 312–320, doi: 10.1007/978-3-642-21799-9_35.

24. SPAHIU Tatjana, SHEHI E, PIPERI Erald. Personalized avatars for virtual garment design and simulation. *UNIVERSI – International Journal of Education, Science Technology, Innovation, Health and Environment*, 2015, **1**(3), 56–63.

25. KLEIN, Hartmut, JENEROWICZ, Marcin, TRUBE, Niclas, BOLJEN, Matthias. How to combine 3D textile modeling with latest FE human body models. In *6th International Digital Human Modeling Symposium (DHM2020), Skövde, Sweden, 31 August - 2 September 2020.* IOS Press, doi: 10.3233/ATDE200022.

Sibel Kaplan, Betül Akgünoğlu
Suleyman Demirel University, Textile Engineering Department, West Campus, Isparta, Turkey

Transfer and Friction Characteristics of Sports Socks Fabrics Made of Synthetic Fibres in Different Structures

Prenos tekočin in torne lastnosti sintetičnih pletiv za športne nogavice v različnih vezavah

Corresponding author/*Korespondenčna avtorica*:
Prof. Dr. Sibel Kaplan
E-mail: sibelkaplan@sdu.edu.tr
Phone: 0090 246 2111183
ORCID ID: 0000-0002-7247-135X

Abstract

Sports socks fabrics produced from polyester, polypropylene, their modified forms Thermocool®, Polycolon®, in three different structures (single jersey, piquet, terry) were investigated for their skin-fabric friction, permeability (air and water vapour), liquid absorption and transfer (absorbency, immersion, absorption capacity, wetback and drying) properties. According to the results, the effect of structure is dominant for frictional characteristics but focusing on the material, polypropylene created a bulkier and lighter structure with lower friction coefficients, an advantage for sports socks. The effect of structure is greater than the material also for some thermal comfort parameters, e.g. air permeability and absorbency. Focusing on materials, besides their better liquid transfer characteristics, modified forms of both fibres had worse performances for air permeability and absorbency compared to their standard forms. Absorption capacity, wetback and drying performances were related to fabric density besides the polyester's higher regain capacity. While Polycolon® had superiority for wetback performance against standard polypropylene, this was not the case for Thermocool®; however, both modified materials showed apparent superiority for drying periods. Piquet structures were advantageous for absorption capacity and wetback performances for polypropylene. For sports socks parts, specific needs can be met by changing the fabric structure. Considering the materials, polypropylene and Polycolon® can be recommended for both thermal and tactile aspects.
Keywords: sports socks, Thermocool®, Polycolon®, friction, liquid transfer

Izvleček

Na levo-desnih pletivih za športne nogavice, izdelanih iz poliestra, polipropilena in njunih modificiranih oblik Thermocool® in Polycolon® v treh vezavah, tj. enostavni levo-desni, pike in frotir, so bili preizkušani trenje pletiva ob kožo, prepustnostne lastnosti (zračna prepustnost, prepustnost vodne pare), absorpcija in prenos tekočine (vpojnost, omočljivost pri potapljanju, zmogljivost vpojnosti, povratno vlaženje in sušenje). Glede na rezultate ima vezava prevladujoč vpliv na torne lastnosti, pri osredotočenju na material pa je pletivo iz polipropilena lažje in bolj voluminozno ter ima nižji koeficient trenja, kar je za športne nogavice prednost. Vpliv vezave je večji od vpliva materiala tudi za nekatere dejavnike toplotnega udobja, kot sta zračna prepustnost in vpojnost. Če se osredinimo na materiale, modificirani tipi vlaken Thermocool® in Polycolon® bolje prenašajo tekočine ter imajo slabšo zračno prepustnost in vpojnost kot standardni tipi vlaken. Vpojnost, povratno vlaženje in sušenje so bili povezani z višjo reprizo poliestra in gostoto pleti-

va. Medtem ko je bil za Polycolon® prenos vlage na hrbtno stran večji kot pri standardnem polipropilenu, to ne velja za Thermocool®; oba modificirana materiala sta občutno boljša glede časa sušenja. Vezava piké ugodno vpliva na zmogljivost vpojnosti in povratno vlaženje pletiva iz polipropilena. Za sestavne dele športnih nogavic je zadovoljevanje specifičnih potreb mogoče doseči s spremembo vezave pletiva, glede izbire materiala pa sta z vidika toplotnih in taktilnih lastnosti priporočljiva polipropilen in Polycolon®.

Ključne besede: toplotna udobnost, tipna udobnost, prenos mase

1 Introduction

Consumers require multifunctional apparel products with superior comfort performance and sports socks is one of the clothing groups for which both thermal, pressure and tactile comfort performances are crucial. Socks comfort has a big influence on the performance of sports people and it is difficult to enable dryness, necessary insulation and mechanical comfort for different kinds of sports shoes as it is a closed system. Compression support, minimisation of foot blisters as a result of cyclic friction under high temperature and relative humidity within the shoes [1], moisture management properties, anatomically placed cushioning and shock absorbing properties [2] can be listed as characteristics of optimal sports socks. Sweating, which may reach up to 0.5 litres per foot during a sports activity within shoes not allowing adequate liquid, and water vapour transfer is the main reason for dampness sensation, decreased insulation, foot injuries occurring as a result of softer skin or wet fabric having a higher friction coefficient, some health problems sourcing from microorganisms and increased fatigue feeling [3–10]. Therefore, besides liquid absorption period and capacity, good athletic socks fabric must also transport sweat away from the foot surface not to create the above mentioned problems. Mechanical interactions between the skin and fabric are the sources of skin irritations for some specific garments such as socks and fitted sports clothing, e.g. swimwear, leggings etc. [11]. The mentioned friction characteristics of fabrics produced from different materials and fabric structures are generally evaluated by subjective tests [12–14] and fabric surface analyses with a reciprocating linear tribometer [15–17], horizontal platform method [18] and 3D biomechanical models with computational simulations [19].

The material and fabric structure of sports socks are the determinant factors of comfort and deformation related problems. Ideally, under pressure, an athlete should wear hydrophobic socks in regions prone to blister formation and shoes with a hydrophilic inner liner [20]. Sports socks are usually produced from standard or modified synthetic fibres and their blends for insulating and moisture wicking abilities without absorption and lighter weight upon sweating, enabling less energy expenditure [21–24]. Polyester, polyamide, polypropylene, acrylic (generally as pile structure) and elastane are the most common fibres used in sports and active wear [22, 24]. Polypropylene and its modified forms are increasingly being used in the sportswear market for generally inner layers [21] with their very low moisture absorbency, insulation retaining performance, excellent moisture vapour permeability and transplanar/in plane wicking capabilities [11]. A worsted spun yarn, Polycolon®, was suggested for cold weather protective gloves [25] and for shoe insoles with its good capillary wicking abilities [26]. Bioceramics (1%) were also used for socks and managed moisture on foot better than cotton/polyester [27]. Generally single jersey, false rib, terry and piquet structures are used on different parts of sports socks for thermal comfort enhancements, to decrease friction and pressure on specific parts [2].

In this study, permeability, liquid absorption/transfer and skin-fabric friction characteristics of sports socks fabrics produced from polyester, its modified form Thermocool®, polypropylene and its modified form Polycolon® were investigated. Single jersey (without elastane), piquet and terry fabrics were knitted to simulate structures on different parts of functional sports socks.

2 Materials and methods

2.1 Materials

Socks fabrics were knitted from Ne 26 standard polyester, its modified form Thermocool®, Ne 34 standard polypropylene and its modified form Polycolon® staple yarns, the characteristics of which are summarised in Table 1. Thermocool® is a unique blend of fibres with a hollow core that enables light weight,

Table 1: *Characteristics of yarns used for socks fabrics*
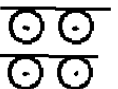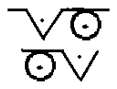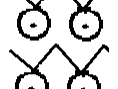
Fabric code	Knit type	Material	Yarn count	Twist coefficient (αe) [S.D.] [a]
PESA	Single jersey	100% polyester	227 dtex	4.34 [0.12]
PESB	Piquet	78% polyester/15% polyamide/7% elastane	227 dtex PES + 20/40dtex /13f PA gimped	–
PESC	Terry			
MPESA	Single jersey	100% Thermocool®	227 dtex	5.34 [0.02]
MPESB	Piquet	78% Thermocool®/15% polyamide/7% elastane	227 dtex PES + 20/40 dtex /13f PA gimped	–
MPESC	Terry			
PPA	Single Jersey	100% polypropylene	174 dtex	3.43 [0.10]
PPB	Piquet	74% polypropylene/17% polyamide/9% elastane	174 dtex PP + 20/40 dtex/13f PA gimped	–
PPC	Terry			
MPPA	Single Jersey	100% Polycolon®	174 dtex	3.29 [0.09]
MPPB	Piquet	74% Polycolon®/17% polyamide/9% elastane	174 dtex PP + 20/40dtex/13f PA gimped	–
MPPC	Terry			

[a] standard deviation

higher insulation and a channelled cross section for better wicking and drying abilities [28]. Polycolon® is a modified, polypropylene-based, worsted-spun long-staple yarn produced by Scholler. It has the lowest surface tension of all synthetic functional fibres and does not absorb moisture. With its good liquid transfer properties, it decreases the risk of blisters when used for socks. It is the lightest functional fibre in the world; around 40% lighter than cotton and 35% lighter than polyester [29].

Fabrics having single jersey, piquet and terry structures were knitted on a Lonati 400 socks knitting machine with 3 3/4 inch diameter, 200 needles and E value of 18. Single jersey fabrics were knitted without any other component to see the material effects clearly, while the piquet and terry structures were knitted with 20/40 dtex/13 f (spandex/polyamide) elastomeric inlay yarn (full plating). The socks parts where investigated knit types are used can be seen in Table 2.

Table 2: *Knitting structures used on different parts of sports socks*

Knit code	A	B	C
Knit type	Single Jersey	Piquet	Terry
Needle diagram			
Regions of knit types on socks			

2.2 Methods

2.2.1   Physical and frictional characteristics

Weight and thickness were tested according to TS 251 and ASTM D 1777 with 5 g/cm² pressure with a James Heal R&B Cloth Thickness Tester (James Heal Corp., UK) in turn. Physical porosity characteristics were calculated according to Equation 1 [22].

$$P = \left(1 - \frac{m}{\rho}\right) x\ 100 \qquad (1)$$

where *P* is porosity (%), *m* is fabric density (g/cm³) and ρ is fibre density (g/cm³).

Friction coefficients of socks fabrics were calculated with friction force measurements conducted according to ASTM D 1894-14 with a Lloyd LR5K Plus (Lloyd Instruments, Inc., USA) tensile strength tester. Static and kinetic friction coefficients were calculated (cf. Equation 2) from force results obtained for wale direction as a result of movement of a sled (3.9 cm × 4 cm) covered with lambskin with a speed of 25 mm/min and normal force of 2.50 g/cm² on a platform covered with the socks fabric (inner side up).

$$\mu = F / N \qquad (2)$$

where *N* is normal force (N) and *F* is static/kinetic frictional force.

2.2.2   Permeability and liquid absorption/transfer characteristics

The air and water vapour permeability values were tested according to TS 391 EN ISO 9237 by FX Textest 3300 (James Heal Corp., UK) and ASTM E96-16 Cup Method in turn. The absorbency and liquid transfer characteristics of samples were tested with drop test according to AATCC 79:2018 and with sinking time (immersion) test according to AATCC 79-Method B. Absorption capacities were calculated according to the modified version of ISO 20158:2018 and drying periods were determined according to a preceding study [30] until the fabrics come to their conditioned weight. From drying graphics, slopes of the weight loss lines (amount of evaporated liquid/evaporation period) that give idea about the drying rates were calculated to have an exact comparison. Transverse wicking (wetback) rates were determined according to a preceding study [31] from the liquid amounts transferred from the wet sample (including liquid equal to their

absorption capacities) to the dry samples 74.5 mm in diameter under the pressure of 15.6 kg/m² after the periods of 5 min, 10 min, 15 min, 20 min, 25 min and 30 min.

All fabrics were washed according to TS EN ISO 6330:2012 in a Wascator FOM71 CLS washing machine (James Heal and Co. Ltd., Halifax, UK) and conditioned under standard atmospheric conditions (20 ± 2 °C, 65 ± 2% RH) according to ASTM D1776-08e1 (2009) before the tests.

2.2.3   Statistical analyses

IBM SPSS 21.0 Statistics Software (SPSS Inc. USA) was used for the Multivariate Analysis of Variance (MANOVA) test to investigate the effects of material and structure on the investigated parameters. MANOVA is used when more than one factor affecting the dependent variable, including all their combinations at different levels, are studied and tested. Duncan and Student Newman Keuls (SNK) tests were used to examine significant differences. Statistical significances were investigated with p values ($p < 0.05$ meaning significant difference). A correlation analysis was conducted to determine the relationships among physical and mechanical parameters.

3 Results and discussion

Material (polyester, polypropylene, Thermocool®, Polycolon®), structure/knit type (single jersey, piquet and terry) of the fabrics and their interactions obtained from MANOVA had significant effects on all physical, surface, permeability and liquid transfer characteristics, as it can be seen in Table 3 ($p < 0.05$).

Table 4 shows material effects of socks fabrics grouped according to three different knit types.

3.1 Physical and surface properties

Physical properties of socks fabrics produced from different synthetic yarns in different knit types are compiled in Table 5.

As it can be seen in Table 4, for single jersey fabrics, the lowest weight belonged to polypropylene (PP) followed by Polycolon® (MPP) related to their fibre densities, while the polyester (PES) fabric had significantly the maximum weight. The trend is valid for other structures except for the higher value of MPP for the piquet fabric. Thickness values

Table 3: MANOVA results of main factor-parameter interactions

Dependent variable	Significance values of main factors (p)		
	Material	Structure	Material × structure
Weight	0.00	0.00	0.00
Thickness	0.00	0.00	0.00
Static friction coefficient	0.00	0.00	0.00
Kinetic friction coefficient	0.000	0.001	0.000
Air permeability	0.00	0.00	0.00
Absorption period (drop) test	0.00	0.00	0.00
Immersion period	0.00	0.00	0.00
Absorption capacity	0.00	0.00	0.00

Table 4: Post-hoc test results of fabric properties

Property	Single jersey	Piquet	Terry
Weight	PP < MPP < MPES < PES	PES < PP < MPES = MPP	PP = MPP < PES = MPES
Thickness	PES = MPES < PP = MPP	MPES = PP < PES < MPP	PES < MPES = MPP < PP
Static fric. coeff.	MPP = PP = PES < MPES	PP = MPES = MPP < PES	PP = MPP < MPES = PES
Kinetic fric. coeff.	PP = MPP = PES < MPES	PP = MPES = MPP < PES	PP = MPP < MPES < PES
Air permeability	MPES < PES < MPP < PP	MPP < PP < MPES < PES	MPP < PP < MPES < PES
Absorption period (drop) test	PES < PP < MPES < MPP	PP did not absorb MPP did not absorb PES=MPES	PP did not absorb MPP did not absorb PES < MPES
Immersion period	PP did not sink MPP did not sink PES < MPES	PP did not sink MPP did not sink MPES < PES	PP did not sink MPP did not sink MPES < PES
Absorption capacity	PP = MPP < MPES < PES	Statistically identical	PP < MPP < PES < MPES

(cf. Figure 1) are generally higher for PP and MPP, enabling bulkier structures. However, there are some exceptions that PES had higher thickness than PP for the piquet fabric, and the modified forms of both (MPES and MPP) had identical thickness values for the terry fabric. According to the porosity values compiled in Table 5, higher values belonged to the piquet and single jersey structures for polyester and polypropylene fabrics in turn. The piquet and terry structures generally had identical porosity values due to the tuck and pile loops within the fabric structures in turn. The differences among polyester and polypropylene fabrics were not clear as the porosity equation includes a ratio of fibre and fabric densities, despite the lower fabric (as a result of lower yarn linear density) and fibre densities of polypropylene.

According to friction coefficient results, the minimum and identical static and kinetic friction
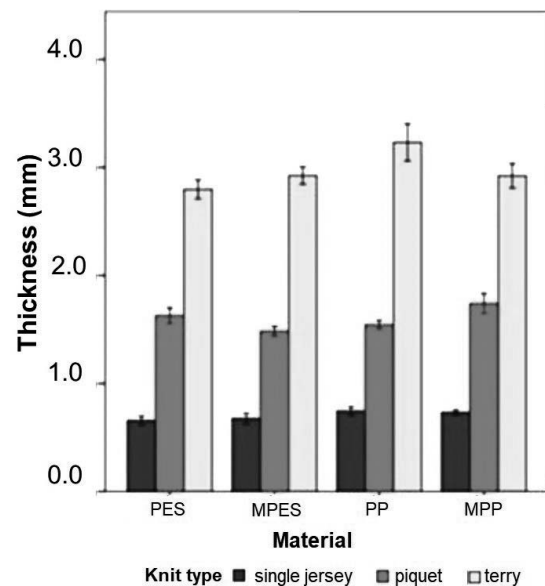
Figure 1: Fabric thickness values

Table 5: Physical properties of fabrics

Fabric code	Courses-wales (1/cm)	Weight (g/m²) [S.D.]	Density (g/cm³) [S.D.]	Porosity (%) [S.D.]
PESA	70-42	255.20 [2.34]	0.39 [0.013]	71.85 [0.92]
PESB	84-50	266.4 [5.48]	0.16 [0.005]	94.81 [0.36]
PESC	80-56	544.62 [26.80]	0.19 [0.013]	85.88 [0.95]
MPESA	70-42	149.60 [9.22]	0.22 [0.013]	83.93 [0.93]
MPESB	88-75	264.87 [3.00]	0.18 [0.003]	87.05 [0.25]
MPESC	92-57	553.35 [25.52]	0.19 [0.007]	86.29 [0.56]
PPA	84-51	93.70 [1.92]	0.13 [0.005]	86.01 [0.55]
PPB	86-38	254.98 [5.01]	0.17 [0.005]	81.63 [0.61]
PPC	84-40	520.98 [4.46]	0.16 [0.006]	82.08 [0.71]
MPPA	72-54	94.98 [1.38]	0.13 [0.001]	85.59 [0.12]
MPPB	80-54	263.40 [3.21]	0.15 [0.004]	83.17 [0.43]
MPPC	74-55	475.33 [12.04]	0.16 [0.007]	81.91 [0.83]

Legend: PES: polyester, MPES: Thermocool®, PP: polypropylene, MPP: Polycolon®
       A: Single Jersey, B: Tucked, C: Terry

coefficients were obtained for PP, MPP (confirming Dyck's study in 1993), maximum values belonged to MPES for single jersey, and PES for the piquet and terry fabrics (cf. Figure 2). For the knit types, while terry fabrics created rougher surfaces for polyester fabrics, single jersey fabrics were rougher for polypropylene according to both static and kinetic friction coefficients. Both material and fabric structure were affective [18]; however, the effect of the fabric structure seems greater on friction coefficients confirming the results by Richie [32].

3.2 Permeability and liquid absorption/ transfer properties

The permeability and absorbency/transfer characteristics of the socks fabrics can be seen in Table 6.
Air permeability results (cf. Figure 3), giving idea about the porous structure of the fabric, show the ranking of PP, MPP, PES and MPES from the maximum values for single jersey fabrics, a result proportional to fabric density and porosity values (cf. Table 4). Worse performances of MPES and MPP, when compared to their standard forms, can be attributed to the rougher surfaces of modified fibres within staple yarn having higher frictional area with air. While terry fabrics had significantly lower air permeability values than piquet fabrics (cf. Figure 3), material trends are the same for both structures. Both standard and modified PES fabrics had higher values than PP and modified PP for piquet and terry fabrics as a result of their higher porosity, confirming a preceding study [33]. As a general look, effects of fabric structure seem greater than material on air permeability, confirming a preceding study [11]. The effect of linear density was not observed for piquet and terry structures including elastomeric inlay yarn.

a)   b)
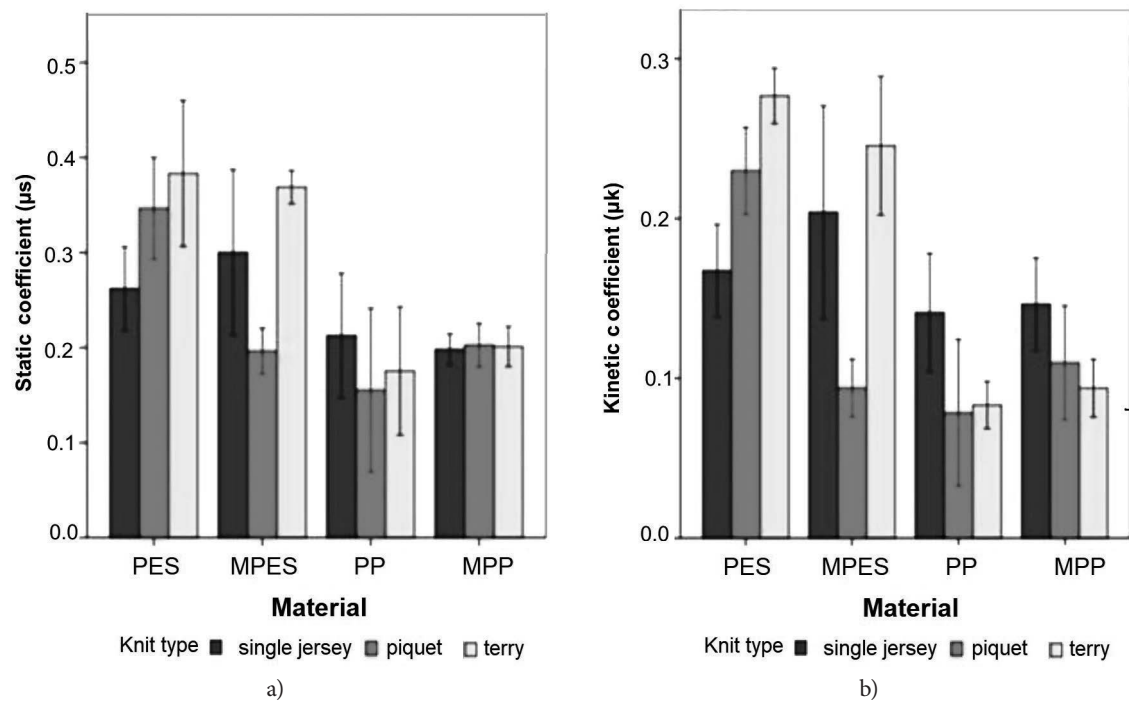
Figure 2: Static (a) and kinetic (b) friction coefficients
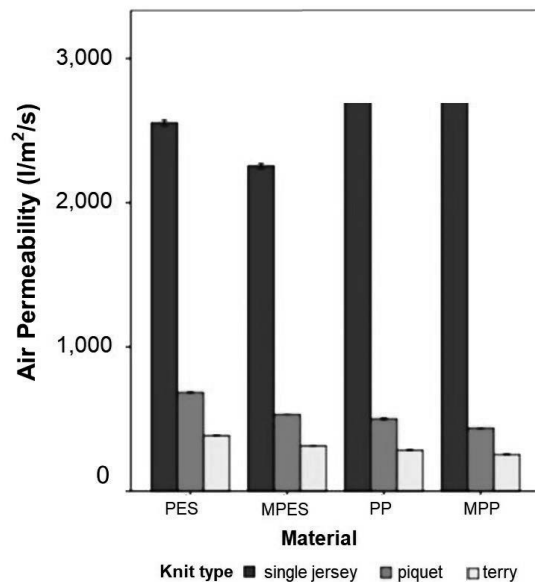
Figure 3: Air permeability values

Water vapour permeability results could not discriminate the fabrics (p > 0.05), probably due to the insufficient precision of the cup method and environmental condition variations (cf. Table 6), despite the test conducted under standard atmospheric conditions.

To move in a fibrous medium, a liquid must wet the fibre surface before being transported through inter-fibre pores by means of capillary action. The fibre-liquid surface attraction force causes wetting action and is determined by fibre and fabric surface characteristics, pore distribution and liquid properties [34–35]. The PP and MPP fabrics did not absorb water within acceptable periods (around 5 seconds), except for the PP single jersey fabric (6.63 s), due to their lowest surface tensions (cf. Table 6). Only single jersey fabrics absorbed liquid within acceptable limits (2.24–8.08) as a result of their open pore structures where liquid can be bound better. MPES and MPP yarn fabrics (mainly designed for better liquid transfer and insulation) absorbed moisture within significantly longer periods than PES and PP as a result of irregular cross sections of these fibres that might decrease contact surface area with water, hence surface energy. Rougher surfaces of piquet and terry fabrics also decreased their surface energy that they absorbed water within 16.45–26.17 seconds contrary to the preceding statement about better wettability of rougher surfaces by well wetting fluids [35]. The procedure and real life simulation ability of the test method should also be considered, namely, sports socks are normally used within shoes under pressure and the surface energy surely differs under these conditions.

Table 6: Permeability and liquid absorption/transfer characteristics

Fabric code	Water vapour permeability (g/m²/24 h) [S.D.]	Absorption period (drop) test (s) [S.D.]	Sinking period (s) [S.D.]	Drying rate/speed (g/h)
PESA	659.57 [191.46]	2.24 [0.20]	102.01 [21.54]	0.477
PESB	561.91 [129.64]	20.14 [6.54]	427.39 [22.92]	0.762
PESC	489.04 [49.33]	16.45 [6.18]	207.71 [19.45]	0.786
MPESA	604.21 [62.04]	8.08 [0.04]	–	0.435
MPESB	566.37 [40.90]	21.51 [0.13]	271.08 [90.14]	0.692
MPESC	616.85 [75.98]	26.17 [0.09]	173.78 [63.69]	0.866
PPA	493.80 [106.63]	6.62 [0.17]	–	0.344
PPB	580.36 [148.15]	–	–	0.779
PPC	569.70 [100.13]	–	–	0.651
MPPA	534.02 [94.58]	11.44 [0.15]	–	0.253
MPPB	609.98 [178.56]	–	–	0.764
MPPC	462.58 [42.32]	–	–	0.807

Legend: PES: Polyester, MPES: Thermocool®, PP: Polypropylene, MPP: Polycolon®
      A: Single Jersey, B: Tucked, C: Terry
      –: did not absorb water or did not sink

The immersion or sinking period results (cf. Table 6) giving idea about both absorption and transfer of liquid within a fabric were also in harmony with the absorption period results that the PP and MPP fabrics did not sink as they did not absorb liquid. Although designed for better transfer capability, the MPES fabric did not have superior performance than standard PES for single jersey fabric showing solely the material effect. MPES Thermocool® had lower sinking periods for both piquet and terry fabrics showing the effects of fibre cross sections and the porous structure of fabrics. The sinking time of about 5 seconds is generally considered satisfactory for well-prepared cellulosic materials [36] and none of the fabrics had a closer performance due to their hydrophobic natures. The absorption capacity values, which affect the dampness sensation, hence comfort, were discriminated more for terry fabrics. For the terry fabrics, MPES had better performances than PES, followed by MPP and PP (cf. Figure 4). Single jersey fabric results showing solely the material effect were the highest for PES; modified forms of both PET and PP could not show superior performances as the absorption capacity is related to the macromolecular structure of the fibre, not its cross section. Better performances of PES against PP can be attributed to their higher moisture regain values (0.4% when compared to 0% of polypropylene) [37]. When the fabric structure is considered, piquet structures had significantly better performances when compared to terry fabrics. Summing up, apart from the fibre macromolecular structure, the fabric structure is also effective on the absorption capacity confirming a preceding study [33].
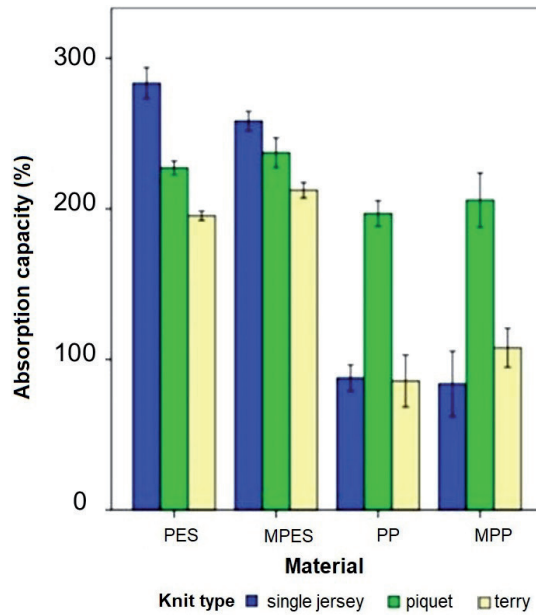
Figure 4: Absorption capacity values

Besides moisture absorption capacity of the socks fabric, its liquid transfer to another clothing layer (wetback) under pressure is important as well. The geometric configuration of pore structures (inter and intrayarn capillaries) and mechanical stress on a fabric play roles on water transport [11]. According to the transplanar wicking under pressure (wetback) test results (cf. Figure 5), standard polyester (PES) transferred the maximum amount

of liquid to the outer dry layer for all structures, hence a drier feeling, having the rating of single jersey (A), piquet (B) and terry (C) fabrics starting from the maximum. MPES fabrics come after PES fabrics for the determined period of 30 minutes and its ranking was obtained as piquet (B), terry (C) and single jersey (A) starting from the maximum. As it can be seen in Figure 5, all standard and modified PP fabrics (PP and MPP) transferred the minimum amount of liquid (ranging from 0.48% to 2.31%) to the outer dry layer proportional to their low absorption capacities and short drying periods. The greater amount of liquid was transferred by MPP Polycolon® when compared to standard PP and by piquet fabrics among other knit types confirming their absorption capacity results.

Moisture on the skin or clothing increases the heat loss of the body and also affects its overall performance and endurance. The drying ability of the knitted fabric is primarily affected by the mass per unit area and thickness [37]. The mentioned phenomenon is valid also for this study that terry fabrics with the maximum weight values (PES and MPES) dried within longer periods in spite of their lower absorption capacities than piquet fabrics (cf. Figure 6). Minimum drying periods belonged to polypropylene single jersey fabrics as expected, followed by polyester fabrics. According to slope calculations (cf. Table 6), terry fabrics made of MPES had the maximum drying speed (0.87), followed
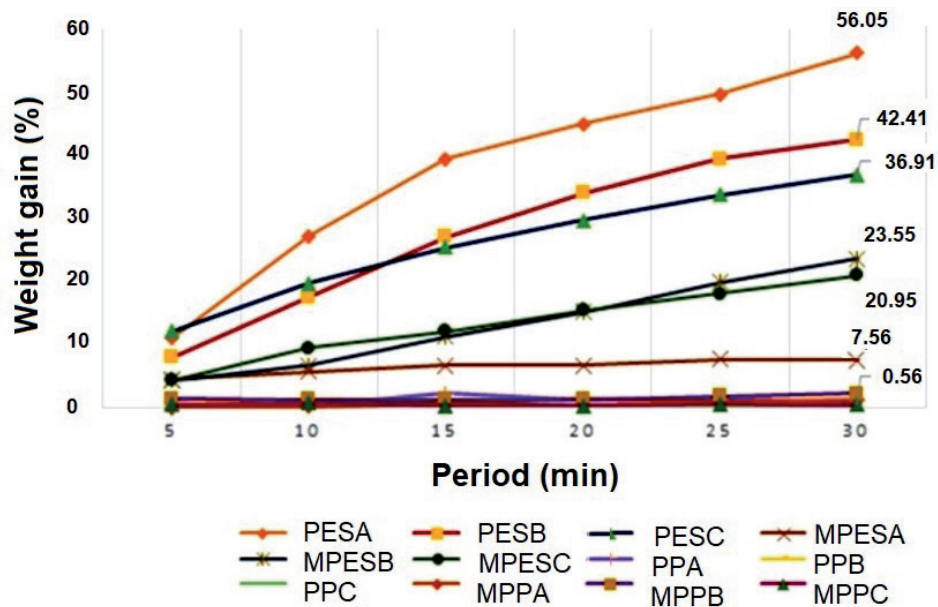
*Figure 5: Transferred liquid from wet to dry fabric (weight gain) under pressure
(A: single jersey, B: piquet, C: terry)*
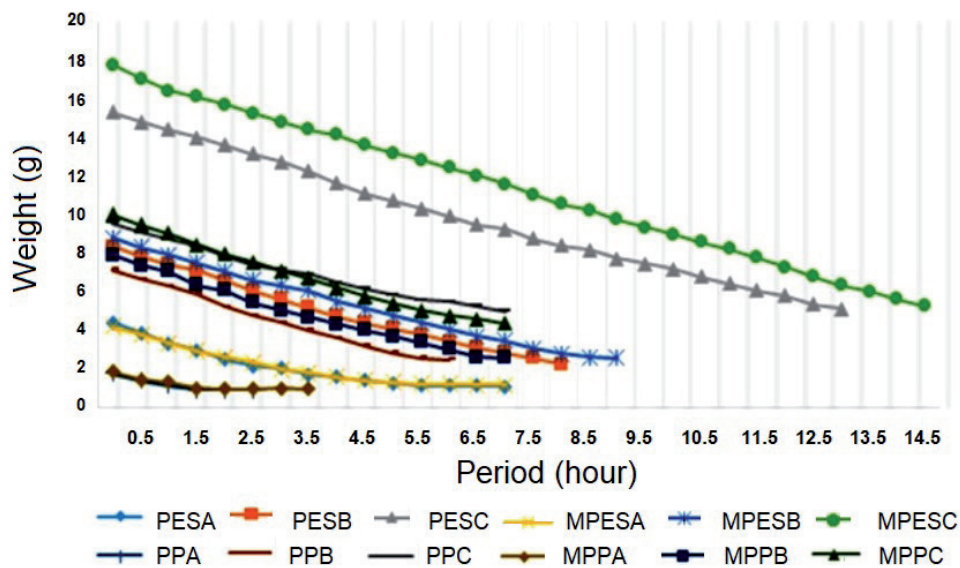
Figure 6: Drying periods (A: single jersey, B: piquet, C: terry)

by MPP Polycolon® (0.81). The drying speed values increased starting from single jersey fabrics (A), followed by piquet (B) and terry fabrics for all materials except for PP. The minimum drying speed belonged to single jersey MPP fabric (0.25) followed by single jersey PP fabric (0.34), MPES (0.44) and PES (0.48) fabrics. It was concluded that drying periods are related more to weight and absorption capacities of fabrics.

According to the correlation analysis results, air permeability is negatively correlated with weight and thickness as expected. The denser the fabric, the less air passes through it. The absorption period (drop) test results are correlated with surface and porosity properties, which shows the effect of surface and structural features on surface energy, hence absorbency of the fabric. Other significant correlation coefficients are compiled in Table 7.

4 Conclusion

Sports socks have a decisive influence on comfort and performance of sports people. The perceived comfort, mainly affected by temperature and dampness feelings, depends on the fibre content and construction of socks. Moreover, frictional deformation occurring on foot skin, perceived by mechanoreceptors, is also important for sports performance. During walking or running, besides cyclic pressure, friction and shear forces resulting from forward or sideways momentum of the athlete, increased moisture level and temperature within sports shoes are the main reasons for foot blisters. Therefore, in this study, friction, permeability and liquid transfer characteristics of socks fabrics produced from standard and modified forms of polyester and polypropylene fabrics in different

Table 7: Correlation analysis results

Property	Weight	Thickness	Water vapour perm.	Static friction coeff.	Kinetic friction coeff.	Porosity
Weight		0.904 [b]				
Air permeability	−0.699 [a]	−0.837 [b]				
Absorption period (Drop)				0.661 [a]	0.630 [a]	0.645 [a]
Absorption capacity			0.678 [a]			
Static friction coeff.					0.975 [b]	

[a], [b]: significant for $p = 0.05$, $p = 0.01$ in turn

structures (single jersey, piquet and terry) were investigated. According to the results, both standard and modified polypropylene Polycolon® gave lighter and bulkier fabrics, which is an advantage for permeability, hence drying performance of the socks. Polypropylene fabrics also created lower friction coefficients, meaning less deformation on wet skin when compared to polyester. Polyester, especially the standard one, has a bigger potential for skin deformation, the effect of fabric structure here being greater. The modified forms of polyester and polypropylene (Thermocool® and Polycolon®) had worse performances for air permeability, which may be related to their higher fibre surface areas. For liquid absorption, polyester was advantageous, but piquet and terry structures of polypropylene did not absorb liquid. The modified polyester Thermocool® did not have a superiority for liquid absorption, but it transferred liquid better for piquet and terry structures. While the absorption capacity is related to the regain capacity of the fibre and fabric density, besides its lower capacity, polypropylene had better performances in piquet structure which is also the case for wetback performance. Polycolon® had better wetback performance when compared to standard polypropylene, which was not the case for polyester. Both Thermocool® and Polycolon® had better performances for drying periods. Yarn linear densities of polyester and polypropylene fabrics surely had influence on fabric density, porosity and hence permeability characteristics, which can be accepted as a weakness of this study. In conclusion, polypropylene, especially modified form Polycolon® and piquet structures, can be suggested for plantar and lateral foot parts where blisters occur during running under high moisture and temperature conditions.

Acknowledgments

References

1. DAN, R., FAN, X. R., XU, L. B., ZHANG, M. Numerical simulation of the relationship between pressure and material properties of the top part of socks. *Journal of the Textile Institute*, 2013, **104**(8), 844–851, doi: 10.1080/00405000.2012.758516.
2. ASHFORD, R. L., WHITE, P., INDRAMOHAN, V. The aerodynamics of running socks: Reality or rhetoric? *The Foot*, 2011, **21**(4), 184–187, doi: 10.1016/j.foot.2011.06.002.
3. HOLE, L. G. Sweat disposal from footwear and health and hygiene of foot skin. *Journal Society Cosmetic Chemists*, 1973, **24**(1), 43–63, https://library.scconline.org/v024n01/41.
4. CAMERON, B. A., BROWN, D. M., DALLAS, M. J., BRANDT, B. Effect of natural and synthetic fibers and film and moisture content on stratum corneum hydration in an occlusive system. *Textile Research Journal*, 1997, **67**(8), 585–592, doi: 10.1177/004051759706700806.
5. LI, Y., ZHU, Q., YEUNG, K. W. Influence of thickness and porosity on coupled heat and liquid moisture transfer in porous textiles. *Textile Research Journal*, 2002, **72**(5), 435–446, doi: 10.1177/004051750207200511.
6. ZHANG, P., GONG, R. H., YANAİ, Y., TOKURA, H. Influence of clothing material properties on rectal temperature in different environments. *International Journal of Clothing Science and Technology*, 2002, **14**(5), 299–306, doi: 10.1108/09556220210446112.
7. GERHARDT, L. C., STRÄSSLE, V., LENZ, A., SPENCER, N. D., DERLER, S. Influence of epidermal hydration on the friction of human skin against textiles. *Journal of The Royal Society Interface*, 2008, **5**(28), 1317–1328, doi: 10.1098/rsif.2008.0034.
8. ROSSI, R. M., STÄMPFLI, R., PSIKUTA, A., RECHSTEINER, I., BRÜHWILER, P. A. Transplanar and in-plane wicking effects in sock materials under pressure. *Textile Research Journal*, 2011, **81**(15), 1549–1558, doi: 10.1177/0040517511413317.
9. IRZMAŃSKA, E., DUTKIEWICZ, J. K., IRZMAŃSKI, R. New approach to assessing comfort of use of protective footwear with a textile liner and its impact on foot physiology. *Textile Research Journal*, 2014, **84**(7), 728–738, doi: 10.1177/0040517513507362.

10. TANG, K. P. M., KAN, C. W., FAN, J. T. Evaluation of water absorption and transport property of fabrics. *Textile Progress*, 2014, **46**(1), 1–132, doi: 10.1080/00405167.2014.942582.

11. ZHONG, W., XING, M. M., PAN, N., MAIBACH, H. I. Textiles and human skin, microclimate, cutaneous reactions: an overview. *Cutaneous and Ocular Toxicology*, 2006, 25(1), 23–39, doi: 10.1080/15569520500536600.

12. BERTAUX, E., DERLER, S., ROSSI, R. M., ZENG, X., KOEHL, L., VENTENAT, V. Textile, physiological and sensorial parameters in sock comfort. *Textile Research Journal*, 2010, **80**(17), 1803–1810, doi: 10.1177/0040517510369409.

13. GWOSDOW, A.R., STEVENS, J.C., BERGLUND, L.G. AND STOLWIJK, J. A. J. Skin friction and fabric sensations in neutral and warm environments. *Textile Research Journal*, 1986, **56**(9), 574–580, doi: 10.1177/004051758605600909.

14. HERRING, K.M. AND RICHIE JR, D.H. Friction blisters and sock fiber composition. A double-blind study. *Journal of the American Podiatric Medical Association*, 1990, **80**(2), 63–71, doi: 10.7547/87507315-80-2-63.

15. BAUSSAN, E., BUENO, M. A., ROSSI, R. M. AND DERLER, S. Experiments and modelling of skin-knitted fabric friction. *Wear*, 2010, **268**(9-10), 1103–1110, doi: 10.1016/j.wear.2010.01.010.

16. BAUSSAN, E., BUENO, M. A., ROSSI, R. M., DERLER, S. Analysis of current running sock structures with regard to blister prevention. *Textile Research Journal*, 2013, **83**(8), 836–848, doi: 10.1177/0040517512461698.

17. LI, W., LIU, X. D., CAI, Z. B., ZHENG, J., ZHOU, Z. R. Effect of prosthetic socks on the frictional properties of residual limb skin. *Wear*, 2011, **271**(11-12), 2804–2811, doi: 10.1016/j.wear.2011.05.032.

18. VAN AMBER, R. R., LOWE, B. J., NIVEN, B. E., LAING, R. M., WILSON, C. A., COLLIE, S. The effect of fiber type, yarn structure and fabric structure on the frictional characteristics of sock fabrics. *Textile Research Journal*, 2015, **85**(2), 115–127, doi: 10.1177/0040517514530029.

19. DAI, X.Q., LI, Y., ZHANG, M., CHEUNG, J. T. M. Effect of sock on biomechanical responses of foot during walking. *Clinical Biomechanics*, 2006, **21**(3), 314–321, doi: 10.1016/j.clinbiomech.2005.10.002.

20. BAUSSAN, E. *Tribological study and modeling of skin-sock contact application to running. Doctoral Thesis.* Mulhouse : Haute Alsace University, 2010.

21. DYCK, W. A review of footwear for cold/wet scenarios. Part 2: Socks, liners, and insoles (Technical note DREO-TN-93-28). Ottawa : Defence Research Establishment, 1993, https://apps.dtic.mil/sti/citations/ADA280317.

22. BABU, B.S., SENTHILKUMAR, P., SENTHILKUMAR, M. Effect of yarn linear density on moisture management characteristics of cotton/polypropylene double-layer knitted fabrics. *Industria Textila*, 2015, **66**(3), 123–130.

23. BABU, B.S., SENTHİLKUMAR, P., SENTHİLKUMAR, M. Effect of yarn type on moisture transfer characteristics of double-face knitted fabrics for active sportswear. *Journal of Industrial Textiles*, 2020, **49**(8), 1078–1099, doi: 10.1177/1528083718805717.

24. *High performance technical textiles.* Edited by R. Paul. 1st edition. Hoboken : John Wiley & Sons, 2019, 37–52.

25. ANTTONEN, H., PIETIKAINEN, P., RINTAMAKI, H., RISSANEN, S. Cold protective gloves in meat processing industry-product development and selection. In *Ergonomics of protective clothing. Proceedings of NOKOBETEF 6 and 1st European conference on protective clothing.* Edited by K. Kuklane and I. Holmer. Stockholm : Arbetslivsinstitutet, 2000, 212–215.

26. BERGER, C., MANZ, G.R. *Climate configurable sole and shoe. US patent no. 6817112. 2004-16-11.*

27. MARTÍNEZ NOVA, A., MARCOS-TEJEDOR, F., GÓMEZ MARTÍN, B., SÁNCHEZ-RODRÍGUEZ, R., ESCAMILLA-MARTÍNEZ, E. Bioceramic-fiber socks have more benefits than cotton-made socks in controlling bacterial load and the increase of sweat in runners. *Textile Research Journal*, 2018, **88**(6), 696–703, doi: 10.1177/0040517516688631.

28. ADVANSA ThermoCool introduced at OR [online]. RIS [cited January 20, 2020]. Available from: <https://risnews.com/advansa-thermocool-introduced-or>.

29. POLYCOLON [online]. Scholler the spinning group an Indorama Ventures Company [cited January 20, 2020]. Available from: <https://polycolon.com/en/>.

30. FOURT, L., SOOKNE, A. M., FRISHMAN, D., HARRIS M. The rate of drying of fabrics.

Textile Research Journal, 1951, **21**(1), 26–33, doi: 10.1177/004051755102100107.

31. ZHUANG, Q., HARLOCK, S. C., BROOK, D. B. Transfer wicking mechanisms of knitted fabrics used as undergarments for outdoor activities. *Textile Research Journal*, 2002, **72**(8), 727–734, doi: 10.1177/004051750207200813.

32. RICHIE, D.H. Socks: hosiery-essential equipment for the athlete [online]. Athletic Equipment Managers Association [cited January 20, 2020]. Available from: <http://buildyourownnewsletters. com/content/socks-hosiery%E2%80%94essen-tial-equipment-athlete>.

33. SUGANTHİ, T., SENTHİLKUMAR, P., DİPİKA, V. Thermal comfort properties of a bi-layer knitted fabric structure for volleyball sportswear. *Fibres & Textiles in Eastern Europe*, 2017, **1**(121), 75–80, doi: 10.5604/12303666.1227885.

34. HSIEH, Y. L. Liquid transport in fabric structures. *Textile Research Journal*, 1995, **65**(5), 299–307, doi: 10.1177/004051759506500508.

35. SIRKOVÁ, B. K., MOUČKOVÁ, E. Analysis possibilities of controlled transport of moisture in woven fabrics. *Autex Research Journal*, 2018, **18**(4), 385–391, doi: https://doi.org/10.1515/aut-2018-0008.

36. PAVKO-CUDEN, A., ELESINI-STANKOVIČ, U. Elastane addition impact on structural and transfer properties of viscose and polyacrylonitrile knits. *Acta Chimica Slovenica*, 2010, **57**(4), 957–962.

37. SUGANTHI, T., & SENTHILKUMAR, P. Moisture-management properties of bi-layer knitted fabrics for sportswear. *Journal of Industrial Textiles*, 2018, **47**(7), 1447–1463, doi: 10.1177/1528083717692594.

Md. Mazharul Islam[1], Md. Reazuddin Repon[2, 3, 4], Md. Shohan Parvez[5], Md. Mahbubul Haque[6], Mohammad Abdul Jalil[5]

[1] *Northern University Bangladesh, Department of Textile Engineering, Dhaka-1213, Bangladesh*
[2] *ZR Research Institute for Advanced Materials, Sherpur-2100, Bangladesh*
[3] *Khwaja Yunus Ali University, Department of Textile Engineering, Sirajgang-6751, Bangladesh*
[4] *Kaunas University of Technology, Department of Production Engineering, Faculty of Mechanical Engineering and Design, Studentu 56, LT-51424, Kaunas, Lithuania*
[5] *Khulna University of Engineering & Technology, Department of Textile Engineering, Khulna-9203, Bangladesh*
[6] *Daffodil International University, Department of Textile Engineering, Dhaka-1207, Bangladesh*

Factors Affecting Apparel Pattern Grading Accuracy: Existing Software Solutions Comparison and Development of New Solution
Dejavniki, ki vplivajo na natančnost gradiranja krojev oblačil: primerjava obstoječih programskih rešitev in razvoj nove rešitve

Corresponding author/Korespondenčni avtor:
Mohammad Abdul Jalil
E-mail: drjalil@te.kuet.ac.bd
Phone: +8801711269630
ORCID ID: 0000-0002-0006-8086

Abstract
Every so often, grading is not 100% accurate due to the conventional system for calculating the grading increment. The aim of this study was to develop a new calculation system of grading increment provided by different software, e.g. Lectra, Gerber, Optitex, Boke CAD etc., and to develop a new mathematical solution that enhances grading precision. For this experiment, three different spec sheets of different buyers were collected, and then combined and drawn to a solitary sketch for both front and back including all points of measures (POM) for a more easy comparison. The solutions for the presence of diagonal and curve measurements were provided with examples using various tools and techniques of different professional garment CAD software. The benefit of the new approach is not only reduced errors of grading but also guaranteed garment fit without distorting style features. However, the drawbacks of the measurement method are complicated and time-consuming. They revolve around the fact that iterative fitting and adjustments are mandatory to improve the fit before bulk production. The study revealed that this new system slightly increases calculation time, whereas the sample approval time for order execution reduces considerably.
Keywords: grading, CAD, pattern making, grading system, Pythagoras grading

Izvleček
Gradiranje pogosto ni 100-odstotno natančno zaradi konvencionalnega sistema za izračun gradirnega prirastka. Namen te študije je razviti nov sistem izračunavanja gradirnega prirastka v primerjavi s tistimi, ki jih ponujajo različna programska orodja, kot so Lectra, Gerber, Optitex, Boke CAD ipd., in razviti novo matematično rešitev, ki izboljša na-

tančnost gradiranja. Za raziskavo so bile izbrane tri tehnične skice različnih proizvajalcev, združene v eno samo skico oblačila, ki prikazuje sprednji in zadnji del oblačila ter vključuje vse mere oblačila za njihovo lažjo primerjavo pri gradiranju. Nato so na primerih z uporabo različnih orodij in tehnik gradiranja z različnimi komercialnimi programi CAD PDS prikazani rezultati gradiranja diagonalnih in krivuljnih mer. Prikazana prednost novega pristopa gradiranja ni le v zmanjšanju napak pri gradiranju, temveč tudi v zagotavljanju prileganja oblačila, ne da bi se spremenila njegova oblika. Pomanjkljivost tega pristopa je v zapleteni in dolgotrajni merilni metodi, ki za izboljšanje rezultatov gradiranja zahteva ročno prilagajanje gradirnega prirastka.
Ključne besede: gradiranje, CAD, konstruiranje krojev oblačil, gradirni sistem, Pitagorovo gradiranje

1 Introduction

Grading is a process of increasing and decreasing pattern dimensions by creating multiple sizes to fit different people [1–3]. In the concepts of pattern grading, it has been described that the grading system is developed from sizing specifications, and sizing specifications are derived from anthropometric surveys [4]. In order to create garments in each size, the increases used to create each new pattern should be based on body measurements associated with that specific size and organised in a size chart. In the late 1960s, computerised grading was developed in the USA, followed by Germany, Italy, Denmark, UK and France to improve the accuracy as well as efficiency [3, 5]. The basic principle of computerised grading is the same as manual grading. The manual procedure of grading is exceptionally tedious and grading efficiency is affected by the grader's experience [6]. The computer was used as a drawing tool. Computerised grading was still tedious and time-consuming; however, the mistake-vulnerable grading process was done satisfactorily with the computerised method. Computer-aided pattern grading systems have become popular in clothing factories as they have become faster, more consistent and accurate, more reliable and manageable than conventional manual grading [7–10]. Generally, grading contains three steps, i.e. determining grade points, determining alteration rules and amounts of each grade point, and joining altered points using the curve smoothing technique [11, 12]. A grade rule can be determined by comparing and calculating mathematical or geometrical differences between the body measurements of each size [1, 13–15]. A grade rule table defines how far each cardinal point of pattern moves in the x and y direction in a Cartesian graph [16]. The way towards grading is extremely dreary and requires an incredible level of acumen and discernment, and frequently the exactness of the graded pattern pieces of clothing is affected by the grader's skills [17]. The proportion of the pattern will vary according to the experience, accuracy and personal judgment of the grader [18]. The problems of assessing the factors affecting apparel pattern grading accuracy were identified and some recommendations were proposed in the first part of this work [19]. This paper, however, focuses on the comparison of different solutions to achieve grading accuracy provided by different software, e.g. Lectra, Gerber, Optitex, Boke CAD etc., and develops a new mathematical explanation. Grading has long remained a neglected area of research in the clothing industry and the classical size charts used by the industry have evolved over the years with a trial-and-error method [20]. Pattern grading is a procedure of efficiently enhancing and reducing the measurements of a piece or sloper into a different number of sizes for large scale manufacturing [4, 17]. The amount and direction into which the pattern increases or decreases has been determined. At the same time, the correct proportions of garments have been maintained without distorting the style features. In order to grade a pattern, increases (or decreases) are applied at specific points of a pattern to make each new pattern in another larger (or smaller) size. The conventional incremental computerised grading is based on a Cartesian graph that has the horizontal (x) and the vertical axes (x) that intersect at right angles and divide an area into four quadrants. In the Cartesian graph, the dimensional changes of patterns are moved to the left or right on the x-axis, and up or down on the y-axis to create new sizes [10, 21]. Consequently, horizontal increments are placed on the x-axis and vertical measurements on the y-axis. Diagonal measurement increments are based on the assumption that they will increase in the same amount as the amount on the x- or y-axis. Nevertheless, scientifically this is not true and will lead to measurement problems. Again, during the grading of the curve line, the amount that should change in the x and y directions to get the desired length of the curve is

unknown and complex. Hence, grading increments must be changed more than once until the required curve length is achieved. As it can be seen in the first part of this paper, different problems arise due to the presence of diagonal and curved lines in a spec sheet [22, 23]. The problem is in the calculation method; therefore, the calculation should be done properly to minimise grading errors. The presence of diagonal and the presence of curve measurements are only two major problems. Their presence in the spec sheet leads to other problems, as it affects the selection of base size, number of sizes present in the spec sheet etc. If they can be avoided, then other problems will be automatically minimised. For instance, if there is no diagonal measurement, then whatever the base is selected, it will not lead to grading errors. In some spec sheets, it is possible to avoid diagonal and curve measurements but not in all types of product spec sheets. Therefore, solutions to these problems are highly needed.

2 Experimental design

2.1 Materials
For this experiment, three different spec sheets of different buyers were collected, combined and drawn to a solitary sketch for both front and back (cf. Figure 1 and Table 1), including all points of measures (POM) to compare them more easily. The measurement points and their descriptions of all three spec sheets are shown in Table 1.

2.2 Methods
The solutions for the presence of diagonal and curve measurements are provided below with examples using different tools and techniques of professional garment CAD software, e.g. Lectra, Optitex,

Gerber, Tuka CAD, Boke CAD. If these CADs are not available and are techniques unknown to the grader, then another mathematical solution was developed by the authors, which is not only applicable in software but also in the manual process. It is called "Pythagoras Grading" as authors use the "Pythagoras formula" to calculate new grading increment values. All techniques are described and compared with the existing or conventional grading system. Finally, some recommendations are given to choose which solution should be used in what situation.

The conventional system is based on the increment of the given measurement of apparel for different sizes, e.g. "body length from high point shoulder" is increased by 2 cm for each size; hence, points H and G should increase by 2 cm in the negative y direction. For the T-shirt specs A, B and C, cardinal points (represented by A, B, C, E, G, H for front and back, and A, B, C, D, E, F, G for sleeve) and Cartesian coordinate values of grading increments are shown in Figure 2.

3 Experimental work

To solve the grading error due to the presence of diagonal and curve measurements, there are different solutions possible, which are described below.

3.1 Solutions to problem 1 – presence of diagonal measurements

3.1.1 Solution 1 to problem 1 – manual manipulation of grading increment
When grading is required in a particular point, an increment only from the base size to the next higher size is calculated. However, there are two problems
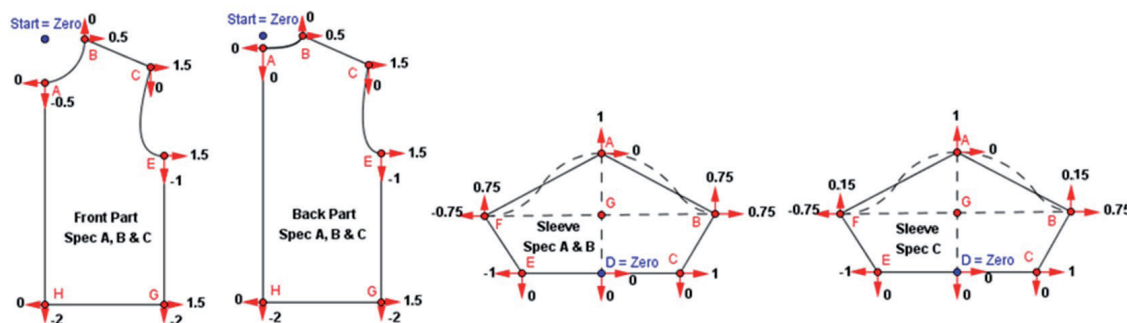

Figure 2: Cardinal points and Cartesian coordinate values of T-shirt specs A, B and C

Table 1: Measurement points and their descriptions of all three specification sheets

Figure 1: Combination of all measurement points of T-shirt

Points	Description	POMs
A	Back neck drop or depth	BND
B	Front neck drop or depth	FND
C	Neck width or opening	NW
D	Across shoulder width or shoulder to shoulder	AS
E	Shoulder length	S
F	Shoulder drop or slant	SD
G	Armhole straight	AHS
H	Armscye depth	ASD
I	Half chest	HC
M	Body length from high point shoulder	BLfHPS
Q	Sleeve length	SL
R	Sleeve opening	SO
S	Under sleeve	US
T	Sleeve width or upper arm	SW
X	Sleeve cap height	SCH
Y	Shoulder slant in degree	SSD

POM	Reference spec A					Reference spec B					Reference spec C				
	S	M	L	XL	XXL	S	M	L	XL	XXL	S	M	L	XL	XXL
BND	1.50	1.50	1.50	1.50	1.50	1.50	1.50	1.50	1.50	1.50	1.50	1.50	1.50	1.50	1.50
FND	8.00	8.50	9.00	9.50	10.00	8.00	8.50	9.00	9.50	10.00	8.00	8.50	9.00	9.50	10.00
NW	16.00	17.00	18.00	19.00	20.00	16.00	17.00	18.00	19.00	20.00	16.00	17.00	18.00	19.00	20.00
AS	–	–	–	–	–	45.00	48.00	51.00	54.00	57.00	45.00	48.00	51.00	54.00	57.00
S	15.00	16.00	17.00	18.00	19.00	15.00	16.00	17.00	18.00	19.00	–	-	-	-	-
SD	5.00	5.00	5.00	5.00	5.00	–	–	–	–	–	5.00	5.00	5.00	5.00	5.00
AHS	24.00	25.00	26.00	27.00	28.00	24.00	25.00	26.00	27.00	28.00	–	-	-	-	-
ASD	–	–	–	–	–	–	–	–	–	–	29.00	30.00	31.00	32.00	33.00
HC	48.00	51.00	54.00	57.00	60.00	48.00	51.00	54.00	57.00	60.00	48.00	51.00	54.00	57.00	60.00
BLf-HPS	70.00	72.00	74.00	76.00	78.00	70.00	72.00	74.00	76.00	78.00	70.00	72.00	74.00	76.00	78.00
SL	21.00	22.00	23.00	24.00	25.00	21.00	22.00	23.00	24.00	25.00	21.00	22.00	23.00	24.00	25.00
SO	18.00	19.00	20.00	21.00	22.00	18.00	19.00	20.00	21.00	22.00	18.00	19.00	20.00	21.00	22.00
US	14.00	14.50	15.00	15.50	16.00	–	–	–	–	–	–	-	-	-	-
SW	–	–	–	–	–	23.00	23.75	24.50	25.25	26.00	23.00	23.75	24.50	25.25	26.00
SCH	–	–	–	–	–	–	–	–	–	–	9.55	10.40	11.25	12.10	12.95

Note: All units are measured in cm. POM: Points of measure

with that. One is that it is assumed that any horizontal or vertical increment leads to an increase in the same amount in diagonal measurement, which is scientifically not true. For instance, when shoulder length increased e.g. by 1 cm and half neck width by 0.5 cm, then the horizontal increment would be (1 + 0.5 = 1.5 cm) in case of "spec A" and the vertical increment 0 cm as there is no increment in shoulder drop. According to the conventional system, the horizontal increment for shoulder length of spec A is 1.5 cm for all sizes. However, an increment of 1.5 cm in the horizontal direction does not mean that the diagonal (shoulder length) increment would be the same. After the grading, it was found that the measurements are lower than required. Manually, the measurements are initially increased by 0.01 cm in the horizontal direction until the required length is achieved. From the result, it was es-

tablished that at least 0.04 cm should increase along with 1.5 cm measurement, meaning that instead of the 1.5 cm horizontal increment, it should increase by 1.54 cm. And for other sizes, it may be 1.53 or 1.55, since the shoulder angle is not constant. Even if shoulder length increased constantly, e.g. 1 cm (15, 16, 17, 18 and 19 cm for S, M, L, XL and XXL sizes, respectively), the increment should not be the same as the angle of the shoulder for all sizes is not constant, which represents the second problem. To prove this, size spec A of the T-shirt is graded with conventional calculation and then the measurement

error is checked, which is shown in Figure 3. After that manual manipulation in grading, the increment is done to rectify the measurements, which is shown in Figure 4. Before and after manipulation measurements for the shoulder are shown below in Figures 3 and 4 along with their grading increment values.

Based on Figures 3 and 4, it can be said that if the diagonal measurement exists in a spec sheet, then the measurement checking and manual manipulation in grading increment should be done to rectify the measurements.
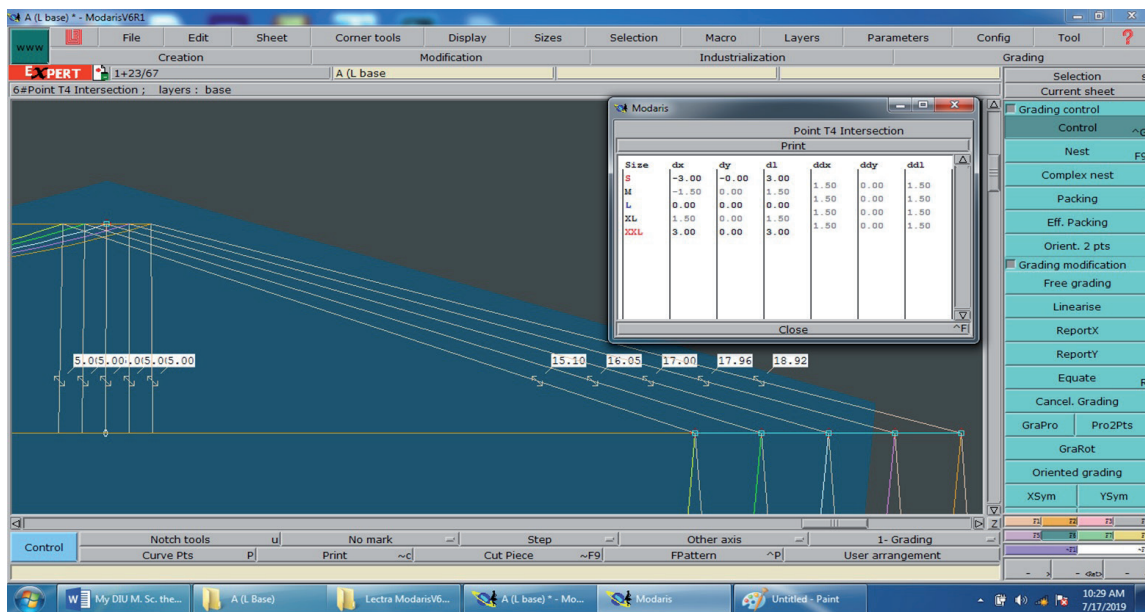

Figure 3: Shoulder length measurements and their grading increment values before manipulation (spec A)
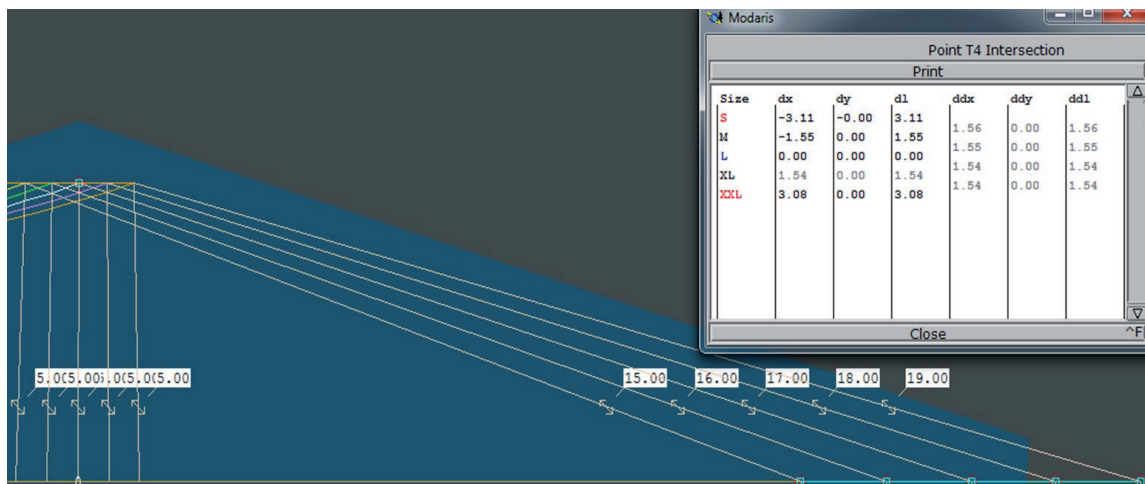

Figure 4: Shoulder length measurements and their grading increment values after manipulation (spec A)

3.1.2 Solution 2 to problem 1 – segment editing with Optitex or TukaCAD

Manual manipulation is time-consuming; therefore, different software companies provide different solutions for grading rectification, e.g. "measure and segment editor" in Optitex and TukaCAD software. The shoulder length before measurement and segment editing is designated in Figure 5, and after measurement and segment editing is given in Figure 6.

In segment editing, the "last horizontal" option is chosen since shoulder length can only increase or decrease in the horizontal direction. If the vertical option is chosen, then the shoulder drop measurement will change. The selection of the segment editor option depends on the measurement location, e.g. in spec A of the T-shirt, shoulder length and shoulder drop are given. The shoulder drop change has to plot in the vertical direction and the shoulder length change has to plot in the horizontal direction. In the case of spec B of the T-shirt, shoulder length and across shoulder are given. Hence, the across shoulder change has to plot in the horizontal direction and the shoulder length change has to plot in the vertical direction. In this case, the "last vertical" option must be chosen in the segment ed-
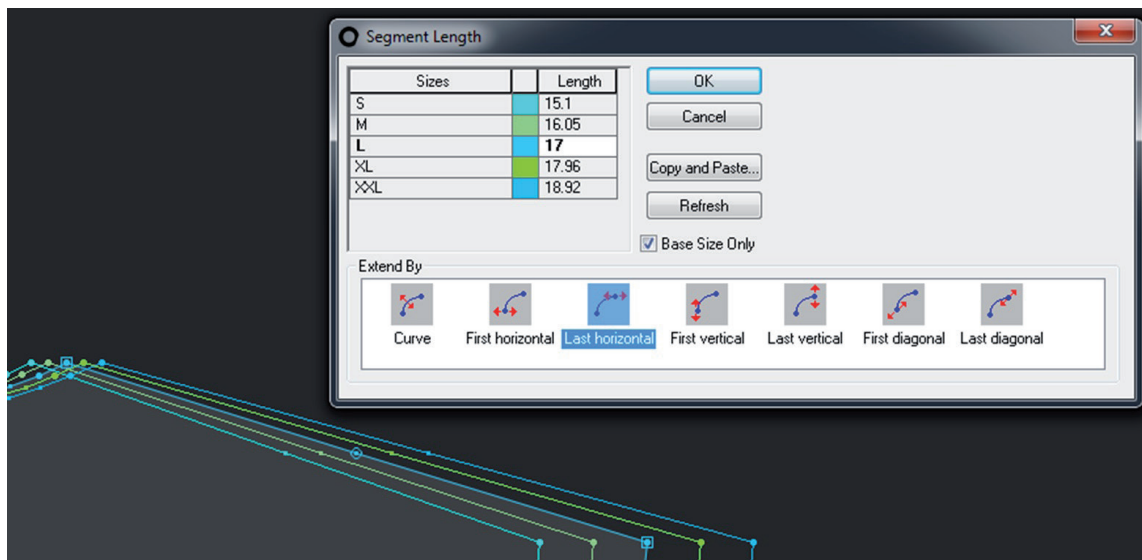
Figure 5: Shoulder length before segment editing (spec A)
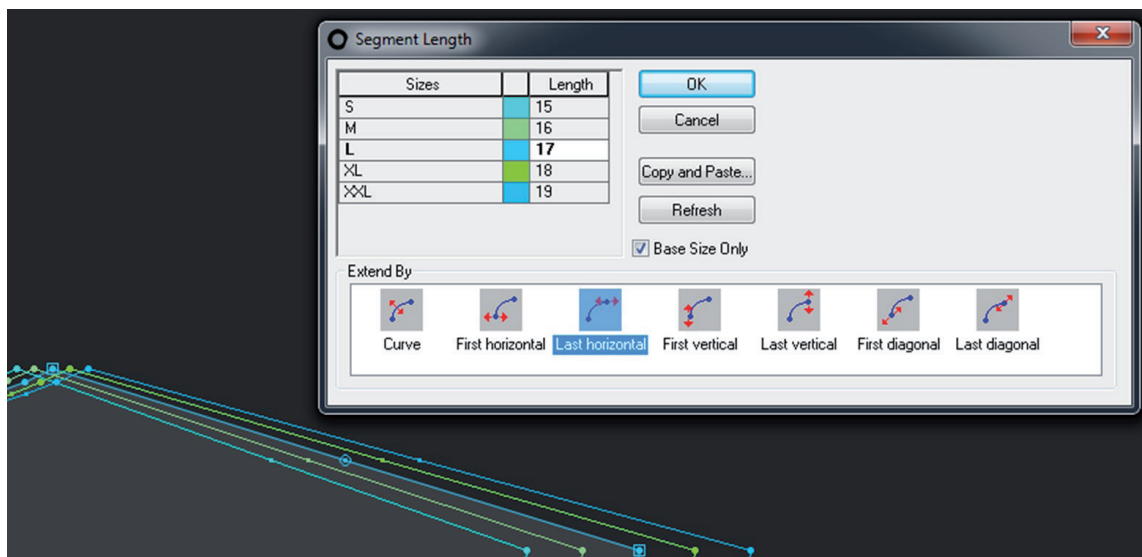
Figure 6: Shoulder length after segment editing (spec A)

itor. Another reason for choosing "last vertical or last horizontal" instead of "first horizontal or first vertical" is due to the shoulder point being the last point and side neck point being the first point of the shoulder line, and in Optitex or Tuka CAD software, points are counted in the clockwise direction. After segment editing, it was established that there is no diagonal grading error.

3.1.3 Solution 3 to problem 1 – automatic grading with BokeCAD

Automatic grading is available only in BokeCAD as far as the authors know. There is a difference between automatic grading and conventional Cartesian coordinate grading. In Cartesian coordinate grading, firstly, a base should be selected and a pattern should be drawn according to the base size measurements. Then, the grading increment calculation is done according to the given measurements
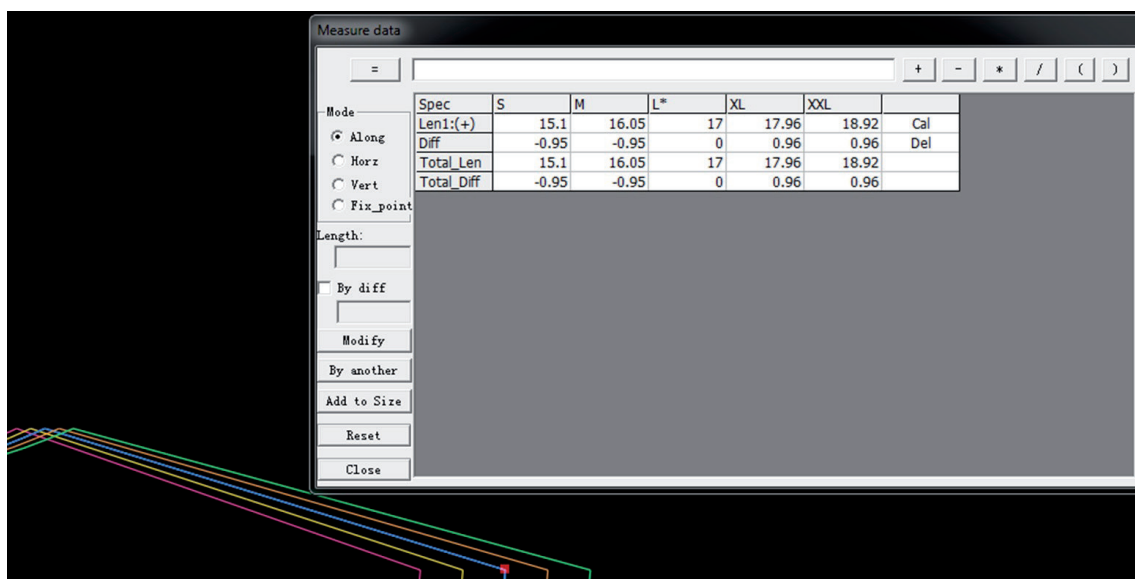
Figure 7: Shoulder length after conventional grading (spec A) with BokeCAD

Figure 8: Shoulder length after automatic grading (spec A) with BokeCAD

in the size chart and their input in the x and y directions of the Cartesian coordinate grading. However, in automatic grading, the first whole measurements from the spec sheet should be plotted in the size chart of the software. Then, a base size should be selected and a pattern drawn by the measurement points not by the measurements. When the grading button is clicked, it will automatically grade the whole pattern. The advantages of the system are: a) grading increment calculation is not n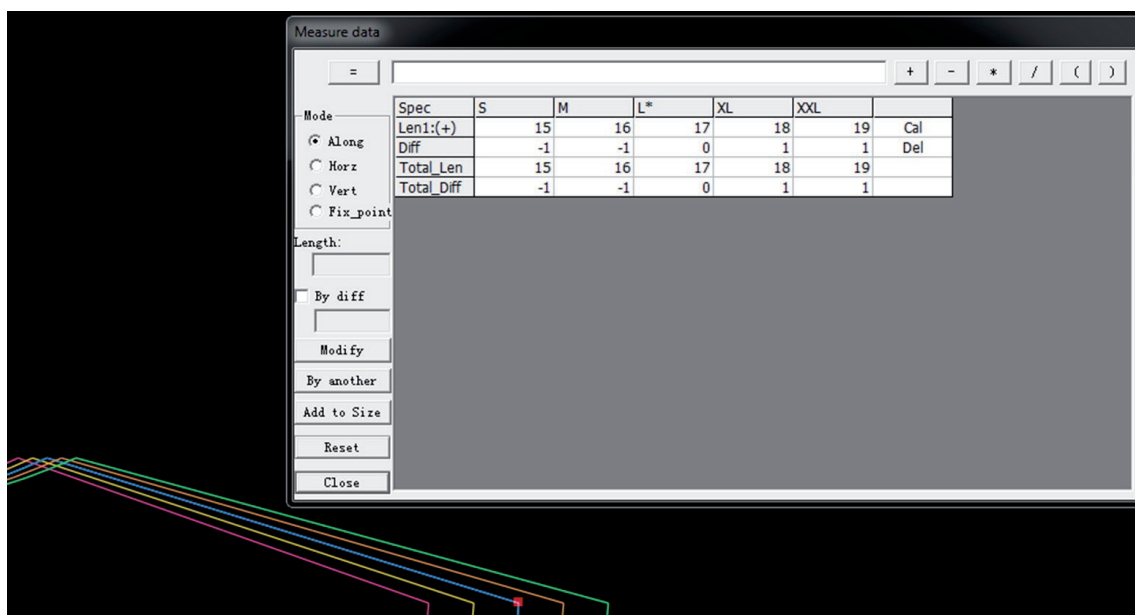eeded, hence no possibility of miscalculation; b) diagonal measurements are automatically adjusted, hence manual manipulation is not needed for the diagonal grading rectification; c) curve grading is almost accurate, as sometimes up to 0.02 cm grading error is found in the case of curve line grading, which is negligible.

For the experiment, "spec A" of T-shirts was selected and graded with both conventional Cartesian coordinate (x, y) grading and automatic grading method. The results are shown in Figures 7 and 8. From Table 2, it can be seen that graded measurements are more precise after automatic grading than conventional grading.

3.1.4　Solution 4 to problem 1 – Pythagoras grading system

It was seen that the diagonal measurements grading increments create grading errors. To minimize the latter, a new grading increment calculation system was developed. For this experiment, specs A and B of T-shirts were selected. The details follow below:

Table 2: Diagonal length comparison of body part (spec A) with conventional and automatic grading of BokeCAD

| Point of measures	Measurement comparison	Size					Unit
		S	M	L	XL	XXL	
Shoulder	Error after conventional grading	+0.10	+0.05	0.00	−0.04	−0.08	cm
	Length acquired after conventional grading	15.10	16.05	17.00	17.96	18.92	
	Length required	**15.00**	**16.00**	**17.00***	**18.00**	**19.00**	
	Length acquired after automatic grading	15.00	16.00	17.00	18.00	19.00	
	Error after automatic grading	0.00	0.00	0.00	0.00	0.00	
Armhole straight	Error after conventional grading	+0.01	+0.01	0.00	0.00	0.00	cm
	Length acquired after conventional grading	24.01	25.01	26.00	27.00	28.00	
	Length required	**24.00**	**25.00**	**26.00***	**27.00**	**28.00**	
	Length acquired after automatic grading	24.00	25.00	26.00	27.00	28.00	
	Error after automatic grading	0.00	0.00	0.00	0.00	0.00	
*Note: * indicates base size*							
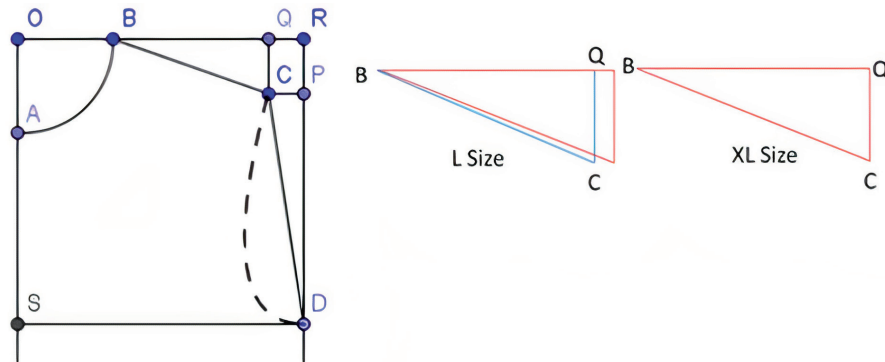
Figure 9: Points to calculate Pythagoras grading for pattern pieces of T-shirt body part (spec A)

(a) Pythagoras grading for pattern pieces of T-shirt body part (spec A)

Pattern construction of a T-shirt body part can be divided into some geometries that are shown in Figure 9.

From Δ BQC (cf. Figure 9), according to Pythagoras law:

$$BQ^2 + QC^2 = BC^2 \tag{1},$$

for L size:

$$Q_L = \sqrt{BC_L{}^2 - QC_L{}^2} = \sqrt{17^2 - 5^2} = 16.25 \tag{2},$$

and for XL size:

$$BQ_{XL} = \sqrt{BC_{XL}{}^2 - QC_{XL}{}^2} = \sqrt{18^2 - 5^2} = 17.29 \tag{3}.$$

The x-axis value of shoulder point C = (17.29 – 16.25) + (x-axis change in B point) = 1.04 + 0.5 = 1.54, and y-axis value of shoulder point C = 0 (due to no change in shoulder drop). According to conventional calculation, C = (1, 0) which should be replaced with (1.54, 0).

From Figure 9, OR = SD = ¼ chest; QC = RP = shoulder drop;

$$\therefore CP_L = QR_L = OR_L - OB_L - BQ_L = (\text{¼ chest})_L - (\text{½ neck width})_L - BQ_L$$

$$\therefore CP_L = 27 - 9 - 16.25 = 1.75$$

and $CP_{XL} = QR_{XL} = OR_{XL} - OB_{XL} - BQ_{XL} = (\text{¼ chest})_{XL} - (\text{½ neck width})_{XL} - BQ_{XL}$

$$\therefore CP_L = 28.5 - 9.5 - 17.29 = 1.71$$

From Δ CPD (cf. Figure 9), according to Pythagoras law:

$$PD^2 + CP^2 = CD^2 \tag{4},$$

for L size:

$$PD_L = \sqrt{26^2 - 1.75^2} = 25.94 \tag{5},$$

and for XL size:

$$PD_{XL} = \sqrt{27^2 - 1.71^2} = 26.95 \tag{6}.$$

The x-axis value of armpit point D = 1.5 (due to change in ¼ chest) and the y-axis value of armpit point D = 25.94 – 26.95 = –1.01.

According to conventional calculation, D = (1.5, –1) which should be replaced with (1.5, –1.01).

After applying Pythagoras grading, the grading increment values of T-shirt body parts are changed, as shown in Figure 10.

After the grading with new grading increments of points C and D, the measurements found are presented in Table 3.

From Table 3, it can be seen that after applying Pythagoras grading, errors were minimised considerably.
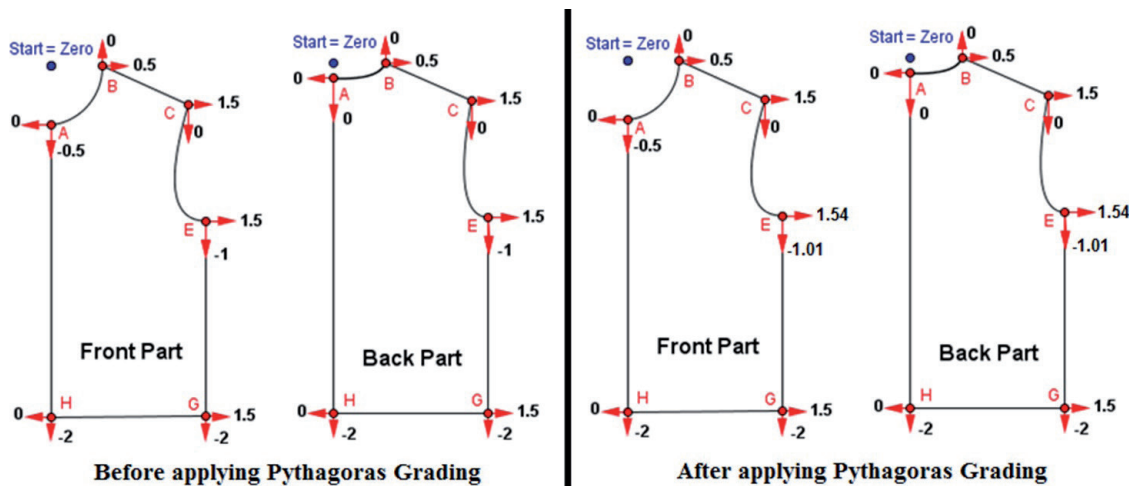

Figure 10: Grading increment of spec A for pattern pieces of T-shirt body parts before and after Pythagoras grading (L size as base size)

Table 3: Diagonal length comparison of pattern pieces of T-shirt body parts (spec A) before and after applying Pythagoras law

Point of Measures	Measurement comparison	Size					Unit
		S	M	L*	XL	XXL	
Shoulder	Error before applying Pythagoras law	+0.10	+0.05	0.00	−0.04	−0.08	cm
	Length acquired before applying Pythagoras law	15.10	16.05	17.00*	17.96	18.92	
	Length required	**15.00**	**16.00**	**17.00***	**18.00**	**19.00**	
	Length acquired after applying Pythagoras law	15.02	16.01	17.00*	18.00	19.00	
	Error after applying Pythagoras law	+0.02	+0.01	0.00	0.00	0.00	
Armhole straight	Error before applying Pythagoras law	+0.01	+0.01	0.00	0.00	0.00	cm
	Length acquired before applying Pythagoras law	24.01	25.01	26.00*	27.00	28.00	
	Length required	**24.00**	**25.00**	**26.00***	**27.00**	**28.00**	
	Length acquired after applying Pythagoras law	24.00	25.00	26.00*	27.01	28.01	
	Error after applying Pythagoras law	0.00	0.00	0.00	+0.01	+0.01	
*Note: * indicates base size*							

(b) Pythagoras grading for the pattern pieces of T-shirt body part (spec B)

From Δ BQC (cf. Figure 9), according to Pythagoras law:

$$BQ^2 + QC^2 = BC^2 \qquad (7),$$

where $BQ_L = OQ_L - OB_L$ = (half across shoulder – half neck width) of size L = 25.5 – 9 = 16.5.

For L size:

$$QC_L = \sqrt{BC_L{}^2 - BQ_L{}^2} = \sqrt{17^2 - 16.5^2} = 4.09 \qquad (8)$$

and for XL size:

$$BQ_{XL} = \sqrt{18^2 - 17.5^2} = 4.21 \qquad (9).$$

The y-axis value of shoulder point C = (4.09 – 4.21) = −0.12 and the x-axis value of shoulder point C = 1.5 (due to change in across shoulder), hence the grading increment value of C = (1.5, −0.12) instead of traditional (1.5, 0.).

From Δ CPD (cf. Figure 9), according to Pythagoras law:

$$CD^2 + PD^2 = CD^2 \qquad (10),$$

where CD = armhole straight and CP = QR = OR – OQ = (¼ chest – ½ across shoulder).

Therefore,

$$PD_L = \sqrt{CD_L{}^2 - CP_L{}^2} = \sqrt{26^2 - 1.5^2} = 25.96 \qquad (11)$$

and

$$PD_{XL} = \sqrt{CD_{XL}{}^2 - CP_{XL}{}^2} = \sqrt{27^2 - 1.5^2} = 26.96 \quad (12).$$

The y-axis value of armpit point D = (25.96 – 26.96) + y-axis point of C = (−1 – 0.12) = (−1.12) and the x-axis value of armpit point D = 1.5 (due to change in ¼ chest), hence the grading increment value of D = (1.5, −1.12) instead of traditional (1.5, −1).
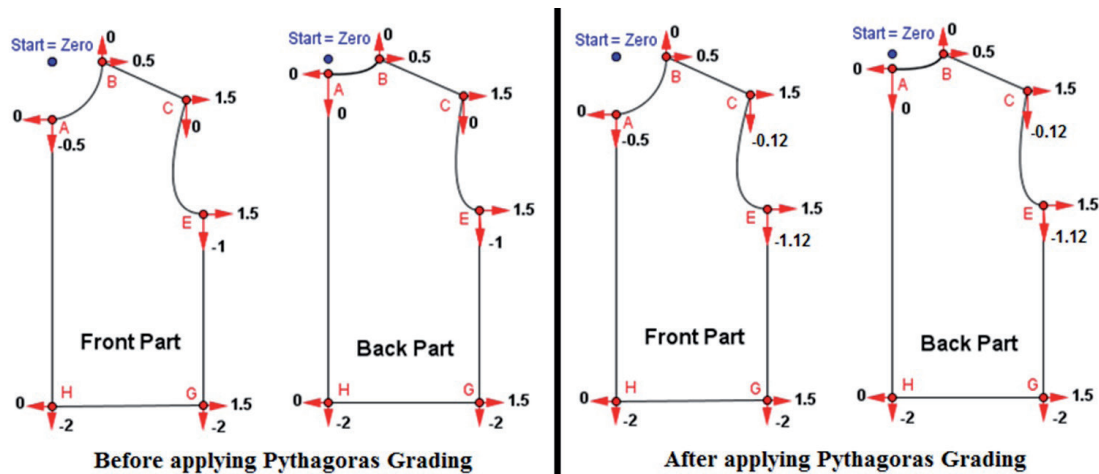
Figure 11: Grading increment of pattern pieces of T-shirt body parts (spec B) before and after Pythagoras grading (L size as base size)

After applying Pythagoras grading, the graded measurements were changed, as it can be seen in Table 4.

Figures 10 and 11, and Tables 3 and 4 show that Pythagoras grading can be used for higher precision grading for diagonal lines.

3.2 Solutions to problem 2 – presence of curve measurements

3.2.1 Solution 1 to problem 2 – segment measuring and manual manipulation of grading increment value

In the first part of the paper [19], it can be seen that the back and front sleeve curves do not match with

Table 4: Diagonal length comparison of pattern pieces of T-shirt body parts (spec B) before and after applying Pythagoras law

Point of measures	Measurement comparison	Size					Unit
		S	M	L*	XL	XXL	
Shoulder length	Error before applying Pythagoras law	+0.07	+0.03	0.00	−0.03	−0.05	cm
	Length acquired before applying Pythagoras law	15.07	16.03	17.00*	17.97	18.95	
	Length required	**15.00**	**16.00**	**17.00***	**18.00**	**19.00**	
	Length acquired after applying Pythagoras law	15.00	16.00	17.00*	18.00	19.00	
	Error after applying Pythagoras law	0.00	0.00	0.00	0.00	0.00	
Armhole straight	Error before applying Pythagoras law	0.00	0.00	0.00	0.00	0.00	cm
	Length acquired before applying Pythagoras law	24.00	25.00	26.00*	27.00	28.00	
	Length required	**24.00**	**25.00**	**26.00***	**27.00**	**28.00**	
	Length acquired after applying Pythagoras law	24.00	25.00	26.00*	27.00	28.00	
	Error after applying Pythagoras law	0.00	0.00	0.00	0.00	0.00	
*Note: * indicates base size*							

the front and back armhole curve length in the conventional grading system. As the armhole straight is
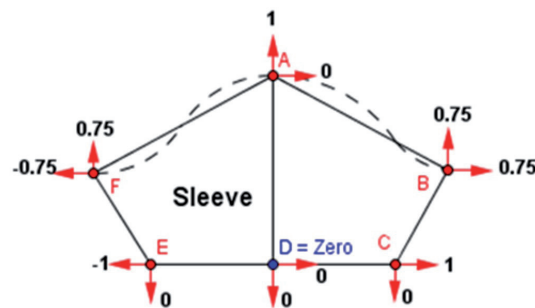
Figure 12: Grading increment for sleeve of T-shirt (spec B) in conventional system

given, after shape correction, armhole curve lengths cannot be modified. Sleeve curves must be manipulated until they match the curve lengths of front and back armhole curves.

For spec B, sleeve width and armhole straight are given. The x-axis of the "F" point (cf. Figure 12) cannot be modified. Instead, a fixed increment must be plotted as sleeve width is given. The y-axis must be modified until the curve length of "AF" (cf. Figure 12) matches the front armhole curve lengths.

Figures 13–16 show that if curve lengths need to match each other, the measurement checking and manual manipulation in grading increment should be conducted to rectify the measurements.

Figure 13: Front sleeve curve before manipulation of grading increment of point F (spec B)

Figure 14: Front sleeve curve after manipulation of grading increment of point F (spec B)
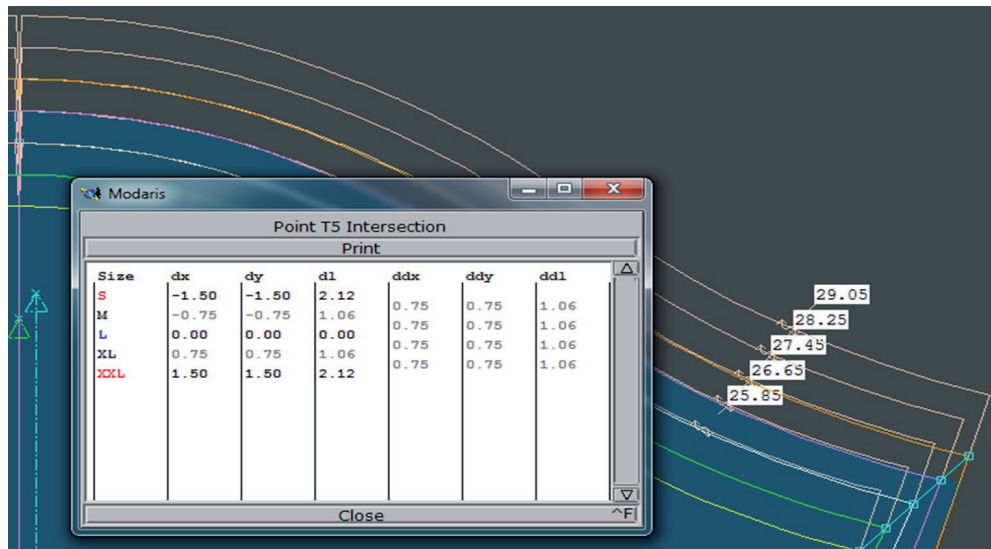
Figure 15: Back sleeve curve before manipulation of grading increment of point B (spec B)
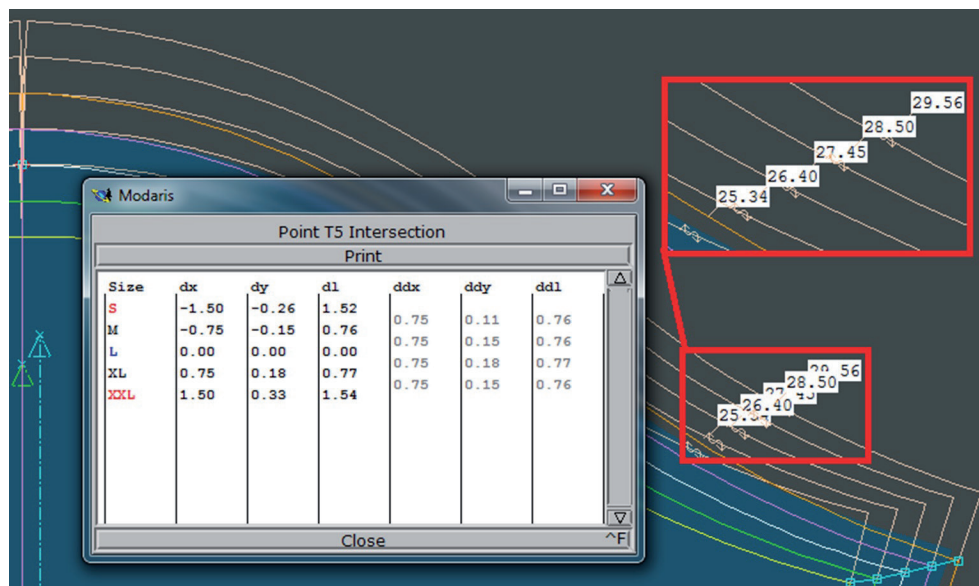
Figure 16: Back sleeve curve after manipulation of grading increment of point B (spec B)

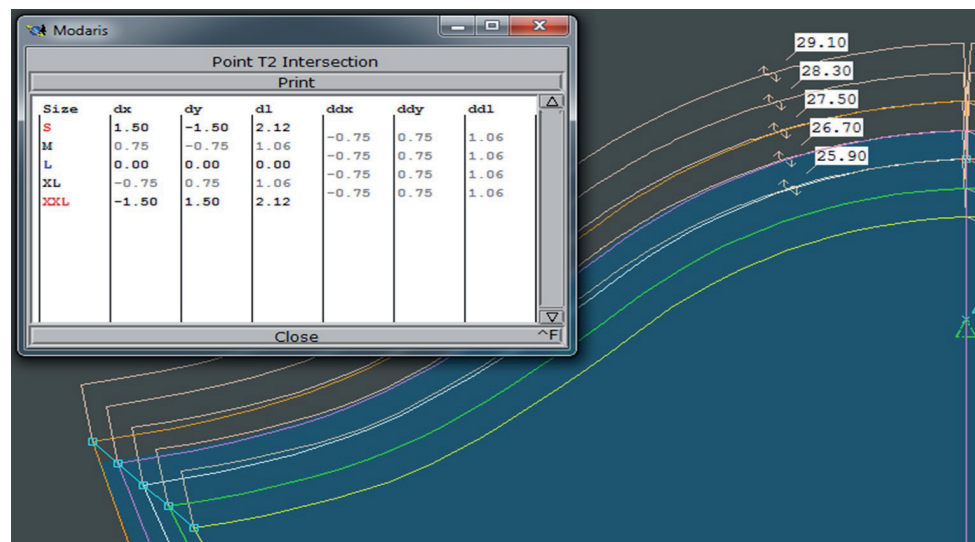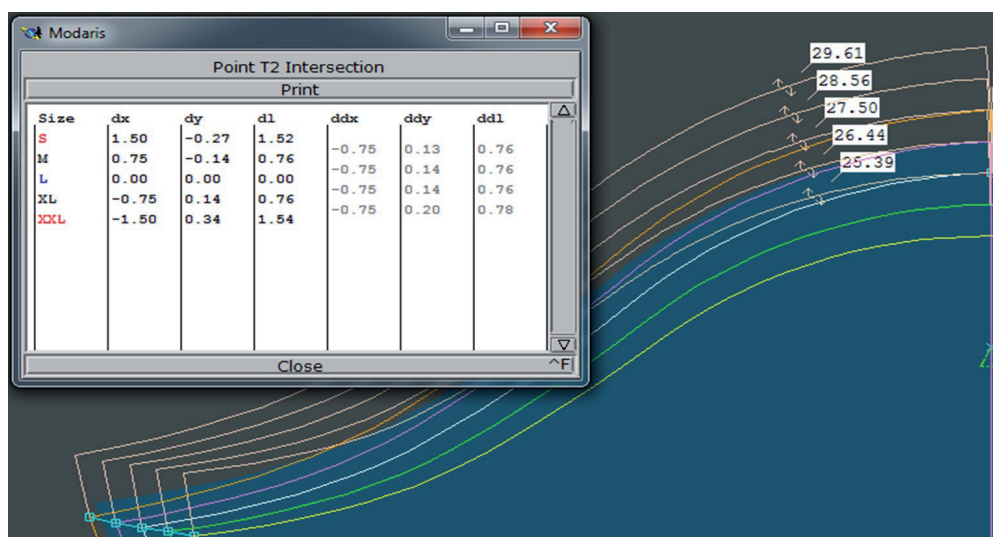However, in the case of spec A, this method cannot rectify the grading errors as the sleeve curve length measurement and under sleeve measurement are connected to only one point (F point in Figure 12). Any change in the x or y direction affects the other line. It can be said that if a combination such as "diagonal and vertical" or "diagonal and horizontal" or "curve and vertical" or "curve and horizontal" is given, then it is possible to rectify the grading with the "segment measuring and manual manipulation of grading increment value" technique. However, if the "diagonal and curve" or "diagonal and diagonal" combination is given, then it is not possible to solve the grading with the "segment measuring and manual manipulation of grading increment value".

3.2.2   Solution 2 to problem 2 – segment editing with Optitex or TukaCAD

Since manual manipulation is time consuming, different software companies provide a different solution for grading rectification, e.g. "measure and segment editor" in the Optitex and TukaCAD software. Before and after the measurement of the front and back sleeve curve before and after segment editing are presented in Figures 17–20.

Figure 17: Front sleeve curve before segment editing (spec B)

Figure 18: Front sleeve curve after segment editing (spec B)

Figure 19: Back sleeve curve before segment editing (spec B)

Figure 20: Back sleeve curve after segment editing (spec B)

In segment editing for the front sleeve curve (spec≈B), the "first vertical" option is chosen and for the back sleeve curve (spec B), the "last vertical" option is chosen, as in the Optitex or Tuka CAD sof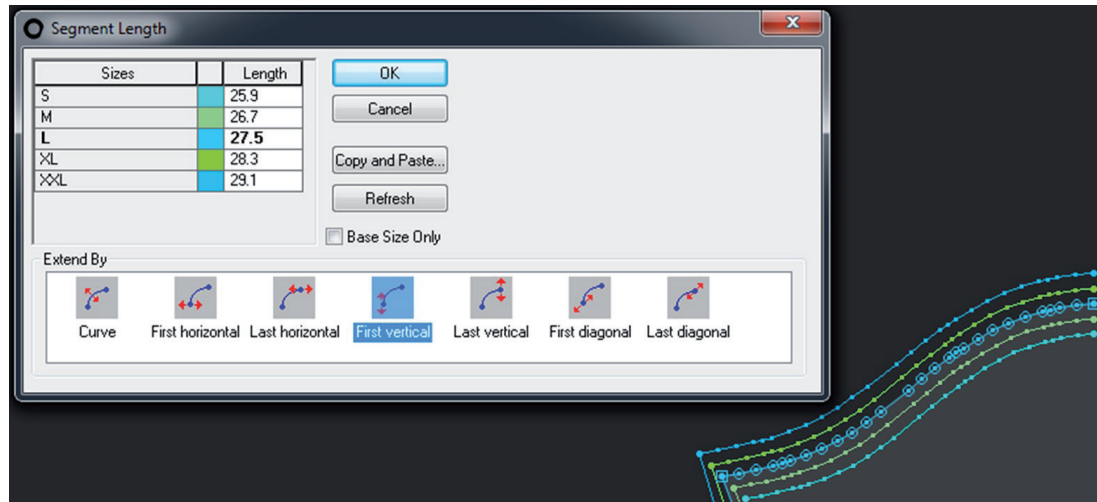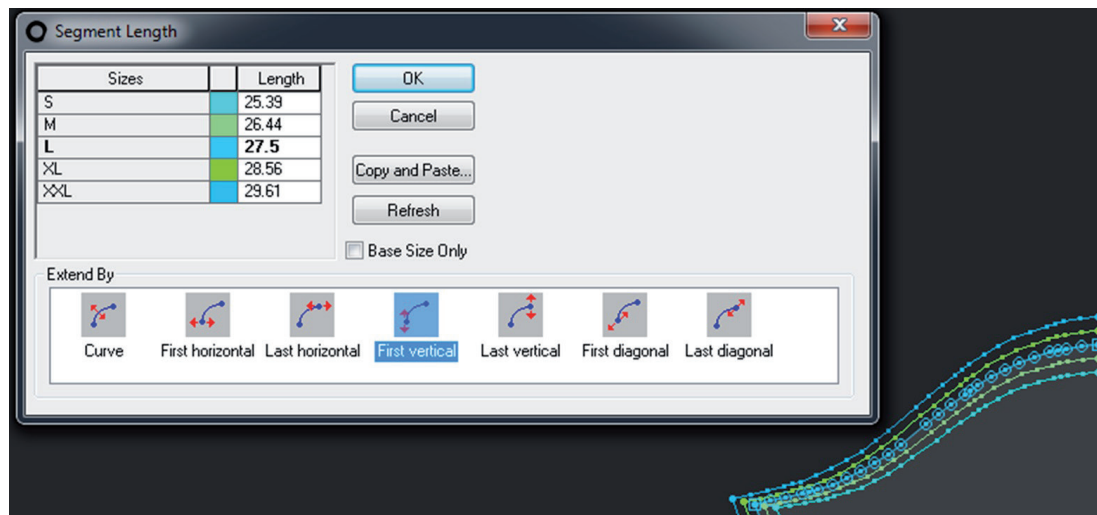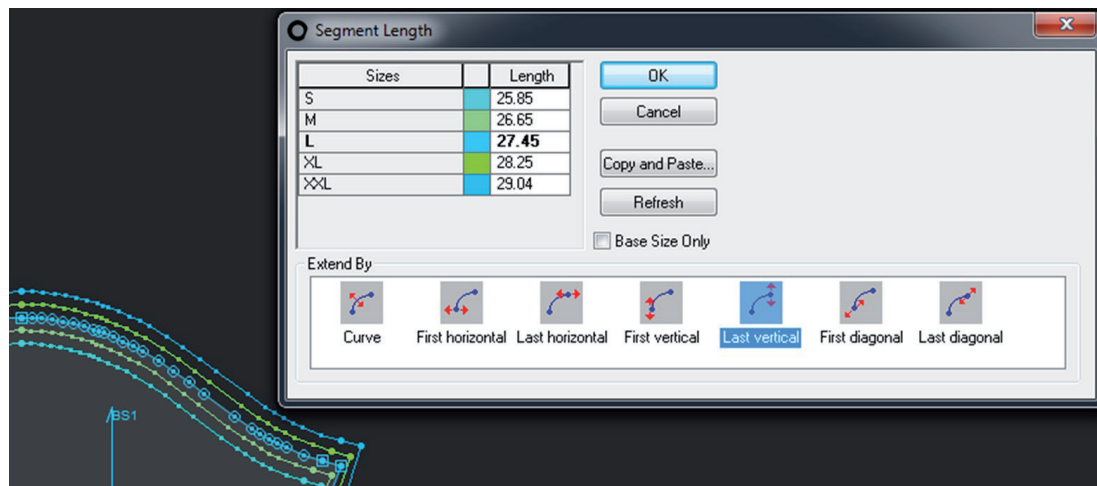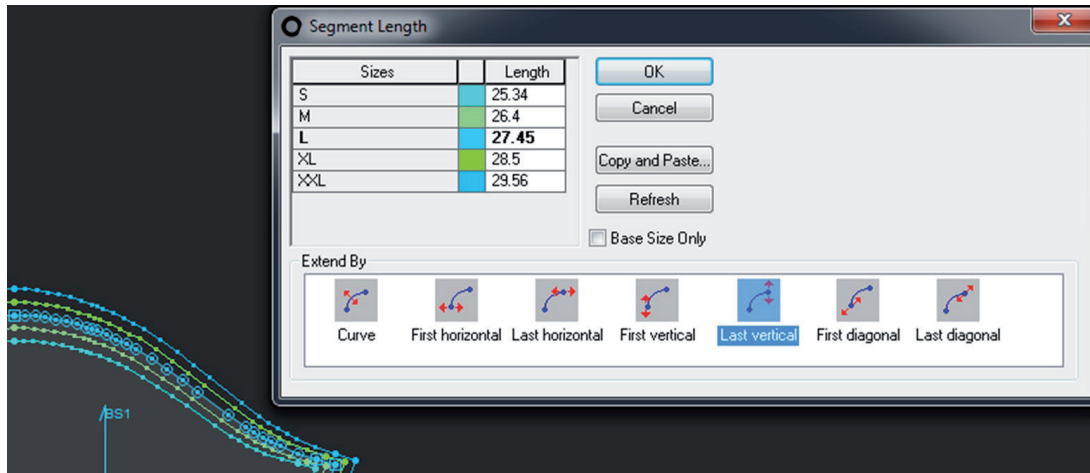tware, points are counted in the clockwise direction. Moreover, it is possible to change front and back sleeve curve in the vertical direction since under sleeve is not given. It is not possible to select the horizontal direction as sleeve width is given in spec B. However, in the case of spec A, the segment editor cannot solve the error of sleeve curve length measurement and under sleeve due to them being connected to only one point (F point in Figure 12). Any change in the x or y direction affects the other line. It can be said that if a combination such as "diagonal and vertical" or "diagonal and horizontal" or "curve and vertical" or "curve and horizontal" is given, then it is possible to rectify the grading with the segment editor. However, if the "diagonal and curve" or "diagonal and diagonal" combination is given, then it is not possible to solve grading with the segment editor (cf. examples above).

3.2.3   Solution 3 to problem 2 – automatic grading with BokeCAD

Sometimes the spec sheet does not have any given curve length. However, due to the matching of some curve lengths, the front and back sleeve curve lengths should be matched with the front and back armhole curve lengths. Sometimes, the curve length depends on diagonal length, e.g. in spec B, armhole straight is 26 cm and after making the curve, the front and back armhole curve lengths are 27.50 cm and 27.45 cm, respectively. To get that length sleeve armhole straight, 27 cm (SAHS = AHS + 1 cm) were

drawn to get 27.5 and 27.45 cm front and back sleeve curve lengths. However, this is not fixed. Only for this spec, 1 cm is added to the armhole straight to match the curve length. For another spec sheet, it will vary according to the measurement. Due to diagonal grading error, curve lengths changed as well. But even if the diagonal grading values are rectified, the curves do not match 100% with each other and a slight error will occur, the latter being negligible. For 100% matching of the curve, a slight modification is quite enough after automatic grading. Therefore, for the experiment, specs A and B of T-shirts were selected and graded with both the Cartesian coordinate (x, y) and automatic method. The results are presented in Tables 5–6.

Tables 5 and 6 show that after automatic grading, there is no diagonal grading error. And up to 0.1 cm, the grading error is found in curve-line grading, which is negligible.

3.2.4   Solution 4 to problem 2 – Pythagoras grading system

As it was seen, diagonal measurement and curve measurements related to diagonal measurement create grading errors. To minimize that, a new grading increment calculation system was developed. The author called it "Pythagoras grading". For this experiment, specs A and B of T-shirts were selected. Details are given below.

3.2.4.1 Pythagoras grading for pattern pieces of T-shirt sleeve (spec B)

Pattern construction of a T-shirt sleeve can be divided into some geometries that are shown in Figure 21.

Table 5: Diagonal and curve length comparison of pattern pieces of T-shirt body part (spec B) with conventional and automatic grading of BokeCAD

Point of measures	Measurement comparison	Size					Unit
		S	M	L*	XL	XXL	
Sleeve armhole straight	Error after conventional grading	+0.43	+0.21	0.00	−0.21	−0.43	cm
	Length acquired after conventional grading	25.43	26.21	27.00*	27.79	28.57	
	Length required	**25.00**	**26.00**	**27.00***	**28.00**	**29.00**	
	Length acquired after automatic grading	25.00	26.00	27.00*	28.00	29.00	
	Error after automatic grading	0.00	0.00	0.00	0.00	0.00	
Front sleeve curve	Error after conventional grading	+0.51	+0.26	0.00	−0.26	−0.51	cm
	Length acquired after conventional grading	25.90	26.70	27.50*	28.30	29.10	
	Length required	**25.39**	**26.44**	**27.50***	**28.56**	**29.61**	
	Length acquired after automatic grading	25.46	26.48	27.50*	28.52	29.55	
	Error after automatic grading	+0.07	+0.04	0.00	−0.04	−0.06	
Back sleeve curve	Error after conventional grading	+0.51	+0.25	0.00	−0.26	−0.52	cm
	Length acquired after conventional grading	25.85	26.65	27.45*	28.24	29.04	
	Length required	**25.34**	**26.40**	**27.45***	**28.50**	**29.56**	
	Length acquired after automatic grading	25.40	26.42	27.45*	28.47	29.49	
	Error after automatic grading	+0.06	+0.02	0.00	−0.03	−0.07	

Note: * indicates base size

Table 6: Diagonal and curve length comparison of body part (spec A) with conventional and automatic grading of BokeCAD

Point of measures	Measurement comparison	Size					Unit
		S	M	L*	XL	XXL	
Sleeve armhole straight	Error after conventional grading	+0.42	+0.21	0.00	−0.21	−0.42	cm
	Length acquired after conventional grading	25.42	26.21	27.00*	27.79	28.58	
	Length required	**25.00**	**26.00**	**27.00***	**28.00**	**29.00**	
	Length acquired after automatic grading	25.00	26.00	27.00*	28.00	29.00	
	Error after automatic grading	0.00	0.00	0.00	0.00	0.00	
Under sleeve	Error after conventional grading	−0.18	−0.10	0.00	+0.12	+0.25	cm
	Length acquired after conventional grading	13.82	14.40	15.00*	15.62	16.25	
	Length Required	**14.00**	**14.50**	**15.00***	**15.50**	**16.00**	
	Length acquired after automatic grading	14.00	14.50	15.00*	15.50	16.00	
	Error after automatic grading	0.00	0.00	0.00	0.00	0.00	

Point of measures	Measurement comparison	Size					Unit
		S	M	L*	XL	XXL	
Front sleeve curve	Error after conventional grading	+0.50	+0.25	0.00	−0.25	−0.50	cm
	Length acquired after conventional grading	25.84	26.65	27.45*	28.25	29.06	
	Length required	**25.34**	**26.40**	**27.45***	**28.50**	**29.56**	
	Length acquired after automatic grading	25.41	26.43	27.45*	28.47	29.48	
	Error after automatic grading	+0.07	+0.03	0.00	−0.03	−0.08	
Back sleeve curve	Error after conventional grading	+0.50	+0.25	0.00	−0.25	−0.50	cm
	Length acquired after conventional grading	25.75	26.55	27.35*	28.15	28.95	
	Length required	**25.25**	**26.30**	**27.35***	**28.40**	**29.45**	
	Length acquired after automatic grading	25.33	26.34	27.35*	28.37	29.38	
	Error after automatic grading	+0.08	+0.04	0.00	−0.03	−0.07	
*Note: * indicates base size*							
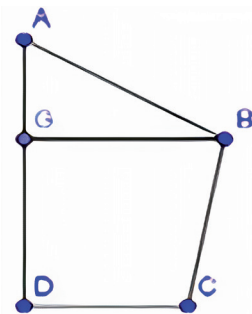
Figure 21: Points to calculate Pythagoras grading for pattern pieces of T-shirt sleeve of spec B

According to Pythagoras law from Δ ABG (cf. Figure 21):

$$AG^2 + GB^2 = AB^2 \tag{13},$$

where AB = sleeve armhole straight and GB = sleeve width.

For L size:

$$AG_L = \sqrt{AB_L{}^2 - GB_L{}^2} = \sqrt{27^2 - 24.5^2} = 11.35 \tag{14},$$

for XL size:

$$AG_{XL} = \sqrt{AB_{XL}{}^2 - GB_{XL}{}^2} = \sqrt{28^2 - 25.25^2} = 12.10 \tag{15}.$$

The x-axis value of point A = 0 and the y-axis value of point A = 12.10 – 11.35 = 0.75; the y-axis value of
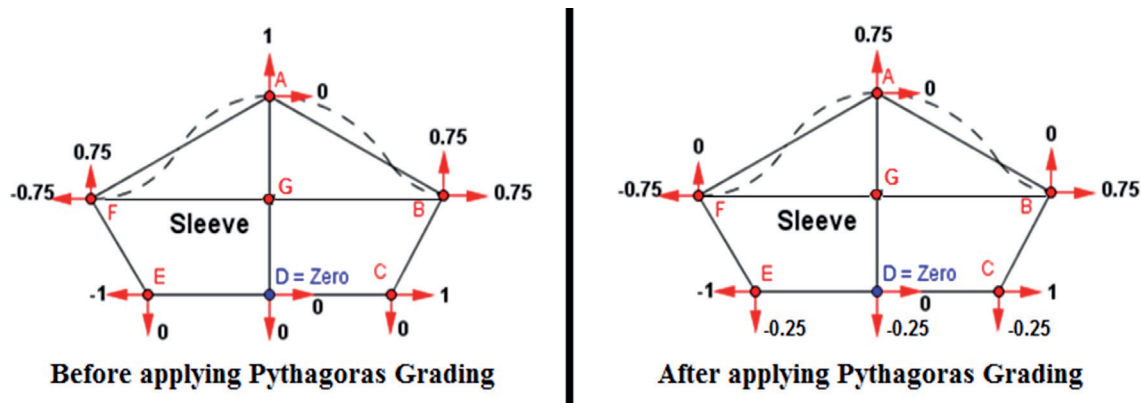
Figure 22: Grading increment of pattern pieces of T-shirt sleeve of spec B before and after Pythagoras grading

point D = (1 − 0.75) = −0.25; and the x-axis value of point D = 0. Therefore, the value of A = (0, 0.75), B = (0.75, 0), C = (1, −0.25), D = (0, −0.25) and G = (0, 0). After applying Pythagoras grading, the grading increment values change, which is shown in Figure 22. The diagonal and curve measurements found after the grading are shown in Table 7.

Based on data in Table 7, it can be said that diagonal and curve grading is up to 0.1 cm error, which is negligible. However, if the under sleeve is given instead of sleeve width, then the calculation is more difficult.

3.2.4.1.1 Pythagoras grading for pattern pieces of T-shirt sleeve (spec A) (method 1)

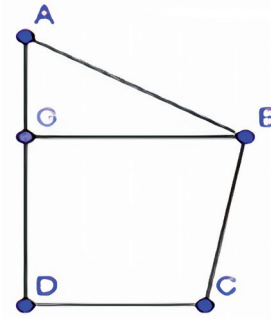The pattern construction of a T-shirt sleeve can be divided into some geometries that are shown in Figure 23.

Figure 23: Points to calculate Pythagoras grading for pattern pieces of T-shirt sleeve of spec B (method 1)

After drawing the pattern and then manually measuring the length, the following measurements were found: AG_L = 9.02 and GB_L = 25.45 (cf. Figure 23). For the grading of sleeve length, the total amount of the grading increment (1 cm) was distributed

Table 7: Diagonal and curve length comparison of sleeve pattern piece (spec B) with conventional and Pythagoras grading

Point of measures	Measurement comparison	Size					Unit
		S	M	L*	XL	XXL	
Sleeve armhole straight	Error before applying Pythagoras law	+0.43	+0.21	0.00	−0.21	−0.43	cm
	Length acquired before applying Pythagoras law	25.43	26.21	27.00*	27.79	28.57	
	Length required	**25.00**	**26.00**	**27.00***	**28.00**	**29.00**	
	Length acquired after applying Pythagoras law	25.02	26.01	27.00*	28.00	29.00	
	Error after applying Pythagoras law	+0.02	+0.01	0.00	0.00	0.00	
Front sleeve curve	Error before applying Pythagoras law	+0.51	+0.26	0.00	−0.26	−0.51	cm
	Length acquired before applying Pythagoras law	25.90	26.70	27.50*	28.30	29.10	
	Length required	**25.39**	**26.44**	**27.50***	**28.56**	**29.61**	
	Length acquired after applying Pythagoras law	25.48	26.49	27.50*	28.52	29.54	
	Error after applying Pythagoras law	+0.09	+0.05	0.00	−0.04	−0.07	
Back sleeve curve	Error before applying Pythagoras law	+0.51	+0.25	0.00	−0.26	−0.52	cm
	Length acquired before applying Pythagoras law	25.85	26.65	27.45*	28.24	29.04	
	Length required	**25.34**	**26.40**	**27.45***	**28.50**	**29.56**	
	Length acquired after applying Pythagoras law	25.44	26.44	27.45*	28.47	29.48	
	Error after applying Pythagoras law	+0.10	+0.04	0.00	−0.03	−0.08	
Note: * indicates base size							

equally on both sides of the zero-point G; hence, $AG_{XL} = (9.02 + 0.5) = 9.52$.

From $\triangle AGB$ (cf. Figure 23), according to Pythagoras law:

$$AG^2 + GB^2 = AB^2 \tag{16},$$

and for XL size:

$$GB_{XL} = \sqrt{28^2 - 9.52^2} = 26.33 \tag{17}.$$

The x-axis value of point B = (26.33 – 25.45) = 0.88 and the y-axis value of point B = 0; the value of point A = (0, 0.5), B = (0.88, 0), C = (1, –0.5), D = (0, –0.5) and G = (0, 0).

After applying Pythagoras grading, the grading increment values change, as shown in Figure 24.

After applying Pythagoras grading, the graded measurements changed and are shown in Table 8.

3.2.4.1.2 Grading calculation for pattern pieces of T-shirt sleeve (spec A) (method 2 – two sleeves drawing from same starting point)

The pattern construction of a T-shirt sleeve can be divided into some geometries when overlapping two consecutive sizes (base size and size next to it), which is shown in Figure 25.

From point D (cf. Figure 25), if the pattern of the sleeve is drawn as AD and A2D = sleeve length for L and XL size, DC and DC2 = sleeve opening for L and XL size, AB and A2B2 = armhole straight for L and XL size, and CB and C2B2 = under sleeve for L and XL size, the calculation can be done as value A = (0, 1), D = (0, 0), C = (1, 0) as in the conventional method.

However, for calculating the increment of B point, 2 lines from B and B2 points must be extended to intersect at point P. Now, the measurement can be performed manually to measure the values of BP

Table 8: Diagonal and curve length comparison of pattern pieces of T-shirt body part (spec A – method 1) with conventional and Pythagoras grading

| Point of Measures	Measurement comparison	Size					Unit
		S	M	L*	XL	XXL	
Sleeve armhole straight	Error before correction	+0.42	+0.21	0.00	−0.21	−0.42	cm
	Length acquired before correction	25.42	26.21	27.00*	27.79	28.58	
	Length required	**25.00**	**26.00**	**27.00***	**28.00**	**29.00**	
	Length acquired after method 1	25.01	26.00	27.00*	28.00	29.00	
	Error after method 1	+0.01	0.00	0.00	0.00	0.00	
Under sleeve	Error before correction	−0.18	−0.10	0.00	+0.12	+0.25	cm
	Length acquired before correction	13.82	14.40	15.00*	15.62	16.25	
	Length required	**14.00**	**14.50**	**15.00***	**15.50**	**16.00**	
	Length acquired after method 1	14.17	14.58	15.00*	15.43	15.86	
	Error after method 1	+0.17	+0.08	0.00	−0.07	−0.14	
Front sleeve curve	Error before correction	+0.50	+0.25	0.00	−0.25	−0.50	cm
	Length acquired before correction	25.84	26.65	27.45*	28.25	29.06	
	Length required	**25.34**	**26.40**	**27.45***	**28.50**	**29.56**	
	Length acquired after method 1	25.42	26.44	27.45*	28.46	29.48	
	Error after method 1	+0.08	+0.04	0.00	−0.04	−0.08	
Back sleeve curve	Error before correction	+0.50	+0.25	0.00	−0.25	−0.50	cm
	Length acquired before correction	25.75	26.55	27.35*	28.15	28.95	
	Length required	**25.25**	**26.30**	**27.35***	**28.40**	**29.45**	
	Length acquired after method 1	25.33	26.34	27.35*	28.36	29.37	
	Error after method 1	+0.08	+0.04	0.00	−0.04	−0.08	
Note: * indicates base size							
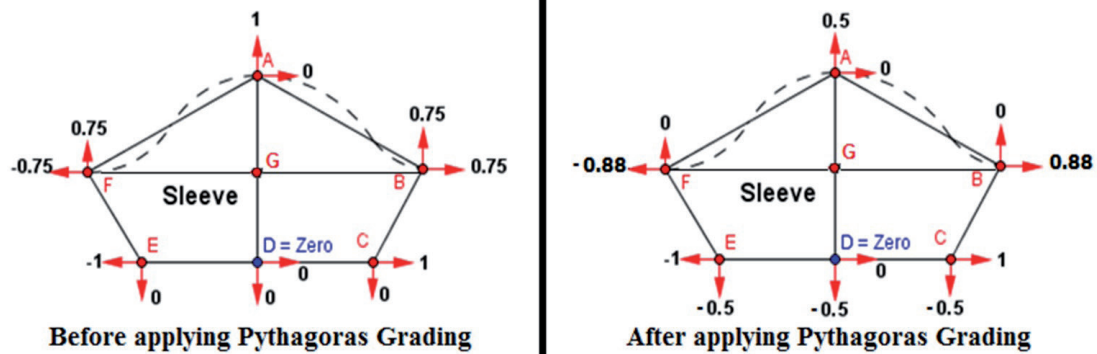
Figure 24: Grading increment of pattern pieces of T-shirt sleeve spec A (method 1) before and after applying Pythagoras grading
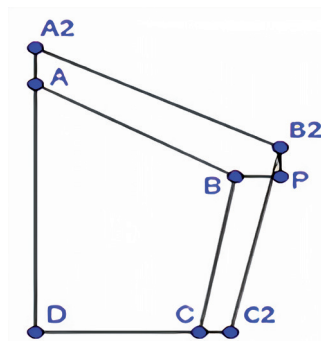

Figure 25: Points to calculate grading increment for the pattern pieces of T-shirt sleeve pattern of spec A (method 2)

and B2P, which are actually the x- and y-axis values of B point. Hence, B = (0.91, 0.57).

After applying method 2, the grading increment values change, which is shown in Figure 26.

The measurements found after the grading can be seen in Table 9.

Regarding data in Table 9, it can be said that there is a minimum deviation from the original measurements, i.e. only up to 0.01 cm error, which is negligible. The values can also be slightly adjusted (increase or decrease as required) to get 100% accurate length. If sleeve width is given instead of under-sleeve, then it is very easier to calculate the grading increments.

4 Recommendation for presence of diagonal and curve measurements

4.1 Recommendation for problem 1 – presence of diagonal measurements

Diagonal measurements should be avoided as much as possible in the spec sheet since they cause grading deficiency. If the diagonal measurement exists in a spec sheet, then the measurement checking and manual manipulation in grading increment should be conducted to rectify the measurements. It can be
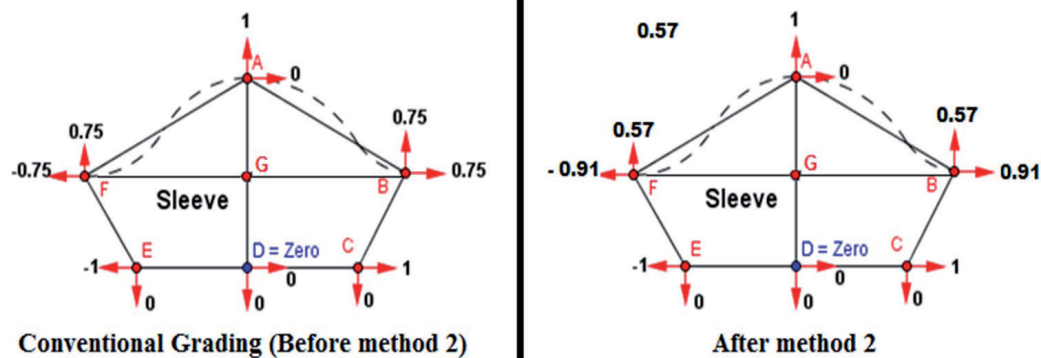

Figure 26: Grading increment of pattern pieces of T-shirt sleeve spec A before and after applying method 2

Table 9: Diagonal and curve length comparison of pattern pieces of T-shirt body part (spec A – method 2)

Point of measures	Measurement comparison	Size					Unit
		S	M	L*	XL	XXL	
Sleeve armhole straight	Error before correction	+0.42	+0.21	0.00	−0.21	−0.42	cm
	Length acquired before correction	25.42	26.21	27.00*	27.79	28.58	
	Length required	**25.00**	**26.00**	**27.00***	**28.00**	**29.00**	
	Length acquired after method 2	25.00	26.00	27.00*	28.00	29.00	
	Error after method 2	0.00	0.00	0.00	0.00	0.00	
Under sleeve	Error before correction	−0.18	−0.10	0.00	+0.12	+0.25	cm
	Length acquired before correction	13.82	14.40	15.00*	15.62	16.25	
	Length required	14.00	14.50	15.00*	15.50	16.00	
	Length acquired after method 2	14.02	14.5	15.00*	15.50	16.01	
	Error after method 2	+0.02	0.00	0.00	0.00	+0.01	
Front sleeve curve	Error before correction	+0.50	+0.25	0.00	−0.25	−0.50	cm
	Length acquired before correction	25.84	26.65	27.45*	28.25	29.06	
	Length required	**25.34**	**26.40**	**27.45***	**28.50**	**29.56**	
	Length acquired after method 2	25.41	26.43	27.45*	28.47	29.48	
	Error after method 2	+0.08	+0.03	0.00	−0.03	−0.08	
Back sleeve curve	Error before correction	+0.50	+0.25	0.00	−0.25	−0.50	cm
	Length acquired before correction	25.75	26.55	27.35*	28.15	28.95	
	Length required	**25.25**	**26.30**	**27.35***	**28.40**	**29.45**	
	Length acquired after method 1	25.32	26.34	27.35*	28.36	29.38	
	Error after method 1	+0.07	+0.04	0.00	−0.04	−0.07	
*Note: * indicates base size*							

done in any garment CAD. However, if Optitex or TukaCAD is available, then the "measure and segment editor" function can be used to minimise the diagonal line grading error. If BokeCAD is available, then "automatic grading" can be used instead of "conventional grading" as both methods are available in BokeCAD. Even if Optitex or TukaCAD or BokeCAD is not available, or we are not familiar with the particular function to rectify grading, then Pythagoras grading can be used to minimise inclined line grading errors.

4.2 Recommendation for problem 2 – presence of curve measurements

Measurement checking and manual manipulation for the grading increment should be performed until the required curve lengths are achieved. If Optitex or TukaCAD is available, use the "measure and segment editor tool" to rectify the curve line grading. If Boke CAD is available, then there is no

need to rectify the grading since it has an automatic grading system for higher precision grading. If that software is not available or we are not familiar with the described tools, then use the Pythagoras grading system developed by the author.

5 Conclusion

During the production, pattern pieces must be increased or decreased geometrically to create a complete range of sizes to produce clothing that fits various body types and sizes. Size specifications vary slightly from manufacturer to manufacturer and each company determines its own grade specifications for each size. Grading is still the most effective method to create multiple sizes from base size according to the size chart for the clothing production (even though the grading calculation can be slightly tricky and complex),

since it is less time consuming and it supports downstream operations such as marker making and cutting. Computerised grading with different 2D and 3D CAD systems are not free from limitations even though they provide the most efficient method of pattern making, grading and marker making. There are different techniques and tools available in different garment CADs to rectify grading errors. However, the tools and techniques provided by different CADs are different from one another and different techniques have different levels of complexity and accuracy. The findings and recommendations will help the pattern grader to minimise and rectify grading deficiencies. If it is successfully implemented, it will not only reduce size-set sample approval time but also develop products that fit well to the wearer's body.

Acknowledgments

References

3. MULLET, K.K. *Concepts of pattern grading: techniques for manual and computer grading.* New York : Bloomsbury Publishing, 2015.

4. PRICE, J., ZAMKOFF, B. *Grading techniques for fashion design.* New York : Fairchild Publications, 1996.

5. PATERSON, M. I. *Pattern grading by computer: unpublished thesis.* University of Bradford, UK, 1978.

6. MOORE, C.L., MULLET, K.K., YOUNG, M.B.P. *Concepts of pattern grading.* New York : Fairchild Publications, 2001.

7. KEISER, S., VANDERMAN, D., GARNER, M.B. *Beyond design: the synergy of apparel product development.* New York : Fairchild Publications, 2003.

8. LIU, Z., HARLOCK, S.C. A computer-aided grading system for both basic block and adapted clothing patterns. Part II: the grading algorithms. *Textile Research Journal*, 1995, **65**(2), 95-100, doi: 10.1177/004051759506500205.

9. ALDRICH, W. *Metric pattern cutting.* Hoboken : Wiley-Blackwell, 2004.

10. ALDRICH, W. *Metric pattern cutting for children's wear and babywear.* Hoboken : John Wiley & Sons, 2009.

11. ALDRICH, W. *Metric pattern cutting for menswear.* Hoboken : John Wiley & Sons, 2011.

12. ALDRICH, W. *Metric pattern cutting for women's wear.* Hoboken : John Wiley & Sons, 2015.

13. ISTOOK, C.L. Enabling mass customization: computer-driven alteration methods. *International Journal of Clothing Science and Technology*, 2002, **14**(1), 61–76, doi: 10.1108/09556220210420345.

14. SAYEM, A. S., KENNON, R. and CLARKE, N. 3D CAD systems for the clothing industry. *International Journal of Fashion Design, Technology and Education*, 2010, **3**(2), 45–53, doi: 10.1080/17543261003689888.

15. WU, Y. *Development of an intelligent pattern making system for skirt design: M. Phil. Dissertation.* The Hong Kong Polytechnic University, Hong Kong, 2013.

16. ISLAM, M.M., HOSSAIN, M. T., JALIL, M.A., KHALIL, E. Line balancing for improving apparel production by operator skill matrix. *International Journal of Science, Technology and Society*, 2015, **3**(4), 101–106, doi: 10.11648/j.ijsts.20150304.11.

17. JALIL, M. A., HOSSAIN, M.T., ISLAM, M.M. and RAHMAN, M. M. To estimate the standard minute value of a polo-shirt by work study. *Global Journal of Research in Engineering*, 2015, **15**(2–G), 25–30, http://engineeringresearch.org/index.php/GJRE/article/view/1342.

18. SHARP, J.R., ELSASSER, V.H. *Introduction to AccuMark, Pattern Design, and PDM.* New York : Fairchild Publications, 2007.

19. KANG, T. J., KIM, M. S. Development of three-dimensional apparel CAD system. Part 1: flat garment pattern drafting system. *International Journal of Clothing Science and Technology*, 2000, **12**(1), 26–38, doi: 10.1108/EUM0000000005318.

20. RANIERI, R.A. *An analysis of the anthropometric measurements of the US Navy male recruit in order to improve garment and pattern design. Doctoral dissertation.* University of North Carolina at Greensboro, Greensboro, 1985.

21. ISLAM, M., JALIL, M. A., PARVEZ, M., HAQUE, M. Assessment of the factors affecting apparel pattern grading accuracy: problems identification and recommendations. *Tekstilec*, 2020, **63**(3), 166–184, doi: 10.14502/Tekstilec2020.63.166-184.

22. KUNICK, P. *Sizing, pattern construction and grading for women's and children's garments.* London : Philip Kunick, 1967.

23. DAI, B.H., WANG, X.Y. Research on intelligent clothing pattern auxiliary input and grading system. *Advanced Materials Research*, 2011, **175-176**, 906–910, doi: 10.4028/www.scientific.net/AMR.175-176.906.

24. GILL, S. A review of research and innovation in garment sizing, prototyping and fitting. *Textile Progress*, 2015, **47**(1), 1–85, doi: 10.1080/00405167.2015.1023512.

25. KIM, D. E., LABAT, K., BYE, E., SOHN, M., RYAN, K. A study of scan garment accuracy and reliability. *The Journal of The Textile Institute*, 2015, **106**(8), 853–861, doi: 10.1080/00405000.2014.949502.